Building the colon epithelial microenvironment *in vitro* for investigation of intestinal disease mechanisms

Angelo Massaro

A dissertation
Submitted in partial fulfillment of the
requirements for the degree of

Doctor of Philosophy

University of Washington
2024

Reading Committee:
Nancy L. Allbritton, Chair
Cole DeForest
Marta Scatena

Program Authorized to Offer Degree:
Department of Bioengineering

University of Washington

Abstract

Building the colon epithelial microenvironment *in vitro* for investigation of intestinal disease mechanisms

Angelo Massaro

Chair of the Supervisory Committee:
Nancy L. Allbritton
Department of Bioengineering

Colonic epithelium is situated directly above the lamina propria which houses fibroblasts and resident immune cells that provide support and protection for proliferative stem cells and terminally differentiated epithelial cells. In health, fibroblasts maintain the extracellular matrix (ECM) and provide signals to help enforce spatial organization in the epithelial layer. In the case of injury or inflammation, resident immune cells initiate the immune response while fibroblasts help to rebuild a healthy tissue, though in some cases persistent, pathological fibroblast activity may lead to tissue thickening and stiffening inducing fibrosis. Disruptions in the epithelium-fibroblast relationship play a role in many diseases including colorectal cancer (CRC) while epithelium-immune cell interactions are critical for maintaining intestinal homeostasis, yet the complexity of the intestinal microenvironment makes it challenging to study these relationships *in vivo*. To better understand intestinal disease initiation and progression, *in vitro* model systems are needed to recapitulate the direct contact between fibroblasts and epithelial cells and to study the immune cell response within a controlled environment.

This dissertation describes the development and testing of *in vitro* model systems to mimic interplay of multiple cell types present in the colonic mucosa. In Chapter 2, we describe a 3D, fully polarized *in vitro* tissue model with an array of crypts comprised of primary human colonic epithelial cells located above a layer of human primary pericryptal fibroblasts. Model crypts form a stem cell niche in their base and a differentiated cell zone at the luminal end. In this *in vitro* context underlying fibroblasts also support epithelial survival and barrier function while modulating proliferation. This model will enable work towards an improved understanding of the role fibroblasts play in healthy colon tissue and in disease initiation and development. Chapter 3 describes a new model of colonic fibrosis wherein fibroblasts and epithelial cells are grown on two scaffolds that exhibit healthy or fibrotic biophysical characteristics. Though fibrosis is often the result of a persistent inflammatory response, fibrinogenesis is a self-perpetuating process and so we sought to model excessive ECM deposition within a tissue by altering the underlying substrate and then culturing primary fibroblasts and epithelial cells together. The hydrogel scaffolds on which cells were cultured possess diffusivity and stiffness characteristics similar to healthy and fibrotic tissues. Cells exhibited altered morphology and phenotype when cultured on stiff scaffolds, demonstrating the usefulness of this model for future fibrosis related investigations. In chapter 4 a different *in vitro* model system was used to observe the interaction between another pair of cell types present in the colonic mucosa: epithelium and resident immune cells. In this case, a soft, highly permeable hydrogel was used as a model of the interstitial space and the migration of macrophages towards a normal or damaged epithelial layer was measured. The epithelial cell barrier function and phenotype along with immune cell migration in response to stimuli were measured demonstrating the usefulness of this system for

modeling acute inflammation. The model systems described in this dissertation will enable further discovery regarding colonic tissue repair and CRC initiation and progression.

Acknowledgements

This work would not have been possible without encouragement, inspiration, and love from those who supported me along the way. A dissertation can feel like a solitary endeavor at times, but my team of family, friends, and mentors has helped me to become a more thorough scientist and thoughtful person. Thank you for teaching me to be patient, confident, caring, and curious.

Thank you, Mom, Dad, and Julia, for your loving support. Thank you to my advisor, Nancy, for leading me and thank you to all members of the Allbritton Lab, especially Sam Hinman, Cecilia Villegas-Novoa, and Yuli Wang, for your abundant guidance. Thank you, Lorenzo Tozzi, Alessandra Balduini and Louisa Dowel, for encouraging me to pursue bioengineering research. Finally, thank you to my roommates, friends, and family members in Seattle and beyond for helping me to enjoy the ride.

Table of Contents

List of Figures

List of Tables

*Supplemental tables S1-S6 can be found in the accompanying file "massaro_Thesis_SupTables_S1-S6.xlsx"

Chapter 1. Introduction

1.1. The Large Intestine

1.1.1. Intestinal Physiology

The large intestine (colon) is a tubular organ of the gastrointestinal (GI) tract, that absorbs water, electrolytes, and vitamins, and processes indigestible waste[1]. The cecum and ascending colon are suited for absorption while the transverse, descending and sigmoid colon sections primarily form, move and store feces[2]. Like other GI organs, colon tissue is organized into concentrically stratified regions. The mucosa is closest to the hollow lumen where waste passes and the gut microbiota is maintained. Outwards from the mucosa there is the submucosa with connective tissue and blood vessels, the muscularis propria with smooth muscle, and the serosa where nerve connections are found[2]. The innermost mucosa can be further subdivided into the epithelium, lamina propria, and contractile muscularis mucosae[2,3] (Figure 1). Columnar epithelial cells lining the lumen form a barrier, secrete mucus, send paracrine signals, and take up nutrients[4]. The lamina propria houses fibroblasts, immune cells, and blood vessels that all support the epithelium and help provide structure [2,5]. The physical and chemical microenvironment of epithelial cells is heavily influenced by cells in the lamina propria and interactions between these two regions is especially important to intestinal homeostasis. The condition of the intestinal epithelium is crucial to overall health and dysregulation in this barrier has been linked to Irritable Bowel Disease, Crohn's, and Colorectal Cancer (CRC). An enhanced understanding of the interplay between the epithelium and lamina propria will be beneficial to understand disease progression and to study the interactions in the colonic mucosa it is important to consider the architecture of the tissue.

1.1.2. Colon Crypt Architecture

The colon's luminal surface is dotted with an array of 100 μm wide, 500 μm deep invaginations called the crypts of Lieberkühn[6,7]. A cross-section of colon tissue reveals crypts as a series of aligned tubes with a flat inter-crypt space (Figure 1). In postnatal development, colonic crypts form via deepening indentations, in mature individuals, crypts can multiply by fission or asymmetric budding, and in aging colons, crypts are often less frequent[8,9]. Crypts act as a stem cell niche, and in the early 19th century Joseph Paneth and Giulio Bizzozero independently proposed that that dividing cells in the crypt base are the source of epithelium in the luminal surface[10,11]. It has since been proven that the crypt structure enables constant regeneration, with multipotent and long-lived stem cells proliferating in the base of crypts for an individual's entire lifetime[6]. As cells divide, some remain in the base with a stem phenotype while other daughter cells progress towards a certain lineage, first as transit amplifying cells then differentiating into several types of epithelial cells that migrate upwards towards the lumen where they live for about a week and are then sloughed off into the lumen[9]. Cells in the crypt base are physically distanced from the high-sheer, anaerobic, and bacteria filled lumen and the location also keeps them closer to vasculature and the lamina propria where cells like fibroblasts secrete supportive soluble factors[12]. The crypt three-dimensional architecture also has been shown to encourage stemness, as cells are responsive to the tight curvature in the crypt base[13,14].

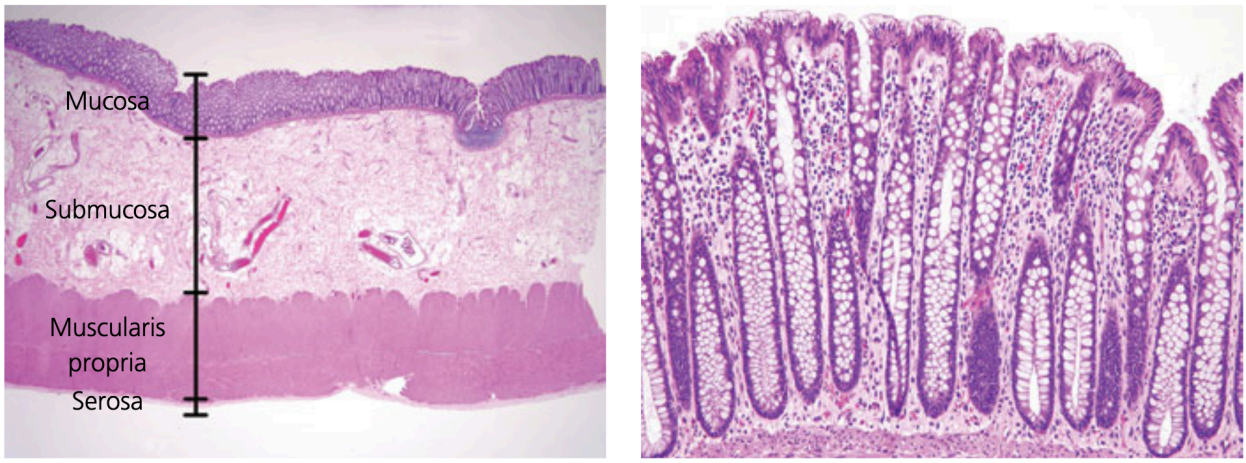

Figure 1.1. Histology of normal human colon. The left panel shows the full, stratified colon tissue while the right panel displays the mucosa. Image from Reinus & Simon 2014[2].

1.1.3. Characterizing Intestinal Epithelial Cells

In early development a tube containing all three germ layers is the structural precursor to the GI system and, as it becomes spatially patterned, the posterior region develops into the hindgut and then the colon while the endoderm in this region develops into epithelium[15]. A radial crypt-villus axis is developed, though colonic villi will be flattened by birth, and multipotent stem cells that will be maintained for an individual's lifetime are established in the base of crypts (Figure 2). Intestinal stem cells can be identified by expression of Leucine-rich repeat-containing G-protein coupled receptor 5 (*Lgr5*) or Achaete-Scute Family BHLH Transcription Factor 2 (*Ascl2*) and they undergo mitosis more rapidly than neighboring cells [16–18]. About 95% of the time stem cells divide asymmetrically i.e., one progeny maintains the parent stem phenotype and the other daughter cell becomes a transit amplifying cell that proliferates 4-5 times before terminally differentiating[6,19]. Otherwise stem cells may divide symmetrically into two stem cells or two transit amplifying cells[20].

Differentiated epithelial cells are mostly absorptive or secretory and they are localized in the upper crypt or inter-crypt space. Colonocytes and goblet cells are the most abundant differentiated epithelial cell types. Notch signaling is said to govern this lineage decision as expression of Notch intracellular domain (*NCID*) leads to colonocyte differentiation whereas Notch inhibition guides towards a goblet phenotype[21,22]. Colonocytes have cilia on their luminal side, are responsible for nutrient absorption, and form tight junctions with lateral neighbors to create the epithelium's physical barrier[23]. Goblet cells secrete mucins into the lumen and the resultant layered mucus enforces the barrier preventing infiltration of bacteria or other pathogens. It is important to note, in the small intestine differentiated Paneth cells are present in the base of the crypt in direct contact with Lgr5+ stem cells, though these are absent in colonic crypts [18]. Other more rare epithelial cell types can be found in intestinal epithelium as well including Tuft cells and Enteroendocrine cells that can aid in the immune response via cytokine release or hormone secretion, directing the immune system or modulating nutrient absorption[23].

1.1.4. Crypt Polarization

The three-dimensional architecture of colonic crypts is crucial for continuous regeneration of the tissue. The shape of these invaginations enables contrasting signals to be delivered near to one another to create a highly ordered environment with conditions in the base that are drastically different than in the top. With contrasting circumstances in the lamina propria versus the gut lumen, chemical concentration gradients are generated across the long axis of intestinal crypts, with a high concentration of a compound on one side and near-zero concentration on the other (Figure 3). For example, oxygen is delivered to the lamina propria via vasculature, but the colon lumen is anaerobic and thus as oxygen diffuses towards the lumen and is consumed, a

gradient is formed with an oxygen rich environment in the base and an oxygen depleted environment in the lumen. To further enforce this gradient, colonocytes in the lumen consume oxygen when available while colonocytes near the base of the crypt conduct fermentation, and do not consume oxygen, leaving more available for metabolically active stem and transit amplifying cells[23]. Oxygen serves as a good example of how formed gradients help maintain the organization within crypts though other signaling factors are perhaps more important to the polarization of the intestinal stem cell niche.

Wnt signaling is a major controller of proliferation in intestinal crypt stem cells[24]. This highly conserved pathway is active when Wnt ligands complex with transmembrane proteins such as Frizzled (Fz) and lipoprotein receptor-related protein (LRP) which subsequently inhibit proteasomal degradation of β-catenin in the cytosol. When β-catenin concentration builds up in the cytosol, it will translocate to the nucleus and activate transcription of Wnt targeted genes[19]. *In situ* RNA hybridization has revealed that activity of canonical Wnt ligands, like Wnt-3, Wnt-6, and Wnt-9b that are associated with proliferation, are localized to the crypt base [24]. Conversely, Wnt ligands associated with noncanonical signaling like Wnt-2b, Wnt-4, Wnt-5a, and Wnt-5b may modulate proliferation and have been observed in mesenchyme near the colonic lumen[24]. Bone morphogenetic proteins (BMP), mainly BMP-2 and BMP-4, inhibit intestinal stem cells[25]. In healthy tissue BMP is excluded from the crypt base and BMP inhibition has been observed to induce proliferation[25–27]. Noggin, a BMP antagonist expressed in the submucosal region, protects proliferating stem cells from BMP signals in the crypt base[25]. R-spondin is another important signaling factor that is a strong agonist of canonical Wnt found in the crypt base[28,29]. While this is not an exhaustive list of all the factors present within the crypt stem cell niche, those mentioned here are most pertinent to this work and with exogenously

provided canonical Wnt, R-spondin, and BMP antagonist Noggin it is possible to maintain intestinal stem cells *in vitro* [30].

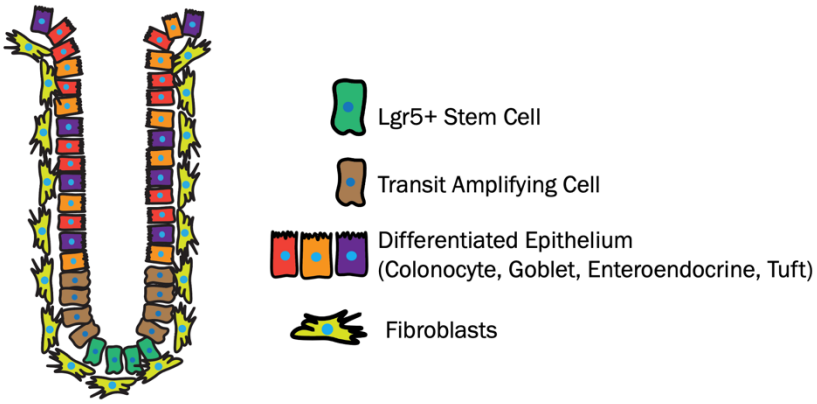

Figure 1.2. Schematic showing the positioning of epithelium and fibroblasts within a colon crypt.

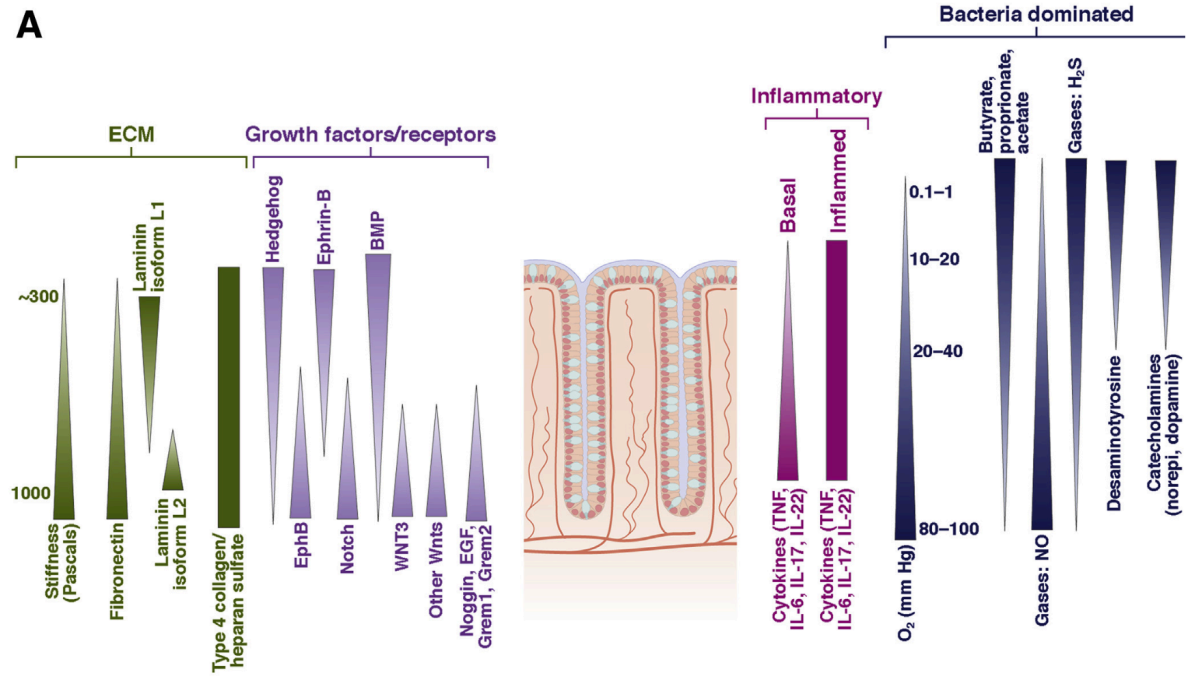

Figure 1.3. Various gradients present in the colon crypt. Figure from Wang et al.[31].

1.2. Role of Fibroblasts

1.2.1. Characterizing Intestinal Fibroblasts

There is ongoing discovery regarding the specific location of a myriad of fibroblast subtypes, which we will not focus on here, but it is important to characterize the main contributors in the lamina propria: intestinal fibroblasts and myofibroblasts can be recognized as CD45-, CD 31-, and CD90+ cells[32]. Vimentin, a cytoskeleton filament protein, is present in both fibroblasts and myofibroblasts while α-smooth muscle actin (α-SMA) is observed in myofibroblasts[33]. Both fibroblasts and myofibroblasts secrete collagens though only myofibroblasts are contractile and there is usually a transition from fibroblasts to myofibroblasts during injury repair[34]. Myofibroblasts can be distinguished from smooth muscle cells by measuring desmin expression which is only expressed in the muscle cells and α-SMA is also more highly expressed in smooth muscle[33]. Further, fibroblasts and myofibroblasts have abundant endoplasmic reticulum and collagen secretion granules, though focal adhesions can only be observed in fibroblasts and inter-cell fibronexus are only observable in myofibroblasts[33,35]. Recently platelet-derived growth factor receptor-α (PDGFR-α) has also been identified in pericryptal fibroblasts and it has been shown that these cells might have different expression levels of PDGFR-α near the top or bottom of crypts indicating that the lamina propria is polarized like the epithelium [36,37].

A note for clarity: When discussing mesenchymal cells of the intestinal lamina propria this can include an array of cell types that share a similar differentiation pathway and have coordinated biological functions[38]. Though this category encompasses mural cells of the vasculature, stromal stem cells, and smooth muscle cells which are all important to the function of the lamina propria, this study will focus on fibroblasts and myofibroblasts. That said, these cells have been observed to have a plastic phenotype i.e., switching back-and-forth depending on

environmental stimuli. While there is an important distinction between the function and impact of fibroblasts versus myofibroblasts, further discussed in chapter 3, herein we will mostly refer to the vimentin-positive supportive cell-type nearest to the epithelium within the lamina propria as pericryptal **fibroblasts**.

1.2.2. Colonic Fibroblasts in Health and Disease

Fibroblasts act in support of stem and differentiated epithelial cells within the large intestine and spatially specific fibroblast signaling helps preserve precise order along the crypt axis. Bidirectional communication between fibroblasts and epithelium occurs via secreted factors, direct cell-to-cell contact, and mechanical cues from the fibroblast-generated ECM[33,39–42]. To help maintain the crypt stem cell niche, fibroblasts near the crypt bottom secrete Wnt (canonical signaling), R-spondin and BMP antagonists Gremlin and Noggin[33,39,40,43]. In contrast, fibroblasts closer to the lumen conduct direct-contact Notch signaling, secrete BMPs and express noncanonical Wnt ligands to direct epithelium differentiation. Fibroblasts also play an important role in establishing the ECM, especially during wound repair. Collagen, fibronectin, and laminin secretion helps build the ECM while MMP secretion and (myo)fibroblast contraction can reorder the physical environment as necessary[33]. Varied ECM production along the crypt axis can also contribute to crypt polarization[31]. As fibroblasts play such an important role in upholding and restoring order within the colonic mucosa, it follows that dysregulation amongst these cells can lead to disease.

Although colonic adenocarcinoma develops from hyperproliferative epithelial cells, recent studies have shown that fibroblasts play an important role in CRC development and progression[44]. An imbalance between epithelium proliferation and differentiation is a hallmark of CRC and this can be a result of atypical fibroblast behavior. As reviewed by Dang and

colleagues, specific alterations in fibroblast-epithelial signaling can lead to CRC related proliferation, invasion, migration, angiogenesis, therapy resistance, immune invasion, and metastasis of epithelial tumor[44]. The immune response can also be aided by fibroblast and again when fibroblast behavior is dysregulated, persistent activation can lead to fibrosis within the colon altering the microenvironment and enabling CRC initiation and progression.

Upon insult or injury to the colonic mucosa, the immune response is set into action by resident immune cells or other local mediators such as epithelial cells or fibroblasts [45]. Several immune-related signaling pathways have been connected to fibrinogenesis including transforming growth factor- β (TGF-β), tumor necrosis factor- α (TNF-α) and interleukins (IL) including IL-1, -17, -4, -13, and -36 [46,47]. While these signaling factors play an important role in activating and recruiting immune cells to prevent further tissue damage, a persisting inflammatory response leads to fibrinogenesis. Continuous ECM deposition complemented by an imbalance in matrix metalloproteases (MMPs) and tissue inhibitors metalloproteinases (TIMPs) results in excessive ECM accumulation [48]. Local mesenchymal cells, the primary cell type responsible for ECM remodeling, also change phenotype to an activated myofibroblast state while more mesenchymal cells are recruited to the area via migration or epithelial and endothelial to mesenchymal transition (EMT) [33,49]. Notably, upregulation of platelet derived growth factor alpha (PDGFα), TGF-β, insulin-like growth factor (IGF), epithelial growth factor (EGF), fibronectin (FN), and N-cadherin (N-cad) in myofibroblasts has been observed in intestinal fibrosis [50,51]. Metabolism in these cells also switches mainly to glycolysis indicative of a highly activated phenotype [50]. Damage to the intestinal barrier can also lead to a host response to pathogens infiltrating from the microbiome resulting in profibrotic activation of fibroblasts and activation of nuclear factor kappa-light-chain-enhancer of activated B cells (NF-

κB) related genes along with contraction within the collagen matrix [45,52]. These changes to mesenchymal cells and the biophysical and biochemical environment have a great impact on the epithelium. While in some isolated regions epithelial hyperplasia may occur, tissue integrity can be lost as epithelial cells flatten, die, and fall off leading to increased gaps between cells [53,54]. Though the impact of fibrosis on mesenchymal cells and epithelium has been studied, much is yet to be learned regarding the complex interplay between mesenchymal cells and epithelium within fibrotic tissue.

1.3. Colorectal Cancer

1.3.1. CRC Burden

Colorectal cancer (CRC) is the third most common cancer and the second most deadly worldwide with 1.93 million new cases and 935,173 deaths caused in 2020[55]. Incidence is higher in Western countries with 55% of global cases, though only 33% of CRC related deaths occurred in Western countries[56,57]. The 5-year survival rate for patients with localized CRC is relatively good at 90%, but the outlook is more grim for advanced or metastasized disease with a survival rate of just 15% [58,59]. It is thus important to understand the mechanism by which CRC is initiated as prevention or early detection could greatly reduce the global burden.

1.3.2. CRC Initiation and the Tumor Microenvironment

In the most common form of CRC, adenocarcinoma, hyperproliferation in the epithelium is the first step which can lead to polyp formation. Hyperproliferation may be due to aberrant Wnt signaling caused by genetic mutation, microenvironmental circumstances influenced by diet and the microbiota, or dysregulation of other cell types in or near the crypt niche[60]. Though colonic polyps are not inherently malignant, they are closely monitored and may be biopsied in

clinic because they indicate an imbalance in the ratio of proliferating versus differentiating epithelial cells. Mutation of the APC gene, a common tumor suppressor, directly affects Wnt signaling and can impede β-catenin degradation in the cytosol leading to a build-up of the transcription factor in the nucleus and increased activity of canonical Wnt signaling. Following epithelial hyperproliferation and APC mutation, further mutations in a rapidly dividing neoplasm within the KRAS, SMAD4 or p53 genes can enable a tumor to grow, invade and metastasize[56,61].

While cancer research often focuses on the genotypic and phenotypic changes in tumor cells, the biophysical characteristic of a microenvironment also plays an important role in tumorigenesis and cancer progression[62]. Cells are responsive to the number of binding sites available, and the stiffness of the surrounding ECM and it has been observed that there is increased stromal collagen deposition in tumor microenvironments [63]. In fact, tissue stiffening, especially in the case of fibrosis, has been shown to encourage tumor growth, metastasis, and inflammation [64–66]. A key property of fibrotic tissue is increased resistance to deformation, i.e., stiffness, and reduced mobility of soluble factors, i.e., diffusion. *Ex vivo* measurement of healthy and fibrotic human colonic tissue reveals the Young's modulus (E') to be 2.9 and 16.7 kPa, respectively [67]. Additionally, it has been observed that apparent diffusion coefficient can be almost 50% lower within a fibrotic stricture when compared to other regions within the same tissue [68,69].

1.4. Models of the Large Intestine

1.4.1. Enabling Discoveries

To date, *in vitro* models of the intestinal mucosa have focused on the epithelium alone since the health and regeneration of the epithelial barrier is integral to human health. In the past 15

years, several paradigm shifting publications have enabled researchers to accomplish the challenging task of maintaining and expanding intestinal stem cells *in vitro*[31]. First, in 2009 Toshiro Sato et al. described methods for isolating Lgr5+ stem cells from whole intestinal tissue for expansion as organoids that were observed to develop intestinal crypt and villus architecture[30]. This seminal work showed that murine intestinal stem cells could proliferate within laminin-rich Matrigel when supplied with Wnt agonist R-spondin, Epithelial Growth Factor (EGF), and BMP antagonist Noggin without supportive mesenchymal cells present[30,70]. Later, Miyoshi and Stappenbeck genetically modified a fibroblast-like cell line to secrete Wnt3a, R-spondin 3, and Noggin (L-WRN) and they described how media conditioned by L-WRN cells could be provided to support intestinal epithelial stem cells *in vitro* in a highly repeatable fashion[71–73]. Sharing this L-WRN cell line (ATCC, CRL-3276™) has enabled researchers around the world to generate their own conditioned media to support *in vitro* intestinal stem cell growth. More recently, methods have been developed for long-term expansion of colonic epithelium *in vitro* atop a flat slab of neutralized collagen without Matrigel embedded organoids[74]. Additionally, a stiff collagen scaffold that mimics the intestinal crypt architecture and is suspended within a well-insert has been employed to grow intestinal epithelium with precise control over the luminal and basal conditions, i.e., chemical gradients, of the tissue[75,76].

1.4.2. Overview of Other Human Fibroblast-Epithelium Intestinal In Vitro Models

Most human *in vitro* models of the intestinal mucosa have focused solely on the epithelium; however, increasingly fibroblasts are integrated into coculture models to investigate the interactions between the two cell types[37,77–88]. Fibroblasts cultured at a distance from the

epithelial cells but sharing a common medium have permitted investigation of paracrine signaling[30,72,73,81,89]. Crucially, this work has enabled long-term *in vitro* culture of intestinal epithelial cells and identified secreted factors playing a role in fibroblast-epithelial cell interactions. Yet these models fail to capture the impact of direct cell-cell communication occurring *in vivo*. Multi-layered planar coculture models have been used to mimic pericryptal fibroblasts and examine direct cell-cell interactions[79,82]. These models have revealed how direct contact between cells influences tissue barrier function; however, these planar systems do not possess the complex 3D architecture or cell compartmentalization of the crypt. Epithelial organoids have been cultured within a fibroblast-laden hydrogel to mimic the fibroblast-filled stroma of the *in vivo* intestine[85,90,91]. These methods revealed that a stroma containing fibroblasts supported the formation of a budding small intestine organoid. Nonetheless, these models did not mimic the pericryptal positioning of fibroblasts or support direct epithelial cell-fibroblast contacts. Microengineered intestine-on-chip systems with accurate crypt architecture and epithelial cell compartmentalization have been developed but to date these physiologically accurate systems do not fully incorporate pericryptal fibroblasts[75,78,80,86,92–94]. Given that surface topography and curvature, direct cell-cell interactions, and cell compartmentalization are known to play critical roles in the physiology of the intestine, an improved understanding of the fibroblast-epithelial cell partnership awaits an architectural accurate model of the colonic epithelium with its pericryptal fibroblasts[14,95]. Thus, we set out to create a system with both primary-derived human cell types in direct contact within 3D crypt architecture where cells behavior could be monitored with spatial specificity.

Chapter 2. Development of an in vitro model of intestinal tissue to study fibroblast and epithelial cell interplay

Chapter 2 is adapted from the following manuscript:
A. Massaro, C. Villegas-Novoa, Y. Wang, & N.L. Allbritton, Fibroblasts modulate epithelial cell behavior within the proliferative niche and differentiated cell zone within a human colonic crypt model (peer review).

2.1. Abstract

To study the fibroblast-epithelial cell interactions, an *in vitro* crypt model was formed on a shaped collagen scaffold with primary epithelial cells growing above a layer of primary colonic fibroblasts. The crypts possessed a basal stem cell niche populated with proliferative cells and a differentiated, nondividing cell zone at the luminal crypt end. The presence of fibroblasts enhanced cell differentiation and accelerated the rate at which a high resistance epithelial cell layer formed relative to cultures without fibroblasts. The fibroblasts modulated cell proliferation within crypts increasing the number of crypts populated with proliferative cells but decreasing the total number of proliferative cells in each crypt. Bulk-RNA sequencing revealed 41 genes that were significantly upregulated and 190 genes that were significantly downregulated in cocultured epithelium relative to epithelium cultured without fibroblasts. This epithelium-fibroblast crypt model suggests bidirectional communication between the two cell types and has the potential to serve as a model to investigate fibroblast-epithelial cell interactions in health and disease.

2.2. Introduction

In this work, a 2D model and a micro-engineered 3D model was developed to enable colonic fibroblast-epithelial coculture. The planar or 2D coculture model was created for fast

optimization of the coculture conditions with assessment of cell viability and surface coverage. This simple model utilized a tissue-cultured fibroblast cell line CCD18-Co derived from normal human colon as fibroblasts. Scaffolding and culture conditions were optimized for the epithelial cells while maintaining the wellbeing of the fibroblasts. The 3D model possessed *in vitro* crypts comprised of primary human colonic epithelial cells and underlying primary pericryptal fibroblasts isolated from normal colonic stroma. The optimized planar conditions were applied to the 3D model or array of crypts with underlying fibroblasts. Fibroblasts and epithelial cells (alone or in coculture) were assessed for their ability to proliferate under different conditions as well as their ability to express cell-type specific markers. Epithelial cell function, for example, creation of a high resistance barrier, was evaluated over time. The impact of the fibroblasts on epithelial cell crypt formation and cell compartmentalization was also evaluated. The impact on stem cell maintenance and proliferation was quantified followed by RNA expression analysis to investigate how the fibroblasts modified epithelial cell physiology. This system will enable an improved understanding of the interconnected relationship between epithelial cells and their partner cells, the pericryptal fibroblasts.

2.3. Results

2.3.1. Design of a platform for epithelial cell-fibroblast coculture

To visualize the *in vivo* location of the epithelial cells with respect to fibroblasts, human colonic tissue was fixed, sectioned, and immunostained for vimentin to identify fibroblasts and EpCAM to label epithelial cells. Fibroblasts were observed throughout the stroma beneath and between the colon crypts (Figure 2.1A, B). Importantly a layer of pericryptal fibroblasts was in close apposition to all epithelial cells including those within the crypts as well as those lining the luminal surface. To recapitulate this close relationship between the pericryptal fibroblasts and

epithelial cells, two *in vitro* systems were developed (Figure 2.1C): *i)* a planar coculture model and *ii)* a 3D crypt coculture model. Both systems employed a scaffolding comprised of a cross-linked collagen that was molded into either a flat surface or a three-dimensional crypt array. The collagen scaffold in both flat and molded-crypt models was placed within a hanging basket to enable control of media conditions on both sides of the scaffolding[96]. The flat collagen slab supported planar growth of the two cell types and enabled rapid screening of coculture conditions to support both fibroblasts and epithelial cells. Once the optimal coculture conditions were determined, a shaped scaffolding to support the crypt arrays was constructed. Screens on the flat collagen slabs employed a tissue-cultured intestinal, fibroblast cell-line (CCD18-Co). The 3D crypt arrays used primary human colonic fibroblasts which are a more restricted resource, but which more closely resembled the *in vivo* cell type than the cell line.

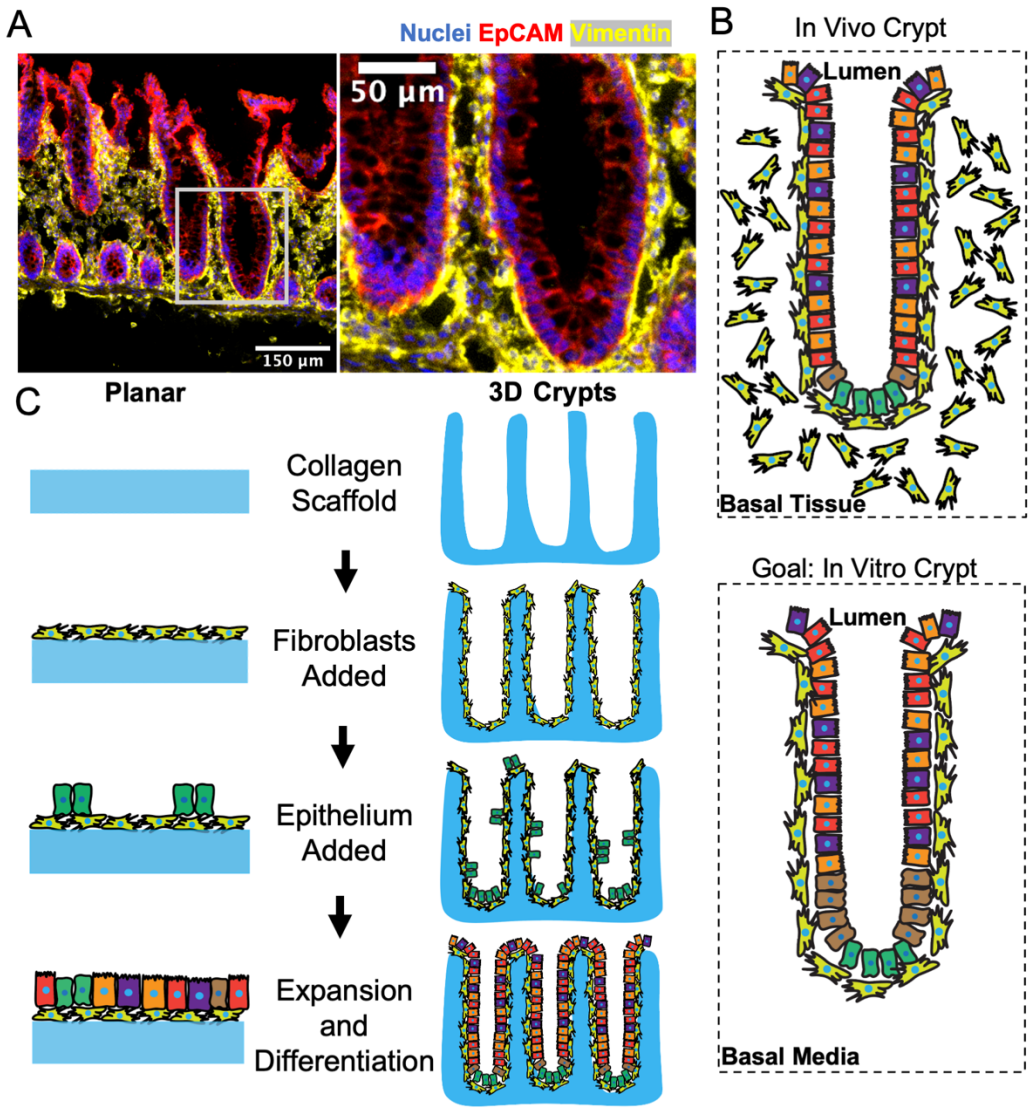

Figure 2.1. Model system to recapitulate the direct interactions of colonic fibroblasts with epithelium. (A) Fluorescence staining of a sliced section of human colon tissue displaying nuclei, epithelium, and fibroblasts. The white box in the left panel locates the higher magnification inset of the right panel. (B) Schematics showing the *in vivo* and *in vitro* positioning of columnar epithelial cells above pericryptal fibroblasts within a crypt. (C) Schematics of the sequential seeding process for generating a planar (2D) and crypt-shaped (3D) coculture model.

2.3.2. Identification of common culture conditions for fibroblasts and epithelial cells

Fibroblasts and epithelial cells are typically cultured under distinct conditions. Fibroblasts grow well in commonly used media such as DMEM supplemented with serum while epithelial cells require a wide range of additives such as B27, Y-27632, A83-01, SB202190, and growth

factors of Wnt, R-spondin, Noggin (WRN) and epithelial growth factor (EGF) to maintain stem cells and support their proliferation (Table 2.1). Fibroblasts are typically cultured on a polystyrene surface (stiffness ~ 3 GPa[97]) while intestinal epithelial stem cells require a much softer matrix (e.g. collagen, Matrigel with stiffness of 0.1-1 kPa) with proper ECM contacts for cell survival[98]. An initial goal of this work was to identify a medium and surface on which both fibroblasts and epithelial cells would be viable and maintain their appropriate phenotype. Since fibroblasts are more tolerant of their culture conditions than epithelial cells, fibroblasts were initially cultured under conditions supportive of intestinal epithelial stem cells. Under these culture conditions, fibroblasts demonstrated poor survival and altered morphology (Figure 2.2 A). To understand which medium additive might be negatively impacting the cells, fibroblasts were cultured on polystyrene 12-well plates in fibroblast medium but with the addition of a single component from the epithelial medium. The impact of WRN, EGF, A83-01, and SB202190 was not assessed since epithelial stem/proliferative cells are critically dependent on these factors[70]. Cell morphology and surface coverage were examined over time. Fibroblasts without the epithelial-cell additives spread across the culture surface and grew to confluence within three days while fibroblasts in the presence of B27 or Y-27632 possessed a spindle-shaped morphology and had either increased turnover or did not grow to cover the substrate (Figure 2.2 B). B27 is a serum-free cocktail of culture supplements originally tailored to optimize neuronal cell culture but commonly used in epithelial *in vitro* culture. Y-27632 is a Rho kinase inhibitor added to the epithelial media formulation to help epithelial cells survive while dissociated during thawing or passage[99]. Since B27 and Y-27632 altered fibroblast morphology and growth properties, both were removed from the medium. Primocin is a potent, broad-spectrum antibiotic used to eliminate fecal bacteria during initial colonic cell isolation and

it was also replaced with more conventional tissue culture antibiotics, e.g., penicillin/streptomycin. All subsequent cultures for fibroblasts and/or epithelial cells used penicillin/streptomycin but not Primocin, B27, or Y-27632 (Table 1).

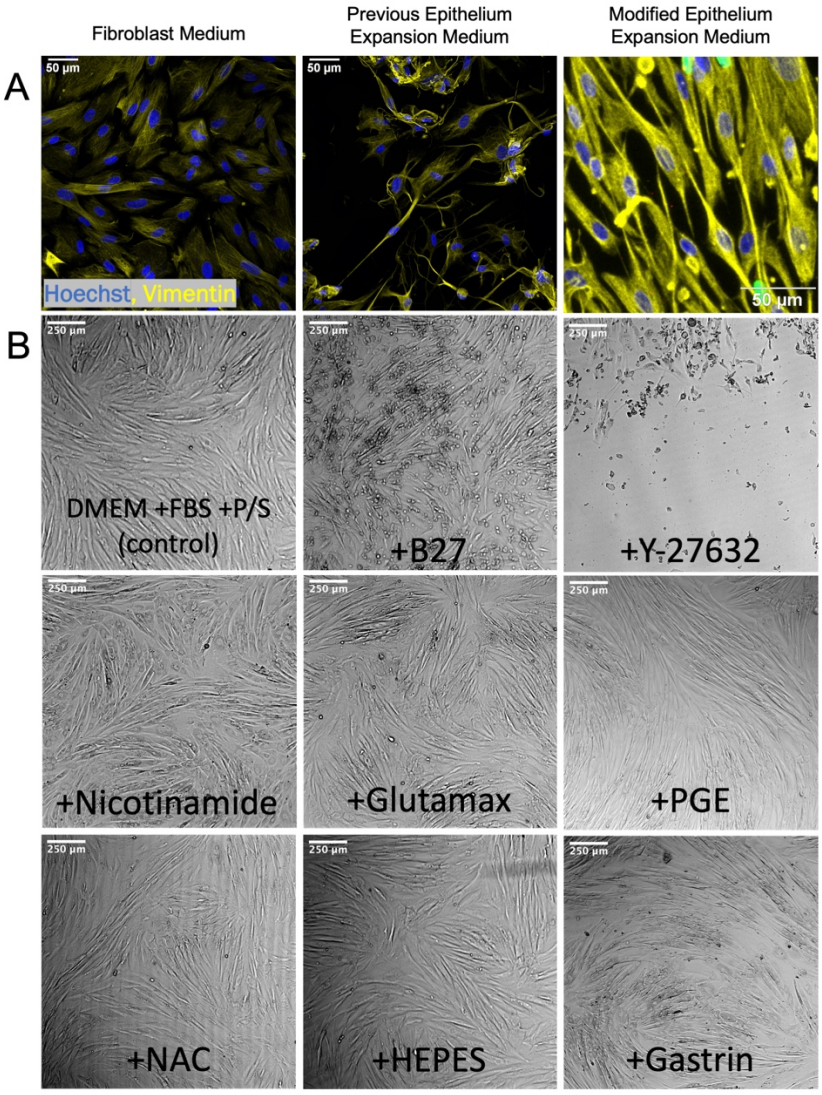

Figure 2.2. Testing media components' impact on fibroblasts. (A) Fluorescence images of fibroblasts stained for Vimentin and Hoechst 33342 to display cell shape and nuclei, respectively. All samples are grown on polystyrene within a 12-well plate with the left top panel displaying fibroblasts grown in the recommended monoculture media (DMEM with 10% FBS and 1% Penn/Strep. In the center top panel fibroblasts were grown with epithelial expansion medium optimized for epithelial monoculture and cell density is diminished while cell shape is altered. In the right-top panel fibroblasts were grown in modified expansion medium (EM) as indicated in Table 2.1.

COMPONENT (VOLUME FOR 500 ML)	MM	EM	SM	DM
L-WRN CONDITIONED MEDIUM	250 mL	250 mL	250 mL	
ADVANCED DMEM/F12 (1X)	250 mL	250 mL	250 mL	500 mL
GLUTAMAX (100X)	5 mL	5 mL	5 mL	5 mL
HEPES (1M)	5 mL	5 mL	5 mL	5 mL
PRIMOCIN (50 MG/ML)	500 µL	(5 mL Pen/Strep)	(5 mL Pen/Strep)	(5 mL Pen/Strep)
NAC (1M)	500 µL	500 µL	500 µL	500 µL
EGF (250 µG/ML)	100 µL	100 µL	100 µL	100 µL
NICOTINAMIDE (1M)		5 mL		
B27 (50X)	10 mL			
GASTRIN (1 MG/ML)	12.5 µL	12.5 µL		
PGE2 (1 mM)		5 µL		
A 83-01 (5 mM)	50 µL		50 µL	50 µL
SB202190 (30 mM)	50 µL	50 µL		
Y-27632 (10 mM)	500 µL			
FBS				50 mL

Table 2.1. Media composition. MM: Maintenance medium. EM: Expansion medium. SM: Stem medium. DM: Differentiation medium. Adapted from Hinman et al.[100]. Fibroblast Medium (FM) consists of 500 mL DMEM, 50 mL FBS, and 5 ml Penn/Strep.

To identify a common substrate on which both epithelial cells and fibroblasts could attach and grow, the two cell types were cultured separately, and together, on a flat cross-linked

collagen surface (stiffness approximately 1 kPa) under the modified medium (Figure 2.4 A, B, C). Cell density was assessed by measuring the area covered by nuclei (Hoechst 33342-stained DNA) and quantifying cell proliferation (EdU incorporation). Cell morphology was judged following immunostaining for EpCAM or vimentin. When cultured alone, epithelial cells grew to confluence with large numbers of proliferative cells (Figure 2.4 D, E). All cells in the epithelial cell culture were EpCAM+ and vimentin- (Figure 2.4 F). Despite removal of Primocin, B27 and Y-27632, the epithelial cells grew well and displayed characteristic markers such as KRT20 and mucin-2 (Figure 2.4 G, H). The fibroblasts also grew to cover the cross-linked collagen surface. Very few proliferative cells were observed in the fibroblast cultures relative to that of the epithelial cells (Figure 2.4 E). As expected, all cells in the fibroblast cultures were vimentin+ and EpCAM- (Figure 2.4 F). Barrier function of the monocultures was assessed by measuring TEER over time. On day 1 after seeding, TEER was near zero and not significantly different between fibroblast and epithelium cultures (Figure 2.4 I). On day 4 and 12, the TEER was significantly greater for the epithelial cells compared to the fibroblasts. The fibroblast and epithelial cells both displayed excellent surface coverage, expected functional behavior and acceptable morphology on the cross-linked collagen which was therefore used for all subsequent experiments.

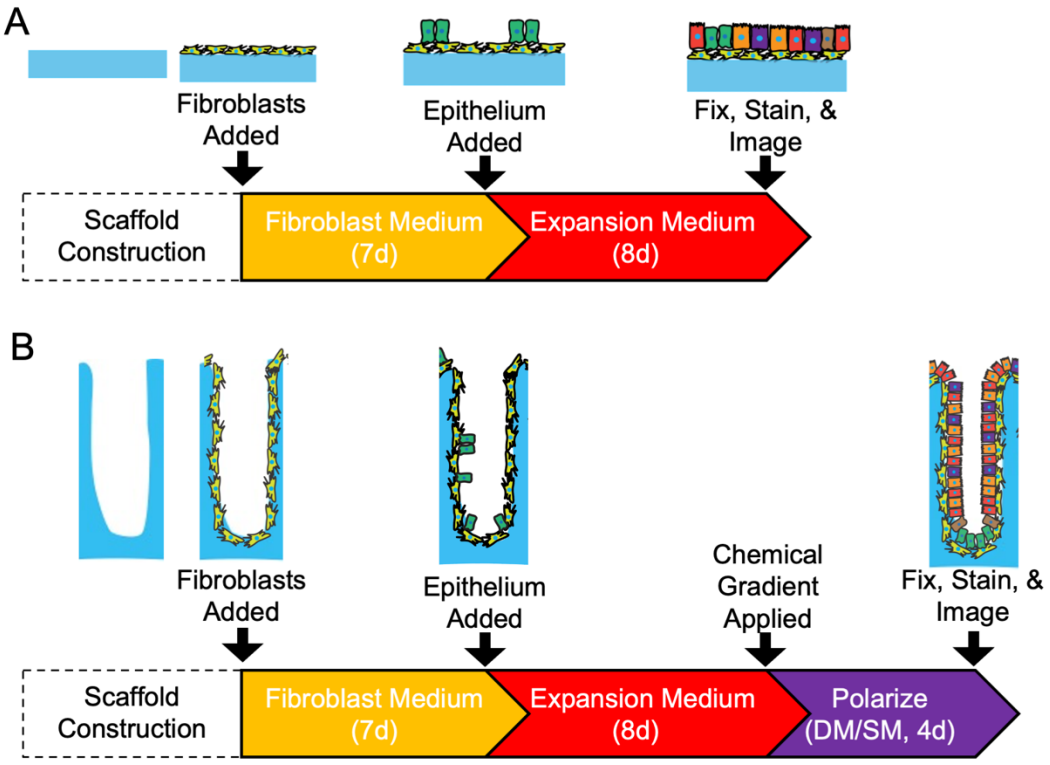

Figure 2.3. Timeline for in vitro tissue seeding. (A) Planar model timeline: Fibroblasts are added first atop a cross-linked collagen scaffold and cultured in FM for one week after which epithelium is added and the full tissue is culture in EM. (B) 3D-crypt model timeline: Like the planar setup, fibroblasts are first added to the scaffold and culture for one week in FM followed by epithelium addition. Cells are cultured in EM (supplied from above and below the scaffold) for eight days and then a chemical gradient is applied with DM supplied at the top of the scaffold within a well-insert and SM is supplied at bottom from below the well-insert. In all cases 0.5 mL of medium is added to the top of the well-insert and 1.5 mL is added below the well insert and the medium is replenished every 24 hours.

2.3.3. Planar coculture of fibroblasts and epithelial cells in the presence of WRN

For coculture, fibroblasts were plated at day 0 on the cross-linked collagen surface and cultured in fibroblast medium for 7 d. Epithelial cells were then plated onto the fibroblast-covered collagen scaffold at day 7 and cultured in EM until the epithelial cells reached confluence above the fibroblasts (8 d) (Figure 2.3 A). The cocultures displayed both EpCAM+ and vimentin+ cells indicating that both epithelial cells and fibroblasts were present on the scaffold (Figure 2.4 C). The measured vimentin+ area was significantly higher in coculture as

compared to epithelium alone indicating that fibroblasts are present though there was a significant reduction in vimentin coverage for the coculture relative to that of the fibroblast only culture (Figure 2.4 F). Fewer fibroblasts were present in the coculture relative to the fibroblast only culture despite plating identical numbers of cells on day 0 so the presence of the epithelial cells appeared to diminish the number of fibroblasts. This was surprising since these cells grow in proximity *in vivo*. The Hoechst 33342+ surface area was not statistically different for coculture as compared to epithelial cells alone (Figure 2.4 D). The surface area occupied by EdU+ cells was significantly lower for coculture as compared to epithelial cells alone (Figure 2.4 E). The normalized expression of KRT20+ (a pan-differentiation marker for epithelial cells) was significantly greater for cells in coculture compared to that of epithelial cells alone although Muc2 (a marker for goblet cells) was not significantly different (Figure 2.4 G, H). The decreased EdU incorporation and increased KRT20 expression suggested that in this simple planar system, the fibroblasts act to decrease epithelial cell proliferation and encourage their differentiation. The TEER was significantly lower on day 4 for epithelial cells alone versus coculture (Figure 2.4 I). A high TEER signifies the presence of mature colonocytes with tight cell-cell interconnections again suggesting that the fibroblasts promote epithelial cell differentiation towards colonocyte lineage. By culture day 12, TEER was not significantly different between monoculture and coculture suggesting that both systems eventually grew to confluence with a majority of colonocytes. These data suggest that the fibroblasts modulate epithelial cell proliferation while encouraging mature colonocyte differentiation and tissue barrier function (even in the presence of exogenous WRN). However, limitations of this simple planar coculture system include the absence of discrete cell zones and the high concentration of WRN throughout the culture so that

subtle impacts of the fibroblasts on epithelial cells particularly the stem/proliferative cells might be obscured.

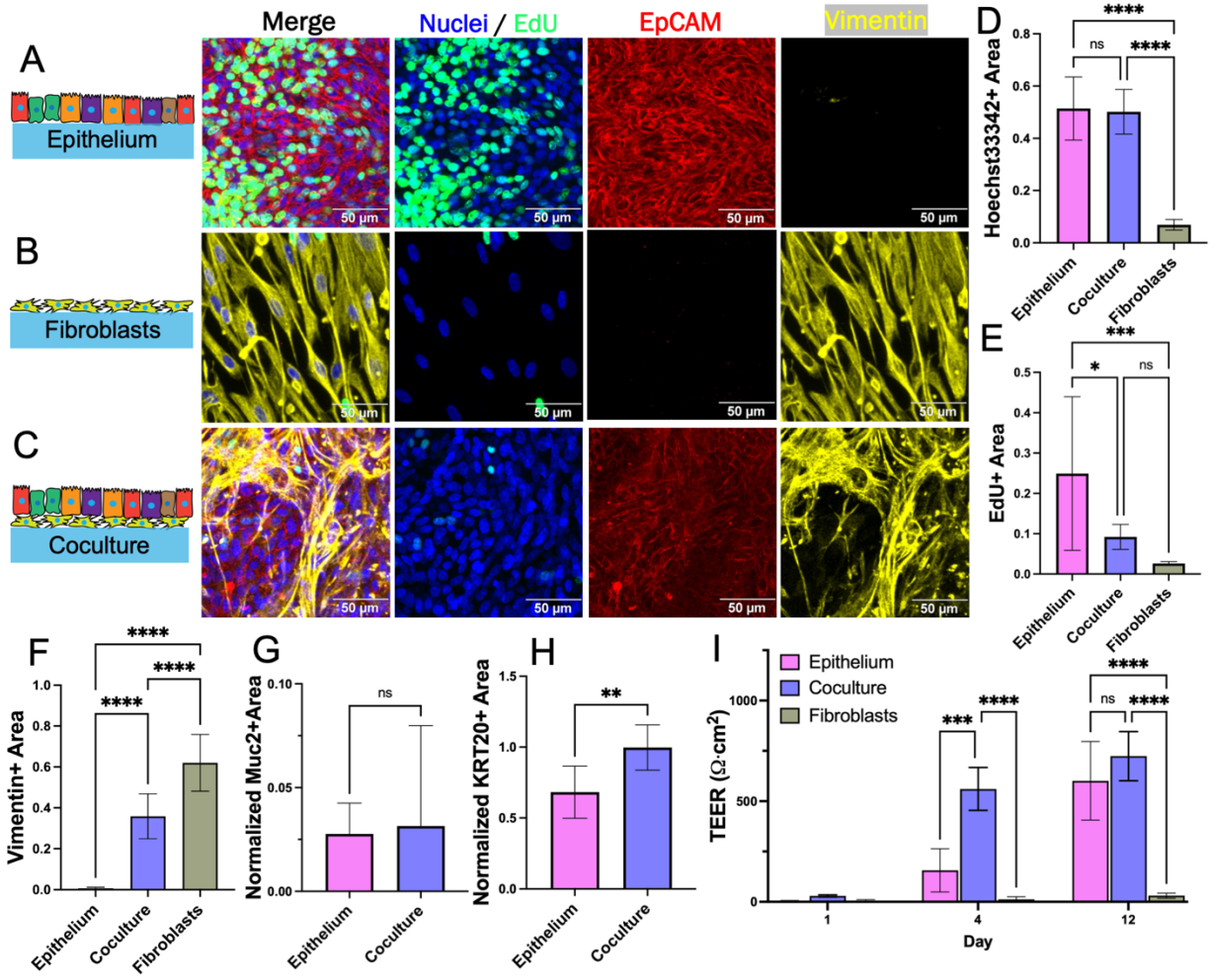

Figure 2.4. Evaluation of fibroblast and epithelial cell coculture on a 2D scaffold. (A) Epithelium alone after 8 days, (B) fibroblasts alone after 7 days, and (C) coculture after 15 days total (7d fibroblasts only, then 8d after epithelium addition) in planar culture stained for Hoechst 33342, EdU incorporation, and EpCAM and vimentin immunofluorescence. (D-F) The fluorescence area positive for (D) Hoechst 33342, (E) EdU incorporation, and (F) vimentin staining was plotted for each culture system. The area positive for each of these markers was determined as that above an empirically set threshold. (G-H) Shown is the normalized fluorescence area positive for (G) mucin 2 and (H) KRT20 immunofluorescence. The normalized area was calculated by dividing the area positive for mucin 2 and KRT20 (above an empirically set threshold) with the area positive for Hoechst 33342 fluorescence (above an empirically set threshold). (I) TEER (n=4) measured on different days for the cultures. ns = not significant, * = p-value < 0.05, ** = p-value < 0.01, *** = p-value < 0.001, **** = p-value < 0.0001. Panels D-I

display the average data with a single standard deviation marked by the error bar. In panels D-H, n=3 biological replicates for each with 3 technical replicates for each sample.

2.3.4. Planar coculture of epithelial cells with fibroblasts without exogenous WRN

In vivo, a major source of Wnt supporting the colonic stem cell niche is pericryptal fibroblasts[33]. To determine whether cocultured fibroblasts might provide supportive factors for the epithelial cells in this model, epithelial cells with or without fibroblasts were cultured in the absence of exogenous WRN. Just as before, fibroblasts were first cultured in simple fibroblast medium on the cross-linked collagen scaffold until confluent (5-7 d). Epithelium was then added above the fibroblasts for coculture or directly onto a collagen scaffold for monoculture and then cultured with optimized medium without WRN. A marked difference was observed in the cell coverage, proliferation, and lineage allocation of epithelium monoculture and coculture with and without WRN after 12 days in culture (Figure 2.4 A). On the first day after addition of the epithelial cells, TEER was near-zero for all cultures (Figure 2.4 B). On day 4 and 12 there was a significantly higher electrical resistance in the cocultures relative to that of day 1 as well as the epithelium only cultures on any day. Epithelial cells without WRN or fibroblasts were not able to proliferate to cover the scaffolding and thus never achieved an elevated TEER. In coculture, epithelial cells proliferated to cover the scaffold with an increased TEER, suggesting that fibroblasts were able to mitigate the absence of exogenous WRN to some degree. On day 12, Hoechst 33342-stained nuclei covered almost four times more area in the cocultured cells compared to epithelial cells alone, again indicating that the fibroblasts supported an increased epithelial cell number in the absence of WRN (Figure 2.4 C). Notably, Hoechst 33342 coverage in coculture without WRN was not significantly different than previously measured coculture with WRN, indicating that these tissues reach similar levels of cell density. By day 12, both the coculture and epithelium monoculture possessed few EdU+ cells, a significant decrease

compared to both culture systems when exogenous WRN was provided (Figure 2.4 D). These data suggest that the fibroblasts partially compensated for the absence of WRN. Next, the presence of differentiated cells on day 12 was examined by staining the cultures for KRT20 and Muc2. The normalized area occupied by both markers was significantly diminished in coculture as compared to monoculture (Figure 2.4 E, F). The removal of exogenous WRN is known to induce rapid differentiation in epithelial cells and the presence of the fibroblasts partially mitigated this effect. Under these conditions fibroblasts appeared to support epithelial cells by slowing differentiation; however, fibroblasts alone did not mimic the full impact of exogenously added WRN. Thus, the fibroblasts appeared to be capable of supporting undifferentiated as well as differentiated epithelial cell states with the dominant effect dependent on the presence or absence of exogenous WRN. However, the absence of distinct cell compartments made these opposing impacts difficult to investigate motivating the construction of a 3D architecturally accurate model of the colonic crypt with an underlying layer of fibroblasts.

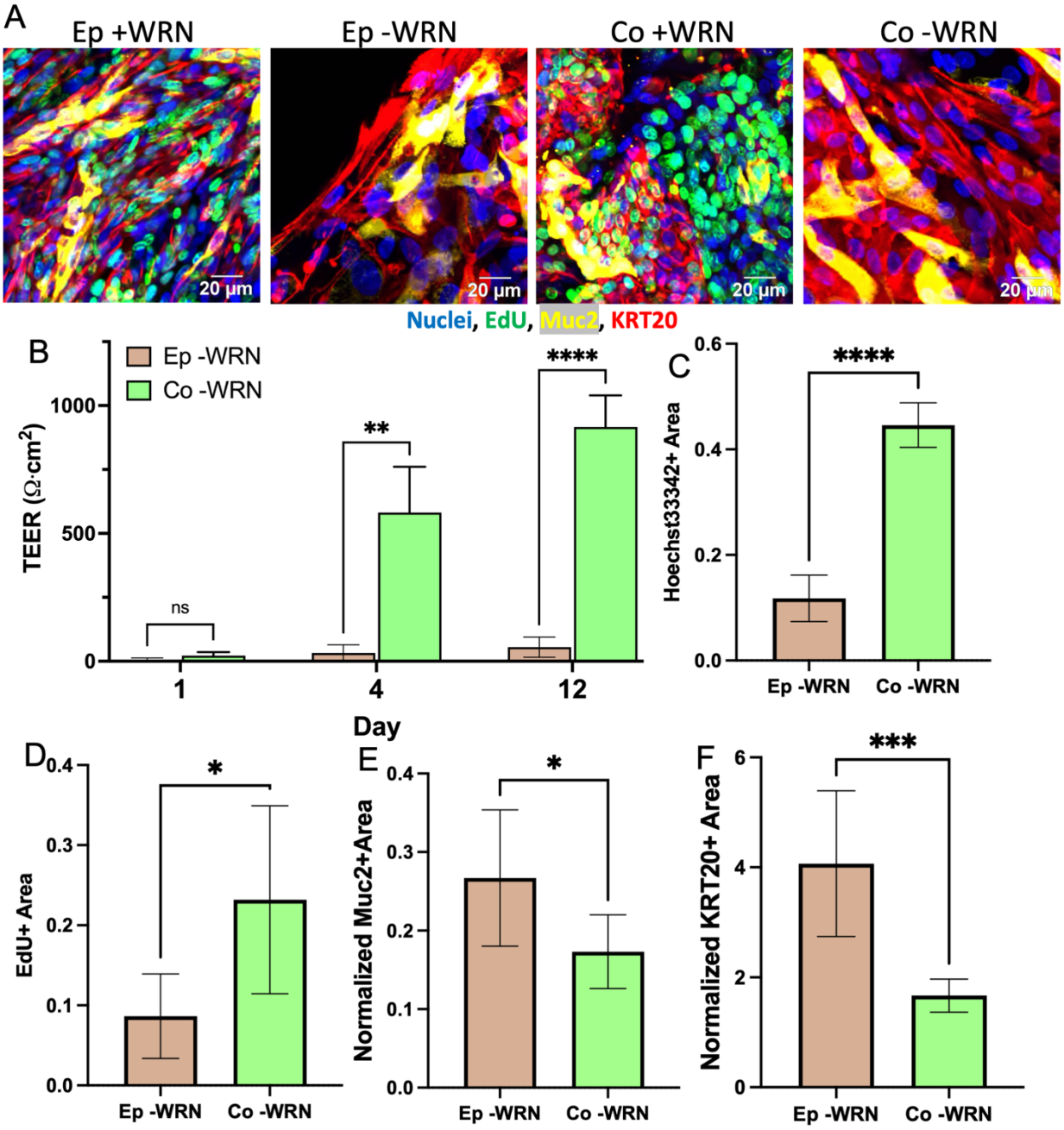

Figure 2.5. Impact of removal of exogenously added growth factors. (A) Epithelium with (Co) and without (Ep) fibroblasts cultured in the presence or absence of growth factors (+/- WRN). Images taken eight days after epithelium addition. (B) TEER measured over time for the epithelium monoculture and coculture after removal of exogenously added WRN. (C-D) The fluorescence area positive for (C) Hoechst 33342, and (D) EdU incorporation was plotted for each culture method. The area positive for each of these markers was determined as that above an empirically set threshold. (E-F) The normalized fluorescence area positive for (E) mucin 2 and (F) KRT20 immunofluorescence. The normalized area was calculated by dividing the area

positive for MUC2 and KRT20 (above an empirically set threshold) with the area positive for Hoechst 33342 fluorescence (above an empirically set threshold). ns = not significant, * = p-value < 0.05, ** = p-value < 0.01, *** = p-value < 0.001, **** = p-value < 0.0001. Panels B-F display the average data with a single standard deviation marked by the error bar and n=3 biological replicates with 3 technical replicates for panels C-F.

2.3.5. 3D coculture of fibroblasts and epithelial cells in a colon crypt architecture

To enable deeper insights into the fibroblast-epithelial cell interactions, crypt arrays were formed on a molded cross-linked collagen scaffold positioned within the luminal compartment of a hanging basket (Figure 2.6A and 2.7 A). When fibroblasts were cultured on the arrays in fibroblast medium, the cells grew to confluence across the surface of the arrays and down into the microwells without occluding the microwells over 6-8 d (0% of crypt lumens obstructed, n = 88, Figure 2.7 B and 2.6 B, C). Fibroblasts expressed vimentin but not EpCAM and the cells established a continuous monolayer along the base and walls of crypts and over the inter-crypt luminal surface (Figure 2.7 B, C). Additionally, little EdU incorporation was observed in fibroblast monoculture suggesting that the cells were very slow growing under these conditions.

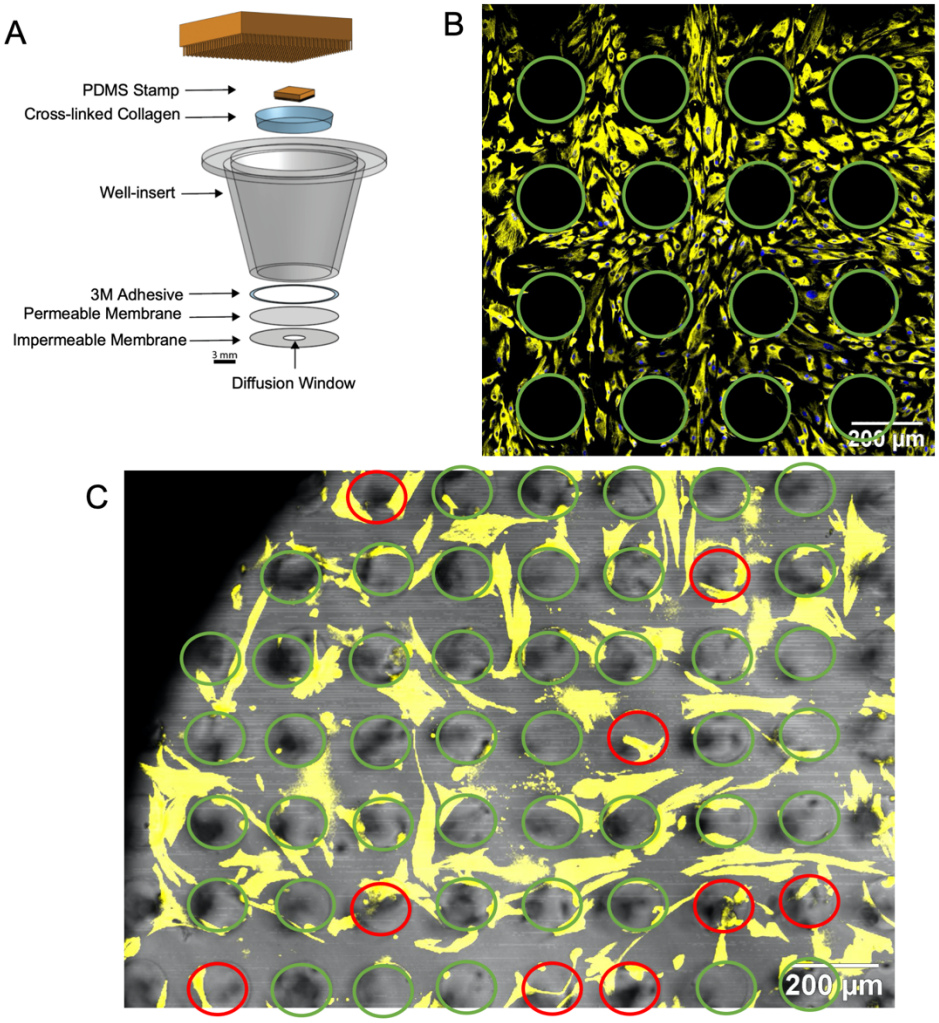

Figure 2.6. Expanding the size of crypts to accommodate fibroblasts. (A) An exploded view of the components within modified well-inserts with a 3 mm diffusion window that are used in both the planar and 3D-crypt models. (B) Immunofluorescence image displaying fibroblasts on a scaffold with 150 µm-wide crypts (yellow = Vimentin, blue = Hoechst 33342). The focal plane for this image is at the top of the scaffold near the crypt openings and it shows that 100 % of crypts with a wider 150 µm opening are not blocked by spanning fibroblasts. (C) Immunofluorescence image displaying fibroblasts atop a scaffold with 80 µm-wide crypts (yellow = Vimentin). Red circles over an opening show a crypt that is occluded by fibroblasts into which epithelial cells could not be added and green circles denote clear opening (9/53 crypts occluded, 17%).

For coculture, epithelial cells were placed atop fibroblasts after 7 days and then cultured for a further 12 days. Once the epithelial cells formed a confluent layer above the fibroblasts (day 8), the medium in the luminal reservoir of the hanging basket was replaced with differentiation

medium without WRN (DM, Table 2.1). Stem cell medium with WRN was maintained in the basal reservoir (SM). Prior work has demonstrated that a standing gradient of WRN is created along the long axis of the crypts under these conditions and that this gradient supports formation of a stem/proliferative cell niche and differentiated cell zone in epithelial cell only cultures (Figure 2.7 D)[75]. After culture for 4-5 d under the WRN gradient, cells on the coculture crypt arrays were assayed for proliferation and protein markers. As expected, EpCAM+ cells were identified in coculture and epithelium-only cultures while vimentin+ cells were present in coculture and fibroblast-only cultures (Figure 2.7 C, D, E). The vimentin+ cell volume in the crypt arrays was significantly lower for coculture crypts compared to fibroblast-only crypts suggesting that addition of the epithelial cells diminished the number of fibroblasts as observed on the planar scaffolds (Figure 2.7 F). The number of nuclei (Hoechst 33342+ objects) was significantly greater for the epithelium only and coculture crypts relative to the fibroblasts as predicted by the planar culture results (Figure 2.7 G). EdU+ cells were localized to the crypt base of the epithelium only and the coculture arrays suggesting that a WRN gradient successfully formed along the crypt long-axis under both conditions (Figure 2.7 D, E). Finally, high magnification imaging revealed that flattened fibroblasts were established in close apposition to columnar epithelial cells within the 3D coculture (Figure 2.7 H). Overall, the attributes measured for the crypt arrays are consistent with the trends observed in the planar model.

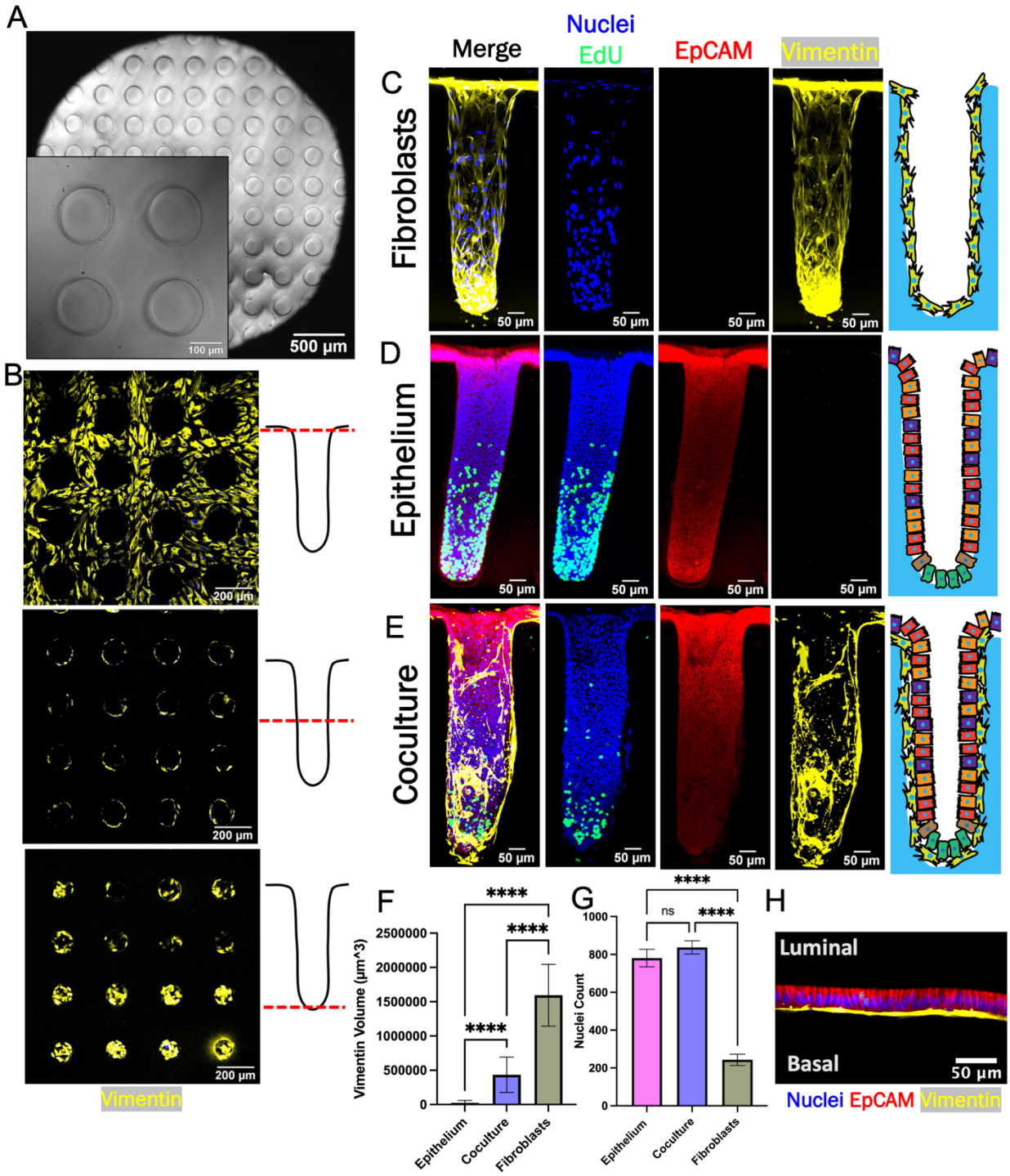

Figure 2.7. Epithelium and fibroblasts cultured as 3D crypts. (A) Brightfield top-view image of a fabricated collagen crypt array. (B) Fluorescence image of fibroblasts growing on a crypt array. Images were obtained at different focal planes (dashed red line) along the length of the crypt as shown in the accompanying schematics (right panels). (C) Sideview maximum z-projection of crypt with only fibroblasts. (D) Sideview maximum z-projection of a crypt with only epithelial cells. (E) Sideview maximum z-projection of a crypt with cocultured fibroblasts and epithelium.

(F) Measured volumetric area (vimentin +) occupied by fibroblasts (n= 3 biological replicates, n = 34, 45, and 10 crypts for epithelium, coculture and fibroblast, respectively). The vimentin + area was that measured to above an empirically set threshold. (G) The total number of nuclei per crypts (n=3 biological replicates, n = 34, 45, and 10 crypts for epithelium, coculture and fibroblast, respectively). (H) Confocal image (X-Z plane) of fibroblasts beneath epithelium (red =EpCAM immunofluorescence, blue = Hoechst 33342, yellow = vimentin. ns = not significant, **** = p-value < 0.0001. Panels F and G display the average data with a single standard deviation marked by the error bar.

To understand the impact of the fibroblasts on the stem/proliferative cell zone, 89 individual crypts across 27 arrays were characterized with respect to the number and location of the EdU+ cells. The number of crypts in the coculture arrays possessing at least one EdU+ cell was significantly greater than that of arrays with only epithelial cells (Figure 2.8 A, B). Since the arrays were seeded with similar numbers of cells, the large number of epithelium-only crypts without an EdU+ cell was most likely due to stem cell loss over time and thus a loss of cells competent to divide. In contrast, the underlying fibroblasts in coculture arrays appeared to maintain a more durable stem/proliferative cell compartment on the arrays. For crypts that did possess at least one EdU+ cell, the number of EdU+ cells/crypt was highly variable for both culture systems (Figure 2.8 C, D). Crypts with fibroblasts supporting the epithelial cells possessed a range of 20 to 230 EdU+ cells/crypt while the epithelial cell-only cultures possessed a range of 19 to 285 EdU+ cells/crypt. However, the mean number of EdU+ cells/crypt in the epithelial cell-only crypts was significantly greater than that of the coculture crypts (Figure 2.8 E). Interestingly, although more of the epithelium-only crypts had zero EdU+ cells, those crypts with at least one EdU+ cell possessed a greater number of proliferative cells compared to crypts with underlying fibroblasts. Thus, the fibroblasts appear to act as a stabilizing influence on the proliferative cells supporting their survival yet diminishing their proliferation.

The impact of the fibroblasts on the spatial extent of the stem/proliferative cell zone was assessed for crypts that possessed at least one EdU+ cell. The distance between each EdU+ nucleus and the crypt base was measured. Significantly more EdU+ cells were found within the bottom half of epithelium-only crypts compared to the fibroblast supported crypts, and the average location of the EdU+ nuclei in the fibroblast-supported crypts was significantly closer to the crypt base than for crypts with only epithelial cells (Figure 2.8 F, G). In addition to modulating the numbers of EdU+ cells, the fibroblasts diminished the height of the proliferative cell zone along the crypt long axis creating a more compact proliferative cell zone. The 3D crypts revealed the subtle differences in the impact of fibroblasts on the proliferative cell compartment not observable in the simple planar model.

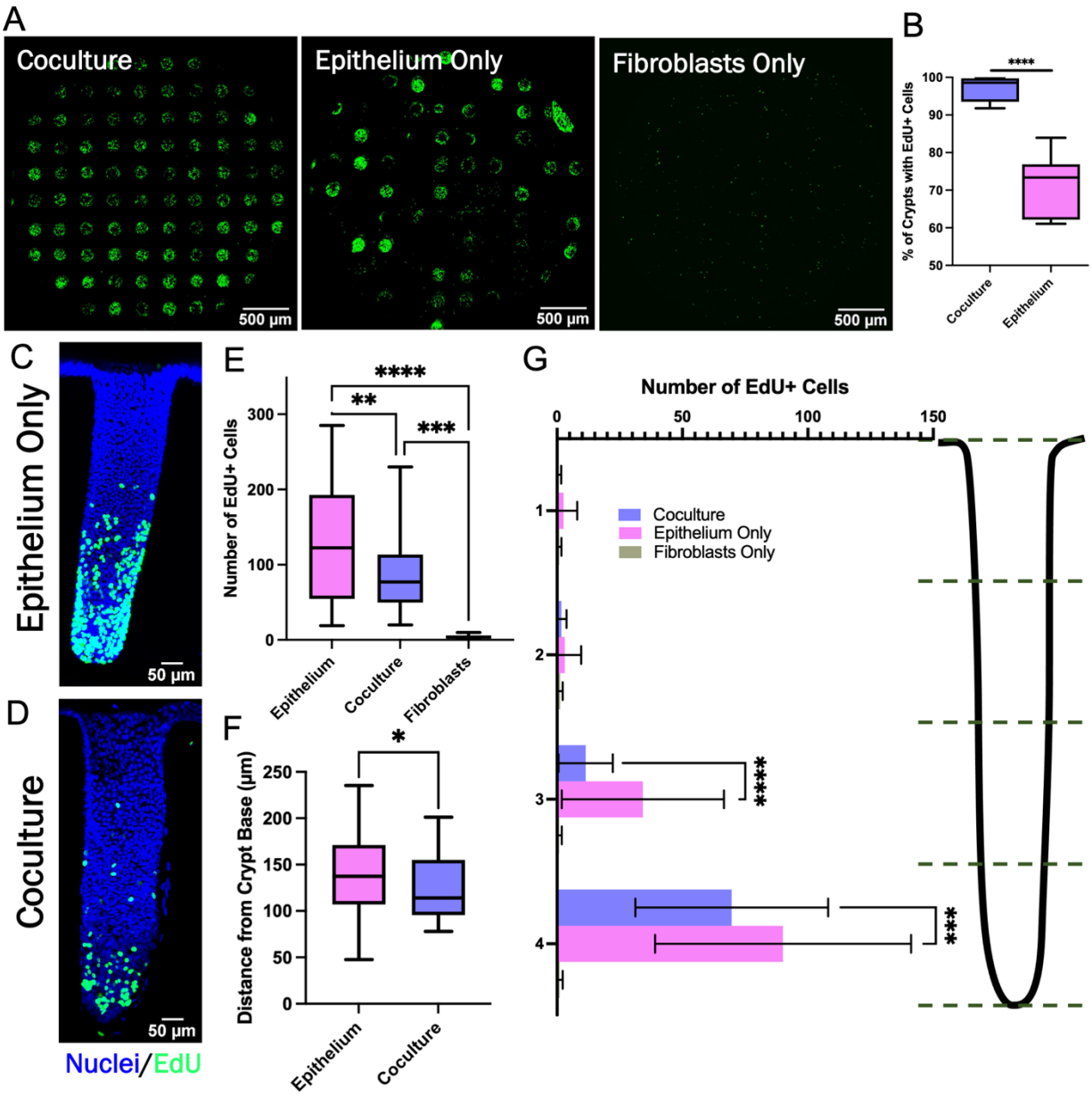

Figure 2.8. Characterization of the stem/proliferative cell zone. (A) Confocal image stack maximum z-projection of full crypt-arrays displaying cells that have incorporated EdU (green). (B) The percentage of crypts containing at least one visible EdU+ cell (n=5 biological replicates i.e., full crypt arrays, n=443 individual coculture crypts, n=410 epithelium monoculture crypts). (C-D) Sideview of a representative epithelium only and coculture crypt stained with Hoechst 33342 and for EdU incorporation. (E) The number of EdU+ cells/crypt (n=3 biological replicates, n = 34, 45, and 10 individual crypts for epithelium, coculture and fibroblast, respectively). (F) The average position of EdU+ cells within individual crypts (n=3 biological replicates, n = 34 individual crypts for epithelium and 45 for coculture). (G) The number of EdU+ cells/crypt location plotted for four regions along the vertical axis of the crypts. Bins

correspond to the accompanying schematic, i.e., bin 4 represents the bottom quartile of a crypt. * = p-value < 0.05, ** = p-value < 0.01, *** = p-value < 0.001, **** = p-value < 0.0001. Box plots in panels B, E, and F display the mean value marked by the central horizontal bar while the box displays the extents of the middle two quartiles (25-75%) and the whiskers mark the minimum and maximum. Panel G displays the average data with a single standard deviation marked by the error bar.

2.3.6. Bulk RNA-sequencing reveals differential gene expression in coculture

To understand how the fibroblasts support the stem/proliferative cell compartment yet enhance differentiation, bulk RNA was isolated from whole crypt arrays with epithelium alone or fibroblasts and epithelium in coculture. mRNA for 12844 protein-coding sequences was detected and compared (Figure 2.9 A). Vimentin (*VIM*) mRNA, a fibroblast marker, was present only in cultures with fibroblasts while *EPCAM* mRNA encoding epithelial cell adhesion marker, a pan-epithelial cell marker, was expressed only when epithelium was present (Figure 2.9 B, C). Of the 12844 genes detected, 684 total genes possessed significantly different expression in the cocultured cells compared to epithelium alone. Of these, 305 genes were significantly downregulated, and 379 genes were significantly upregulated in coculture (Supplementary Table S1, S2). To identify which of these differentially expressed genes might be most informative, genes expressed predominantly in differentiated epithelial cells were first examined. *MUC2* mRNA encoding mucin-2 (MUC2), a major constituent of colonic mucus produced by goblet cells was highly expressed in both the coculture and epithelium only samples but with significantly greater *MUC2* expression in the epithelium only culture relative to that of the coculture sample (Figure 6D). Other goblet cell markers such as *TFF3* (trefoil factor 3), *SPDEF* (SAM pointed domain containing ETS transcription factor), *SPINK4* (serine peptidase inhibitor Kazal type 4), *DLL1* (delta like canonical Notch ligand 1), and *DLL4* (delta like canonical Notch ligand 4) were also expressed in epithelial cell cultures with and without fibroblasts but without a

significant difference suggesting that goblet cell numbers may not have been altered in the presence of the fibroblasts (Figure 2.9 E)[101]. *KRT20* mRNA encoding for cytokeratin-20, a marker for all differentiated colonic epithelial cells, was abundantly expressed in both coculture and epithelium samples with no significant difference (Figure 2.9 F). mRNA markers of colonocytes (absorptive cells) such as *CA1* (carbonic anhydrase 1), *CA2* (carbonic anhydrase 2), *SLC26A3* (solute carrier family 26 member 3), *AQP8* (Aquaporin 8), and *GUCA2B* (guanylate cyclase activator 2B) were down regulated in coculture relative to that of the epithelium alone suggesting that the cocultures might possess fewer mature colonocytes in the presence of the fibroblasts (Figure 2.9 G)[101].

Next, markers of stem/progenitor intestinal cells were examined. *LGR5* (leucine rich repeat containing G protein-coupled receptor 5) mRNA, a marker for colonic stem cells, was present at low counts and without significant difference for epithelial cell cultures with and without fibroblasts. *OLFM4* (olfactomedin 4) mRNA, a marker for colonic transit amplifying cells in humans[102], was also present at low counts and without significant difference for epithelial monoculture and coculture. Of the 12 progenitor genes examined, only *AQP10* (Aquaporin 10) mRNA, a marker for colonic progenitor cells was significantly different (downregulated) in coculture relative to epithelium alone (Figure 2.9 H)[101]. Due to the very low numbers of stem/proliferative cells in all the cultures, differences in the stem/proliferative cell gene expression with and without fibroblasts may have been masked by the very large numbers of differentiated epithelial cells in the cultures. Single-cell mRNA expression analysis may be required to see these low frequency stem/progenitor cell types.

To examine a broader set of epithelial genes and remove confounding impacts of the fibroblast gene expression, all genes highly expressed in fibroblast monoculture (>1.0 CPM)

were removed from the data sets obtained from epithelial cells with or without fibroblasts. Of the original 12844 genes, 1835 filtered genes remained with 190 significantly downregulated and 43 significantly upregulated in the epithelial cells with fibroblasts compared to the epithelial cells without fibroblasts (Figure 2.10, Table S3, S4). A GO Analysis (geneontology.org) was conducted with the 43 upregulated genes to determine whether common biological processes might be identified, and genes related to negative regulation of endopeptidase activity were overrepresented in the gene set upregulated in coculture compared to that epithelium monoculture (Table S5. Endopeptidase activity is associated with rapid proliferation with a need to recycle cellular constituents and this aligns with the observed increased proliferation in epithelium-only crypts where a stem/proliferative zone is maintained. A GO Analysis was also conducted for the 190 downregulated genes in coculture compared to epithelium monoculture and several transport related gene groups were overrepresented i.e., triglyceride transport, water transport, and long-chain fatty acid transport (Table S6). These transport genes are associated with a mature differentiated colonocyte consistent with the increased differentiation of the epithelial cells in the presence of fibroblasts observed in planar culture[103].

Next, genes commonly expressed by fibroblasts with the potential to modulate epithelial cell behavior were examined in epithelium alone, fibroblasts alone, and coculture conditions (Figure 2.9 I)[104]. As expected, transcripts for hallmark fibroblast markers such as *VIM* and α-smooth muscle actin 2 (*ACTA2*) and platelet derived growth factor-α (*PDGRFA*) were highly expressed by fibroblasts alone and in coculture (Figure 2.9 K). The fibroblasts were also actively modifying their microenvironment as evidenced by mRNA expression of fibronectin, collagens, and matrix metalloprotease (*FN1, COL15A1, COL14A1, COL4A5, COL1A1, COL1A2, MMP3*. Figure 6I). Epithelial cell physiology is known to be regulated by ECM with components such as collagen

and fibronectin regulating adhesion, morphology and proliferation[105]. A variety of transcripts encoding growth factors were found to be expressed in fibroblast monoculture as well as the epithelium coculture. R-spondin 3 (RSPO3) participates in stem cell maintenance and drives proliferation while Noggin (NOG), a bone morphogenetic protein (BMP) antagonist, inhibits differentiation [104]. Wnt5a was highly expressed by fibroblasts alone and in coculture. This Wnt ligand associated with non-canonical Wnt signaling is often found to be expressed by luminal fibroblasts and it has a context-dependent effect though in the upper crypt region where it decreases beta-catenin signaling thus encouraging epithelial differentiation rather than proliferation [43,71,104,106,107]. Other transcripts identified include Neuregulin 1 (*NRG1*) which drives secretory cell formation and dickkopf 3 (*DKK3*), a WNT signaling pathway inhibitor. Taken together the presence of these transcripts indicate that the fibroblasts actively alter the microenvironment of the adjacent epithelial cells to modulate epithelial cell physiology.

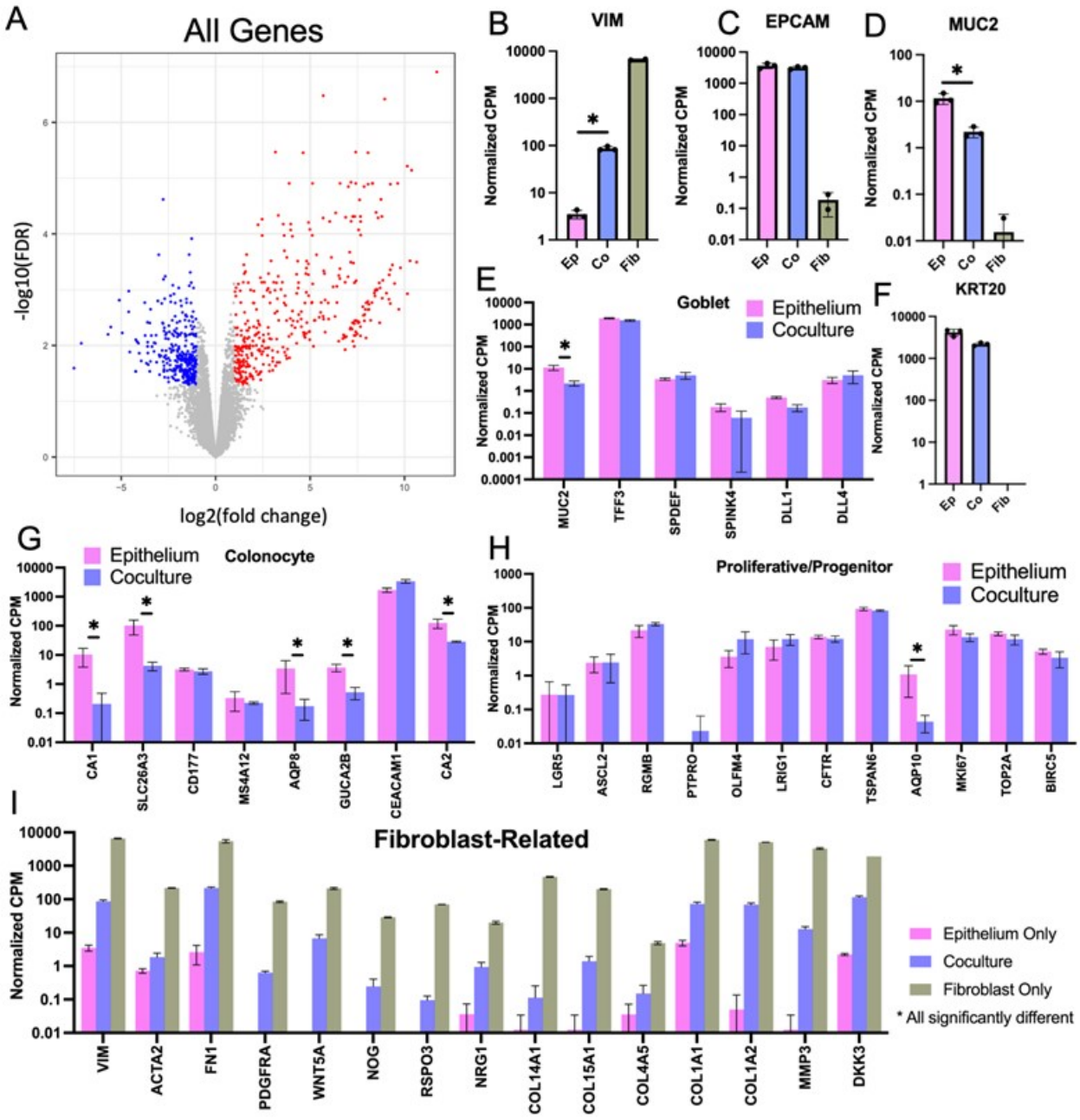

Figure 2.9. Bulk RNA-sequencing cells from 3D crypt arrays. (A) Volcano plot comparing epithelium versus coculture that displays the fold change (FC) and false discovery rate (FDR) for all 12844 genes measured with red indicating significantly upregulated genes in coculture and blue signaling significantly downregulated genes in coculture. (B-D) Normalized counts per million (CPM) for mRNA expression of cell-type specific markers was compared for cultures of fibroblasts only, epithelial cells only and fibroblast-epithelial cell coculture. (B) Vimentin (fibroblasts). (C) EpCAM (all epithelial cells). (D) Muc2 (goblet cells). (E) Expression levels of additional goblet cell-specific mRNA transcripts. (F) Cytokeratin 20 (KRT20, differentiated epithelial cells). Expression levels of genes marking: (G) colonocytes (differentiated absorptive

epithelial cells), (H) progenitor cells (proliferative and not fully differentiated epithelial cells, including transit amplifying cells), and (I) Fibroblast-related genes [104]. N.b., * denotes statistical significance between epithelium monoculture and coculture only, as determined by Benjamini-Hochberg adjusted p-values from comparison of expression fold change.

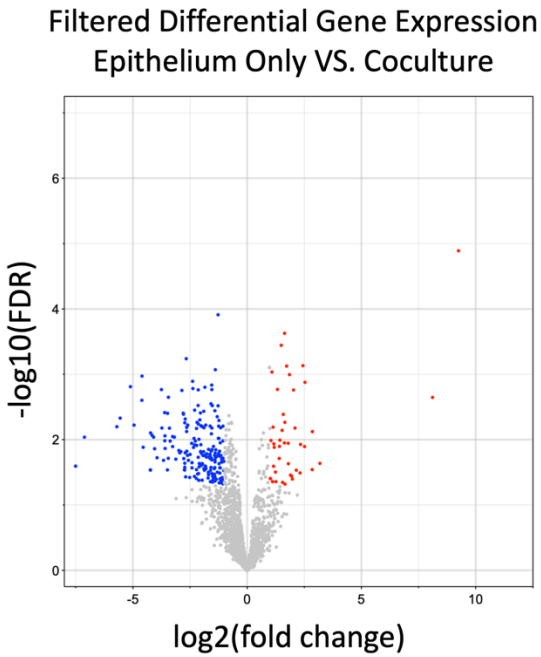

Figure 2.10. Differential gene expression for genes not expressed by fibroblasts. Gray dots display genes that are not significantly different between epithelium only and coculture samples while red dots signify significantly upregulated genes and blue dots show significantly downregulated genes in coculture. N.b., genes with significantly different expression are listed in Supplemental Table S3 and S4

2.4. Discussion

In the large intestine, fibroblasts are found in close association with the epithelial cells throughout the crypt as well as in the luminal region [33]. To mimic this close *in vivo* colonic fibroblast-epithelial cell interaction, primary intestinal fibroblasts were cultured as a supporting layer of cells just below and in contact with epithelial cells. Two models with the two cell types in apposition were employed, an easy-to-build and assay monolayer as well as a more complex 3D model with the ability to reveal greater insights into the inter-cell type connectivity. The two

systems were complementary with the monolayer enabling fast screening of culture conditions with facile assay of outcomes while the 3D crypt array was lower in throughput but provided much richer information. In both systems, cell behavior indicative of enhanced differentiation was observed, and the overall rate of epithelial cell proliferation was diminished while in coculture with fibroblasts. In the absence of exogenously provided growth factors, fibroblasts appeared to enhance epithelial cell survival, though the presence of fibroblasts alone did not provide sufficient support for sustained epithelial cell proliferation i.e., replace the added growth factors. Consistent with this effect was that the presence of fibroblasts appeared to support the maintenance of stem cells at the base of the crypts as evidenced by the presence of EdU+ cells in nearly every crypt across an array of 3D crypts. Thus, in these models, the fibroblasts diminished proliferation while promoting epithelial stem cell survival as well as enhancing the physiologic function of the differentiated cells i.e., increased TEER.

Bulk RNA-sequencing of full crypt arrays revealed differential epithelial cell mRNA expression in coculture, compared to that of epithelial cells cultured without fibroblasts. Genes that were differentially expressed in coculture when compared to epithelium monoculture revealed potential mechanisms for the fibroblast influence [37]. Secreted frizzled related protein 1 (*SFRP1*), a ligand which modulates canonical Wnt-signaling to diminish proliferation of intestinal epithelial cells, was upregulated in coculture relative to epithelial cell monoculture [33,108]. The mRNA of five solute carriers (*SLC6A19, SLC30A10, SLC17A4, SLC3A1, SLC36A1*) and three ATP-binding cassette transporters (*ABCG2, ABCB1, ABCG1*) was significantly down regulated in coculture relative to the epithelial cell monoculture. These transporter proteins, typically found on epithelial cells throughout the digestive tract, are responsible for translocation across membranes of specific molecules (i.e., amino acids,

phosphate, manganese, etc.) or non-specific foreign substrates [109]. This suggests that the fibroblasts can modulate intestinal absorptive behavior. Additionally, two genes which are related to apoptosis (*DAPK2, PRAP1*) were significantly downregulated in coculture relative to the epithelial monoculture. Death-associated protein kinase 2 (*DAPK2*), normally found in the intestinal epithelium, stimulates programed cell death while proline-rich acidic protein 1 (*PRAP1*), also expressed by intestinal epithelium, helps protect cells from oxidative stress-induced apoptosis [110,111]. While these downregulated genes may have opposing influences, the altered expression levels indicate that programmed cell death is modulated by fibroblasts. We do note that our interpretation of these results is limited by the bulk sequencing format. For coculture samples, the two cell types (epithelial and fibroblasts) were intermixed and a complex interplay with each cell type modulating the other's gene expression likely exists. This motivates future experiments focused on single-cell mRNA expression to fully dissect the interplay of these cell types.

In addition to directing growth and differentiation, fibroblasts play key roles throughout the body by synthesizing and secreting ECM to provide a growth surface and support structure for other cell types. Intestinal fibroblasts are known to secrete collagen, laminin, and fibronectin as well as matrix metalloproteinases and they exert physical contractile forces all to build-up or reshape the basement membrane and interstitial space in health and disease[104,112]. Within this model, fibroblasts were actively synthesizing ECM as suggested by the expression of ECM-related genes (e.g., *FN1, COL12A1, FBN1, FMOD*) in both the coculture and fibroblast monoculture. Matrix metalloproteinase 3 (*MMP3*), a protein that degrades collagen, fibronectins and laminins, is expressed by fibroblasts during development and remodeling within the colon and was highly expressed in coculture and fibroblast monoculture [112]. In the colon crypt *in*

vivo, a gradient in fibroblast physiology is thought to exist along the long axis of the crypt with fibroblasts in different crypt regions producing unique ECMs as well as growth and differentiation factors[37]. These distinct fibroblast behaviors support the epithelial cells as they proliferate in the crypt base and then migrate towards the luminal surface developing into mature differentiated epithelial cells. The developed models did not recapitulate this gradient of fibroblasts but rather placed fibroblasts randomly across the scaffolding surface. With further development of this model, it should be possible to tailor fibroblasts behavior along the crypt long axis to display a gradient of phenotypes as occurs *in vivo*.

2.5. Methods

2.5.1. Fabrication of crosslinked collagen scaffolds

2D and 3D collagen scaffolds were constructed on the surface of modified 12-well culture inserts (Corning, cat. no. 354236) according to Hinman and colleagues[113]. Briefly, the factory-supplied membrane was replaced with a permeable membrane (Millipore-Sigma, cat. no. BGCM00010) affixed with a biocompatible adhesive (3M, cat. no. 1504XL). A diffusion window was created by affixing another non-permeable polycarbonate film (McMaster-Carr, cat. no. 8689K44) with a 3 mm hole cut out. For the cross-linked collagen scaffold, N-(3-dimethylaminopropyl)-N ′-ethylcarbodiimide hydrochloride (EDC) and N-hydroxysuccinimide (NHS) were mixed with rat tail type I collagen (Corning, cat. no. 354236) and this mixture, while still liquid, was added to the culture insert atop the diffusion window and then pressed into form by a flat or shaped polydimethylsiloxane (PDMS) stamp. The shaped stamp used for 3D crypt scaffolds contained an array of 150 μm wide by 600 μm tall posts and it was fabricated according to protocols from Hinman and colleagues[113]. To accommodate fibroblast-

epithelium coculture, a photomask with larger hole diameters (150 μm) was used for mold construction and an additional layer of photoresist was added during spin coating to increase crypt height (1,500 rpm for 30 s with an acceleration of 300 rpm/s). Prior to cell plating, the collagen scaffolds were surface treated by overnight incubation with 10 μg/mL type 1 human collagen (Advanced BioMatrix, cat. no. 5007-20ML) in phosphate buffered saline (PBS).

2.5.2. Cell culture

Human colon epithelial stem cells from a transverse colon tissue sample (male, 23 years old, RRID: CVCL_ZR41) were cultured atop a neutralized collagen slab within maintenance media (MM) according to previously described methods[74]. Fibroblasts were expanded within a tissue culture flask in fibroblast medium (FM) containing Dulbecco's Modified Eagle Medium (DMEM, Thermo Fisher, cat. no. 11995065) supplemented with 10% heat-inactivated fetal bovine serum, 100 U/mL penicillin, and 100 μg/mL streptomycin (Table 2.1). For planar experiments CCD18-Co fibroblasts (colon, female, 2.5 months old, ATCC: CRL-1459) were used, and for 3D crypt experiments primary fibroblasts isolated from descending colon (male, 12 years old, RRID: CVCL_D6WE) were used.

For seeding within molded scaffolds, fibroblasts were added to the luminal side of well-inserts in 1mL FM at a concentration of $3x10^5$ – $5x10^5$ cells/mL for both planar and 3D crypt scaffolds. Then FM was replenished every day for up to 7 days, or until confluent. For subsequent epithelium addition, epithelial stem cells grown on 6-well plate above soft neutralized collagen were isolated and dissociated according to previous protocol using collagenase type 4 (Worthington Biochemical Corporation, cat. no. LS004189) and TrypLE express enzyme (Thermo Fisher, cat. no. 12605028)[113]. Epithelial cells were then added directly to the scaffolds for monoculture, or directly on top of fibroblasts for coculture, at a ratio

of 1:3 (1 well from 6-well maintenance plate to 3 well-inserts). N.b. It was critical that epithelial cells were cultured in above collagen in wells for only 3-4 days before isolation and sufficiently dissociated prior to addition to maximize the stem cell population upon initial seeding. In planar culture, the cells were then grown in expansions media (EM, modified from Hinman et al. See Table 2.1) with or without exogenously supplied Wnt, R-spondin, and Noggin (WRN) from L-WRN conditioned media for 12d. In 3D crypts, cells were grown in EM +WRN for 8 d (replenished daily) and then polarization was executed by replacing basal medium with stem medium (SM, Table 2.1) and luminal medium with differentiation medium (DM). After 4 days of polarization (media replenished daily), the samples were fixed and stained for endpoint analysis.

2.5.3. Measuring barrier function

An EVOM2 Epithelial Voltohmmeter (World Precision Instruments) with a chopstick electrode was used to measure transepithelial electrical resistance (TEER) in planar samples. The background resistance was measured in cell-free, molded collagen scaffolds, and the effective surface area was considered 0.9 cm^2, used to calculate TEER (Ohms*cm^2).

2.5.4. Fluorescence staining, imaging, and analysis

5-ethynyl-2'-deoxyuridine (EdU, 1 µg/mL) was added to the culture medium 24 h before sample fixation. Cells were fixed with Prefer fixative (Anatech Ltd., cat. no.NC9053360) for 20 min, permeabilized with 0.5% Triton X-100 at 20°C, and then blocked with 1% bovine serum albumin (BSA) for 1 h. Subsequently, integrated EdU was stained with sulfo-Cy5-azide (1.25 µg/mL) and then primary antibodies were added[114]. In this study, a DNA stain (Hoechst 33342, Sigma-Aldrich, cat. no. B2261) and antibodies for mucin-2 (MUC2, Santa Cruz, cat. no.

sc-15334), cytokeratin-20 (KRT20, Cell Signaling Technology, cat. no. 13063S), epithelial cell adhesion molecule (EpCAM, Bioss USA, cat. no. bs-0593R), and vimentin (VIM, Santa Cruz, cat. no. sc-6260) were used (all 1:500 dilution). After overnight incubation at 4 °C with primary antibodies, the samples were rinsed and matched secondary antibodies with Alexa Fluor 488 (goat anti-mouse, Life Technologies Corp., cat. no. A28175), and Alexa Fluor 555 (donkey anti-rabbit, Life Technologies Corp., cat. no. A31572) fluorophores were added and then rinsed away after overnight incubation at 4 °C. Confocal microscopy was performed with an inverted Olympus Fluoview 3000 equipped with 405, 488, 561, and 640 nm laser diodes and 4x, 10x, or 20x magnifying objectives were used to obtain images.

For image analysis in planar systems, Cell Profiler (cellprofiler.org[115]) was used to segment and measure area occupied by each fluorescent marker. Planar samples were each imaged in three representative sections with the 20x objective and a maximum intensity projection of the z-stack (step size 3.93 μm) was analyzed. Three images from three technical replicates were each analyzed across three repeated experiments. For 3D crypts, 4x overview images were obtained from the top (z-stack, slice 25.4 μm) and a maximum intensity z-projection was used to analyze the number of crypts with EdU+ cells. Next, the membrane was detached from the insert base and cut in half using microdissection scissors, the crypt area was situated perpendicular to the objective and imaged from the side. The 10x objective (step size 4 μm) was used to obtain images and the z-stacks were reconstructed in 3D using IMARIS X64 v9.8.2 (imaris.oxinst.com, Oxford Instruments) for analysis. The number and position of nuclei (Hoechst 33342+), and proliferative nuclei (EdU+) were counted using the IMARIS spots module, and the volume occupied by fibroblasts (vimentin+) was measured using the volume module.

2.5.5. Bulk RNA-sequencing

For gene expression comparison, RNA was extracted from 3D crypt arrays with monoculture epithelium, fibroblasts, or coculture epithelium with fibroblasts (n = 3). To capture only the tissue of interest within crypt arrays, a 3 mm biopsy punch was used to remove the *in vitro* crypt array within well-plate inserts. The extracted tissue portions were then agitated via vortexing and repeated pipetting within RNA lysis buffer (Zymo Research, cat. no. R1057,) and then the RNA was extracted using a Quick-RNA™ MiniPrep Plus kit (Zymo Research, cat. no. R1057,). Sequencing was then conducted on an Illumina NextSeq 2000 (Illumina. San Diego, CA). Software (STAR v2.7.7a), 2-pass mapping was used to align paired-end reads to human hg38 assembly and then GENCODE annotation v38 along with gene-level read quantification was performed[116]. Software (FastQC 0.11.9, RNA-SeQC 2.3.4, RSeQC 4.0.0) were used for quality control with assessment of insert fragment size, read quality, read duplication rates, rRNA rates, gene body coverage and read distribution in different genomic regions[117–119]. Bioconductor package edgeR 3.36.0 was used to detect differential gene expression between sample groups[120]. Genes with low expression were excluded using the edgeR function filterByExpr with min.count = 10 and min.total.count = 15. The filtered expression matrix was normalized by trimmed mean of m-values (TMM) method and subject to significance testing using the quasi-likelihood pipeline implemented in edgeR. A gene was deemed differentially expressed if absolute log2 fold change was above 1 (*i.e.,* fold change > 2 in either direction) and Benjamini-Hochberg adjusted p-values were less than 0.05.

2.5.6. Statistical analysis

For fluorescence and TEER data, a student's t-test was conducted to assess the significant difference between epithelium-only and coculture conditions. Data are presented as mean ±

standard deviation. Differences between means from separate groups (epithelium, fibroblasts and coculture) were determined using 2-way ANOVA followed by Tukey's multiple comparisons, unless otherwise specified. The level of significance is indicated as the p-value in each experiment. Asterisks in figures indicate: *, p-value < 0.05; **, p-value < 0.01; ***, p-value < 0.001, ****, p-value < 0.001; ns (not significant), p-value > 0.05. Statistical analysis and graphical illustrations were performed using GraphPad PRISM 9 software, version 9.5.0(GraphPad Software, San Diego, CA).

Chapter 3: Modeling colonic fibrosis with fibroblasts and epithelium on a stiffened collagen hydrogel

3.1 Abstract

Intestinal fibrosis reduces bowel function and increases an individual's risk of CRC. Yet, there is a lack of understanding surrounding the progression intestinal fibrosis independent of inflammation and there are no approved drugs for treating this pathophysiology. Excessive ECM deposition which leads to fibrosis occurs mainly because of activated mesenchymal cells, a primary focus of previous investigations in fibrosis. However, a tortuous, stiff, and thick tissue also impacts the epithelial layer which makes up the intestinal barrier and which houses proliferative intestinal stem cells that are crucial for healthy tissue recovery. Herein we create an *in vitro* model of intestinal fibrosis involving primary human fibroblasts and epithelial cells on a tunable collagen hydrogel. Two substrates have been formulated to mimic healthy and fibrotic tissue stiffness and diffusivity. We have validated that both cell types can be cultured independently and in coculture atop these new scaffolds and the substrates can be shaped according to experimental needs. Through phenotypic and morphological analysis, it was found that epithelial proliferation and differentiation are impacted by the stiff and soft scaffold differently in the presence and absence of underlying fibroblasts. This model will be useful for future studies on intestinal fibrosis progression and impact.

3.2. Introduction

Intestinal fibrosis is the accumulation of excessive scar tissue in the intestinal wall which results in bowel narrowing and diminished tissue function. Healthy tissue is supplanted with stiff and thick connective tissue which cannot be recovered to a healthy state[121]. Chronic

inflammation is a major cause of intestinal fibrosis as a runaway wound healing process induces excessive extracellular matrix (ECM) deposition and lasting mesenchymal cell recruitment and activation [51,122]. Once it has begun, fibrosis is an independent and self-perpetuating process [50]. As a direct result of fibrosis, individuals experience a decrease in quality of life due to bowel obstruction, nausea, vomiting, and abdominal pain. Additionally, individuals with intestinal fibrosis, often as a result of Irritable Bowel Disease (IBD), are more likely to develop colorectal cancer (CRC) [123,124]. It has been shown that a stiff, tortuous, and disorganized ECM within fibrotic scars supports tumorigenesis [125]. A key mediator in tissue repair after injury is mesenchymal fibroblasts and these cells have proven to play an important role in determining the fate of wound recovery [126].

To date, there are zero approved drugs for treating intestinal fibrosis, though two drugs (Pirfenidone and Nintedanib) have been approved for treating fibrosis in the lungs, which may prove useful for treating intestinal fibrosis. There still exists a pressing clinical need for an intestinal fibrosis model which can be used to study disease mechanics and conduct drug testing [127]. Several mouse models have been used to study fibrosis, as documented by Rieder et al., and these models can be broken down into categories of disease initiation: spontaneous, gene-targeted, chemical, immune-, bacteria, and radiation-induced [128]. Mouse models have provided important insights regarding fibrosis initiation and mechanisms, though animal testing remains a challenge especially within the intestine, as the outcomes do not always match that observed in humans. *In vitro* culture of myofibroblasts has also enabled discovery regarding fibrotic tissues, though these models only focus on the mesenchymal cells and often fail to recapitulate the 3D architecture present *in vivo* [49,67,129]. Organoids are another popular method for modeling intestinal disease, and enteroids have been shown to be responsive to

profibrotic conditions while integrating both mesenchymal and epithelial cells in a 3D architecture [130–132]. These organoids are limited in that the tissue is not accessible from either side and the integration of mesenchyme does not ensure that they are in direct contact with epithelium, a key interface for signaling. A comprehensive model of intestinal fibrosis must include both epithelium and fibroblasts as the former is most important for carrying out the functions of intestinal tissue and the latter is largely responsible for managing ECM deposition, organization, and breakdown. Additionally, the model must capture the spatially ordered nature of 3D intestinal crypts because behavior of both epithelial and mesenchymal cells is different at the luminal and basal sides of the tissue. A model must also ensure that mesenchymal cells and epithelium can be in direct contact with one another while interfacing with a substrate which mimics fibrotic stiffness. Direct contact communication, like Notch signaling, is important for cell interplay and distinct genetic responses can be linked to cytoskeletal response to a stiff or soft underlying substrate.

Herein we describe a model of intestinal fibrosis which integrates primary intestinal fibroblasts and epithelial cells on a substrate with tunable stiffness. A cross-linked collagen substrate was molded to enable planar, layered coculture of fibroblasts and epithelium or molded to mimic the shape of the intestinal mucosa, allowing for the observation of both cells in healthy and fibrotic conditions. With an underlying substrate which has a similar stiffness to healthy and fibrotic tissue it was possible to model the biophysical conditions found in an intestinal fibrotic scar. Additionally, by varying media conditions and monitoring cell behavior over time it was possible to observe how cells grow into an area that was previously absent of cells, for example in the case of injury, and observe how luminal cells behave on varied surfaces after a monolayer is already established. Finally, using these healthy and fibrotic substrates, a molded 3D crypt

architecture allowed the study of pericryptal fibroblasts' and epithelial cells' response to fibrotic tissue while a physiologically relevant chemical gradient of growth factors was applied. Thus, it was possible to study, with spatial specificity, how basal and luminal cells might behave differently on a fibrotic scar.

3.3. Results

3.3.1. Development of substrates with a stiffness representative of normal and fibrotic tissue

Two preparations of a cross-linked collagen hydrogel were used to mimic the fibrotic environment *in vitro*. At first, the two cell-free hydrogels with different collagen concentrations were characterized to determine their resistance to deformation and apparent diffusion coefficient. Shear storage and loss moduli were measured directly via rheometric testing of collagen hydrogel discs with twisting parallel plates. With a hydrogel preparation of 5.75 mg/mL collagen stock, the shear storage and loss moduli were determined to be 2842 ± 123 Pa and 29 ± 14 Pa, respectively. A 12.5 mg/mL collagen hydrogel yielded shear storage and loss moduli of 5287 ± 243 Pa and 58 ± 20 Pa, respectively (Figure 3.1 A). As expected, the hydrogel with a higher concentration of collagen was more rigid while the lower concentration was more flexible. Conversion of the shear storage modulus to Young's modulus (E') showed that the measured stiffness of the 5.75 mg/mL hydrogel was 2.84 ± 0.85 kPa and the 12.5 mg/mL hydrogel is 15.9 ± 0.73 kPa (Figure 3.1 B). These values align with published *ex vivo* measurements and it was determined that each of these hydrogel preparations would be useful to mimic the underlying substrate in healthy and fibrotic conditions.

Another characteristic altered by the density of ECM deposited within a microenvironment is the speed at which molecules diffuse through the tissue. In a fibrotic tissue, with a denser microstructure, one would expect that diffusion might be slowed, especially for

larger molecules. To test this in the experimental scaffolds, fluorescence recovery after photobleaching (FRAP) was monitored after loading the hydrogels with FITC conjugated dextran. The molecular sizes tested were 4, 10, 40, and 150 kDa to capture a range of possible molecules. Importantly, Wnt is a growth signaling factor in the intestinal stem cell niche that is approximately 40 kDa [133]. The apparent diffusion coefficient was calculated for each of the four molecular sizes in both substrates and these data indicate, unsurprisingly, that diffusion is diminished in each substrate as molecule size increases (Figure 3.1 C). Regarding the differences in 5.75 mg/mL versus 12.5 mg/mL substrates, a significant difference was observed in the diffusion of 10 and 40 kDa molecules though there was no difference in the smallest, 4 kDa, or largest, 150 kDa, molecule tested. These data indicate that 10 and 40 kDa molecules move slower within the higher collagen concentration substrate but for compounds that are sufficiently small, i.e., 4 kDa, there is no apparent difference in the rate of diffusion in the stiff or soft scaffolds under the conditions used. Interestingly there is also no difference in the apparent diffusion of 150 kDa dextran through both substrates though this may be because in both hydrogels the larger molecule is relatively immobile, and so any minor difference in diffusion rate is too small to be detected with this method. Rheometric testing, and diffusion measurements show that these two substrates display characteristics that permit it to act as a model of healthy and fibrotic tissue. It was thus determined that comparison of cell behavior on these two substrates *in vitro* could be useful for studying response to excessive ECM deposition.

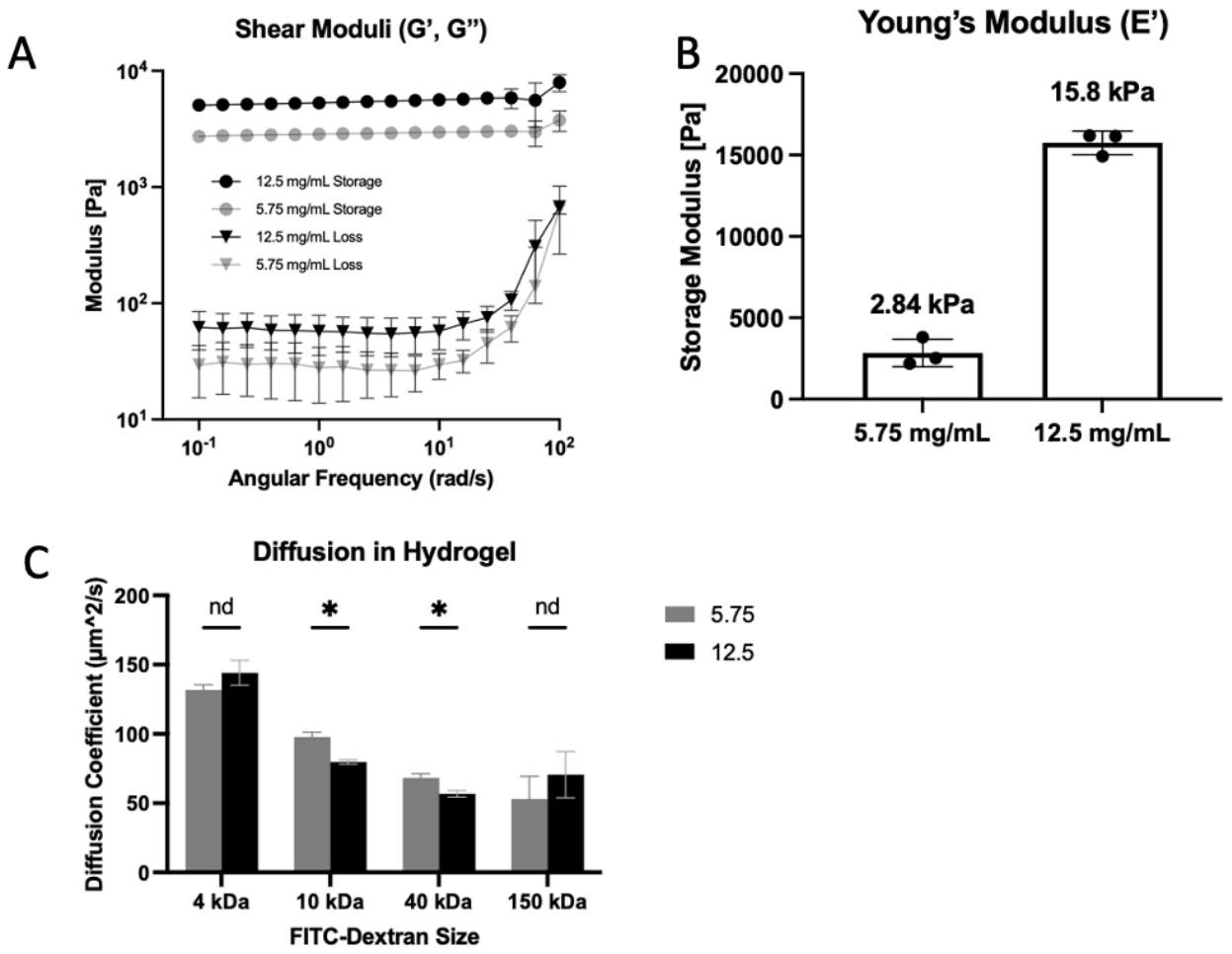

Figure 3.1. Physical characterization of hydrogel scaffolds. (A) Shear storage and loss moduli as measured by a rheometer in a range of angular frequencies (n=3). (B) Converted Young's moduli for soft and stiff scaffolds (n=3). (C) Diffusion coefficient as measured via fluorescence recovery after photobleaching (FRAP) for 4 different sized FITC-conjugated dextran (n=5). nd = no difference detected, * = p-value < 0.05, ** = p-value < 0.01, *** = p-value < 0.001, **** = p-value < 0.0001. Panels A-C display the average data with a single standard deviation marked by the error bar.

3.3.2. Culture of fibroblasts on planar soft and stiff collagen scaffolds

Since fibroblasts are a key player in wound healing and fibrosis, it was important to integrate fibroblasts within both the *in vitro* soft and stiff scaffold models. Primary derived intestinal fibroblasts were cultured atop flat collagen substrates and fibroblast behavior was characterized

under four media conditions. For the purposes of this investigation fibroblast medium (FM), expansion medium (EM), differentiation medium (DM), and stem medium (SM) were used (Table 2.1). FM and EM are the traditional media used for culture of fibroblasts and epithelial cells, respectively, when cultured independently. DM was formulated to mimic the conditions at the luminal side of a crypt (i.e., differentiated cell zone) and so it does not possess WRN. SM reflected the conditions at a crypt base (i.e., stem cell zone) and is simplified compared to EM with nicotinamide, gastrin, pge2, and SB202190 removed but with A83-01 added to encourage an epithelial stem-like phenotype. After five days of culture in each of the four media conditions on the stiff and soft substrates, fibroblasts were fixed and stained for Hoechst 33342 to visualize nuclei, 5-ethynyl-2'-deoxyuridine (EdU)-incorporation to measure proliferation (S-phase cells), as well as fibronectin (FN) and α-smooth muscle actin (αSMA) to measure cellular ECM deposition and myofibroblast activation. The area occupied by EdU, FN, and αSMA fluorescence (above an empirically set threshold) was normalized to the total number of cells i.e., by dividing by the fluorescence area that was Hoechst 33342 positive (above an empirically set threshold). Across all conditions there was no statistically significant difference in cell confluence, FN deposition, or αSMA expression measured, although there was a significant increase in proliferation within FM on softer scaffolds when compared to all other media formulations (Figure 3.2 A-F). Although there is prior evidence suggesting that fibroblasts would express more αSMA on a stiffer substrate *in vitro*, the experiments conducted herein used a primary cell source rather than a cell line (CCD18-Co)[67]. Additionally, SM and DM contain a TGF-β pathway inhibitor which may be inhibiting fibroblast activation.

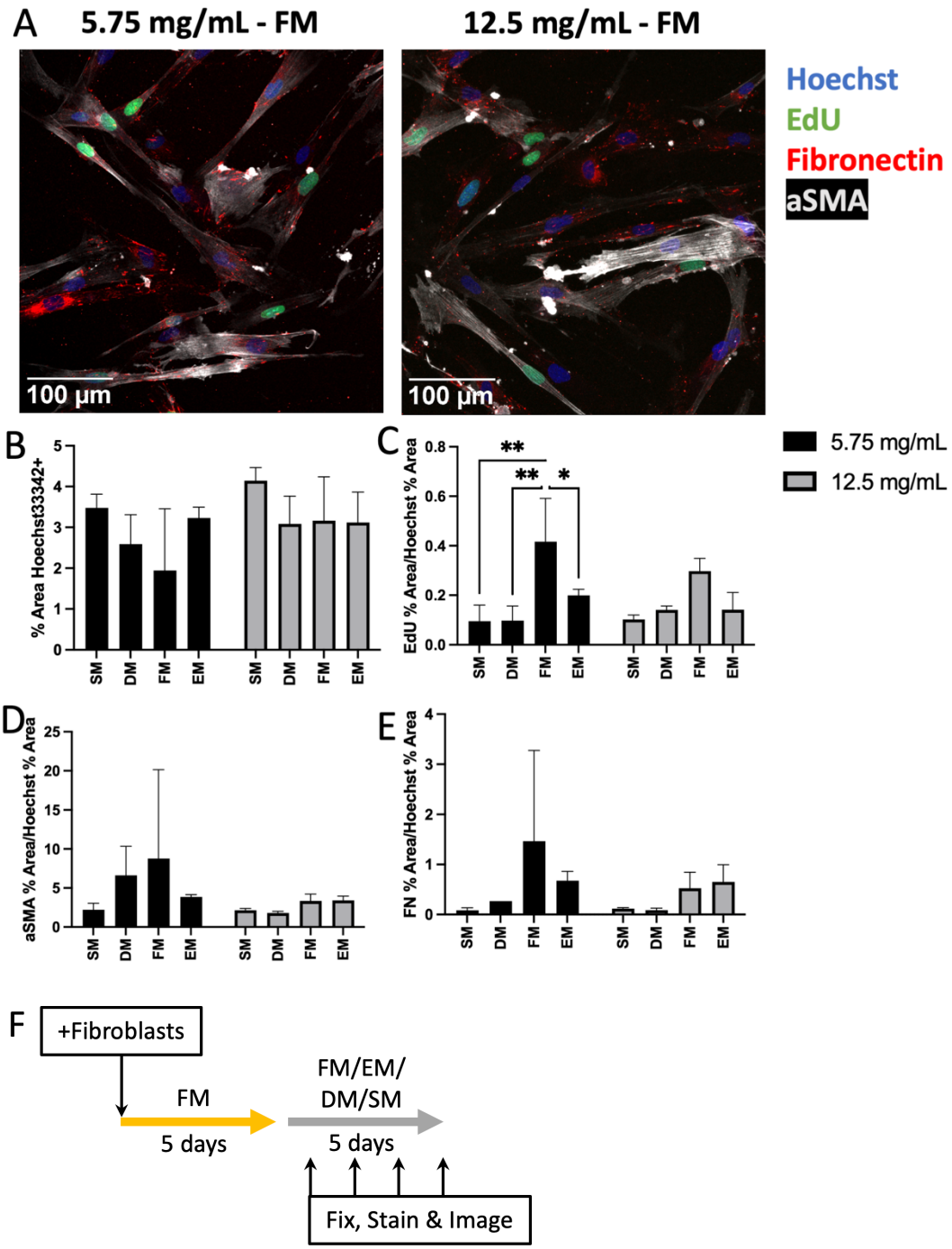

Figure 3.2. Fibroblasts on planar soft and stiff substrates under varied media conditions. (A) Confocal fluorescence images of fibroblasts cultured in FM with Hoechst 33342 in blue, EdU in green, FN in red, and αSMA in white. (B) Hoechst 33342 fluorescent area above an empirical threshold on soft and stiff hydrogels in SM, DM, FM, and EM. (C) EdU, (D) αSMA, and (E) FN fluorescent area above an empirical threshold divided by Hoechst 33342 positive area on soft and stiff hydrogels. (F) Experimental timeline. ns = not significant, * = p-value < 0.05, ** = p-value

< 0.01, *** = p-value < 0.001, **** = p-value < 0.0001. Panels B-E display the average data with a single standard deviation marked by the error bar with n=3 for each bar.

3.3.3. Culture of epithelial cells on planar soft and stiff collagen scaffolds

Epithelial cells line the interior of the intestine, and their function is paramount to the proper physiology of intestinal tissue. Thus, to understand fibrosis, it was important to understand how epithelial cells alone behave when grown on a soft or stiff underlying substrate. At first, epithelial cells were seeded onto flat collagen scaffolds in EM which is rich in growth factors promoting proliferation of epithelial cells. The samples were fixed and stained every 24 h for four days. This condition more closely represents the behavior of cells in proliferative intestinal zones i.e., along the crypt base. Separately, to model the responses of nondividing or differentiated cells, epithelial cells were grown to confluence on the scaffolds in EM for 7 days and then exposed to DM and samples were again fixed and stained every 24 h for four days. Hoechst 33342 was used to visualize nuclei, EdU-incorporation to monitor cells in S-phase, mucin 2 (Muc2) to identify goblet cells, and cytokeratin-20 (KRT20) to mark all differentiated epithelial cells. The area occupied by EdU, Muc2, and KRT20 fluorescence (above an empirically set threshold) was normalized to the total number of cells by dividing by the Hoechst 33342+ fluorescence area.

In the presence of EM, the Hoechst 33342+ area was significantly increased after the third day on the softer, 5.75 mg/mL scaffold when compared to day 1 (Figure 3.3 A, B, E). In contrast, the Hoechst 33342+ area showed no significant differences on the stiffer 12.5 mg/mL scaffold from one day to the next. The soft scaffold also possessed a significantly greater Hoechst 33342+ area on day 3 compared to the cultures on the stiff substrate (Figure 3.3 A, B, E). These data suggested that on the soft substrate the cells were able to increase in number over

time whereas their numbers did not increase over time on the hard substrate. There was no significant difference in EdU integration over four days in EM on both soft and stiff scaffolds (Figure 3.3 A, B, F). With growth factor rich medium replenished daily it makes sense that the proportion of cells in S-phase does not change over time. In EM very little Muc2 signal was detected, and no significant difference was noted across four days on both scaffolds (Figure 3.3 A, B, G). No significant difference was found in KRT20 expression across the four days in EM on both scaffolds as well (Figure 3.3 A, B, G, H). Thus, little change was observed on either scaffold regarding the proportion of proliferating and differentiated cells when the population was exposed to a growth factor rich medium (EM), though the density of cells was significantly different between soft and stiff scaffolds after 3 days.

Under DM conditions, the measured Hoechst 33342+ area was decreasing over time, though there was not a statistically significant difference measured when comparing coverage over four days on both soft and stiff scaffolds. The decrease in Hoechst 33342+ area suggests that fewer cells were present over time in the culture, and this is consistent with the expected cell death and sloughing over time of the mature non-dividing cells (Figure 3.3 C-E). With growth factor depleted media, significantly less EdU+ area was observed when comparing to DM to EM on days one and two. Almost zero EdU signal was detected in samples after 48 hours (Figure 3.3 C, D, F). Area stained positive for Muc2 was observable in DM at first, but by day four there was almost no detectable Muc2 signal, suggesting that few goblet cells were present (Figure 3.3 C, D, G). In DM, KRT20+ area increased over time and was significantly higher after 4 days when compared to EM conditions (Figure 3.3 C, D, H). As expected, the media in which epithelial cells are grown affected their proliferation, survival, and differentiation *in vitro*. Additionally, although there were few differences observed between the stiff and soft scaffold in DM, the

epithelium proliferated more and formed a more densely packed monolayer in EM on a softer, healthy-stiffness substrate as compared to the stiff fibrotic scaffold.

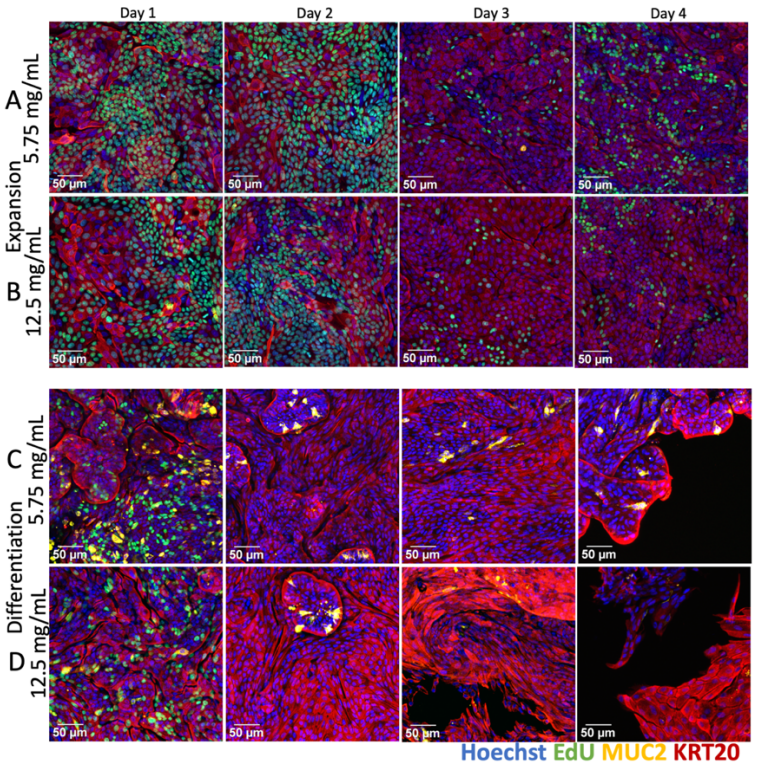
Day 1
Day 2
Day 3
Day 4
A
5.75 mg/mL
Expansion
B
12.5 mg/mL
C
5.75 mg/mL
Differentiation
D
12.5 mg/mL
50 µm
Hoechst EdU MUC2 KRT20

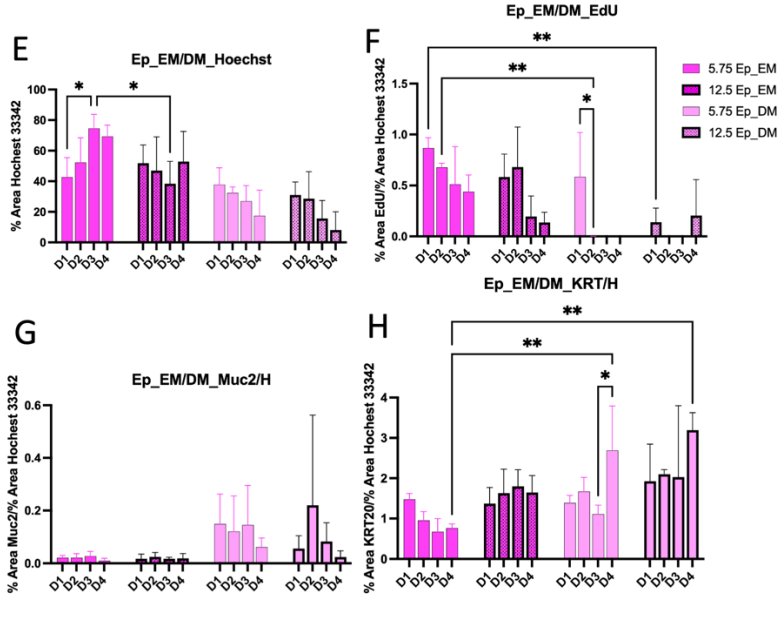
E
Ep_EM/DM_Hoechst
% Area Hochest 33342
F
Ep_EM/DM_EdU
% Area EdU/% Area Hochest 33342
5.75 Ep_EM
12.5 Ep_EM
5.75 Ep_DM
12.5 Ep_DM
G
Ep_EM/DM_Muc2/H
% Area Muc2/% Area Hochest 33342
H
Ep_EM/DM_KRT/H
% Area KRT20/% Area Hochest 33342
D1
D2
D3
D4

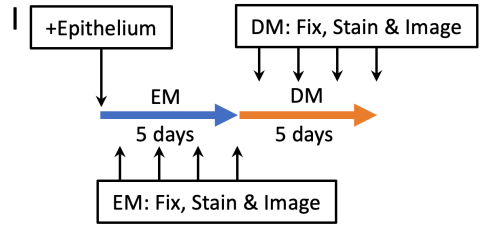
I
+Epithelium
DM: Fix, Stain & Image
EM
5 days
DM
5 days
EM: Fix, Stain & Image

Figure 3.3. Epithelium expansion and differentiation on a soft or stiff substrate. First confocal fluorescence images shown of epithelium in EM over four days on a (A) soft, and (B) stiff hydrogel. Next confocal images shown are epithelium in DM over four days on a (C) soft, and (D) stiff hydrogel. I Hoechst 33342 fluorescent area above an empirical threshold on soft and stiff hydrogels in EM or DM. (F) EdU, (G) Muc2, and (H) KRT20 fluorescent area above an empirical threshold divided by Hoechst 33342 positive area on soft and stiff hydrogels in EM or DM. (I) Experimental timeline. Ns = not significant, * = p-value < 0.05, ** = p-value < 0.01, *** = p-value < 0.001, **** = p-value < 0.0001. Panels E-H display the average data with a single standard deviation marked by the error bar with (n=3).

3.3.4. Coculture of mesenchymal and epithelial cells on planar soft and stiff collagen

Myofibroblasts drive fibrosis and the impact on epithelial cells is what ultimately determines the functionality of the fibrotic tissue. So, it was important to include both cell types within the planar *in vitro* model. Primary mesenchymal and epithelial cells were grown in layers atop the collagen hydrogel with varied stiffness and the behavior of epithelial cells was observed. For coculture, fibroblasts were initially cultured alone on the scaffolds in FM for 5 days prior to adding epithelial cells on top of the fibroblasts. To monitor expansion behavior, cells were cultured in EM and stained and fixed daily for four days immediately after epithelial addition. To observe behavior in differentiated tissue, samples were grown in EM for 8 days before the media was switched to DM and then tissues were again fixed and stained daily for four days. Hoechst 33342, EdU, Muc2, and KRT20 fluorescent area was used to evaluate nuclei density, proliferation, and differentiation.

In EM there was no significant difference between soft and stiff scaffolds when comparing Hoechst 33342+ area over four days (Figure 3.4 A, B, E). Regarding proliferation behavior, EdU+ area was not significantly different over four days on both soft and stiff scaffolds in EM (Figure 3.4 F). Muc2+ area was scarce in EM samples after four days, though no statistically

significant difference was detected when comparing across all four days on both substrates (Figure 3.4 G). The KRT20+ normalized area was not significantly different when comparing across four days on both substrates (Figure 3.4 H).

In DM there was also no significant difference in Hoechst 33342 positive area when comparing across four days on both scaffolds (Figure 3.4 C, D, E). This came as a surprise since epithelium in monoculture within DM was had decreased Hoechst 33342+ area after 4 days and holes in the monolayer were visible. Unsurprisingly, significantly lower EdU+ area was observed in all DM samples as compared to EM samples from day 2 onward (Figure 3.4 C, D, F). Notably, on both soft and stiff scaffolds there was some EdU signal observed on day 2 samples in DM in coculture (about 2% of the normalized Hoechst 33342 area) though this was not significantly different from day 3 and 4. In growth factor depleted DM the fluorescent area that was Muc2+ was not significantly different when comparing across four days, though this area was lower in coculture than in epithelial monoculture.

These data suggest that fibroblasts influence epithelium *in vitro*. The presence of fibroblasts appears to support epithelial survival and mitigate the differential impact of soft versus stiff underlying scaffolds. Specifically, the nuclei density in coculture measured via Hoechst 33342 is unchanged for four days in both EM and DM conditions despite the decrease in proliferation activity observed in DM. Also, no holes in the monolayers were detected in coculture, perhaps meaning the epithelium is not being sloughed off the surface as quickly as when epithelium is grown in monoculture in these conditions. Additionally, in EM conditions with epithelium alone the stiff scaffold seemed to stunt proliferation, but in coculture this effect is not observed. Finally, very few Muc2+ cells were observed in all coculture conditions when compared to epithelium alone suggesting that fibroblasts are limiting this differentiation pathway.

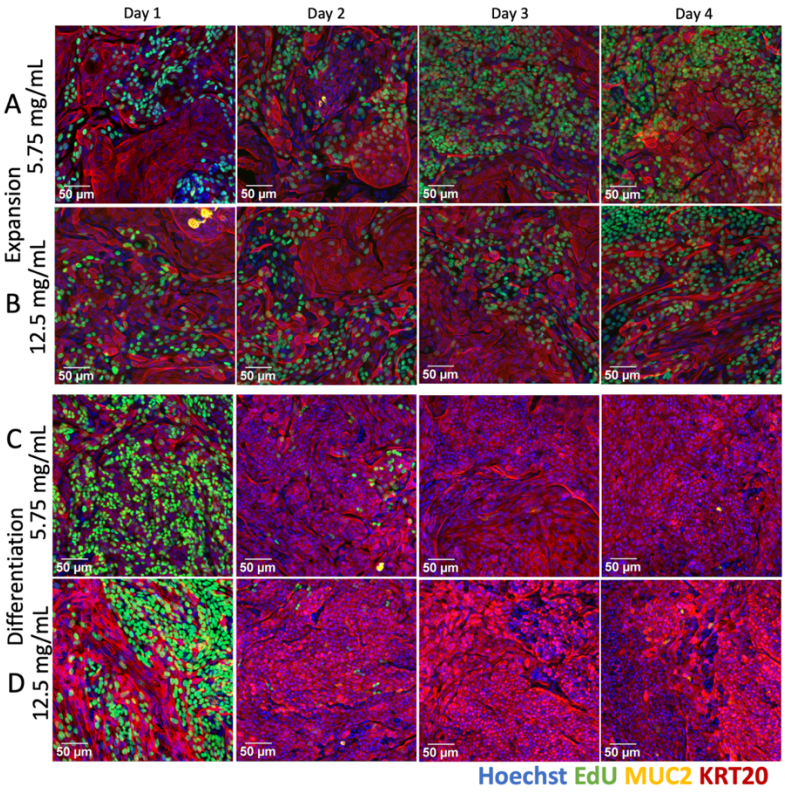
Day 1
Day 2
Day 3
Day 4
A
5.75 mg/mL
Expansion
B
12.5 mg/mL
C
5.75 mg/mL
Differentiation
D
12.5 mg/mL
50 µm
Hoechst EdU MUC2 KRT20

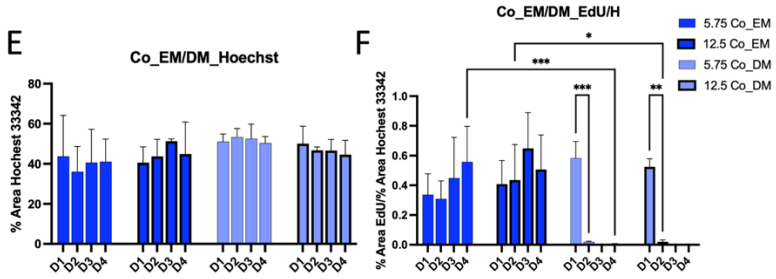
E
Co_EM/DM_Hoechst
% Area Hochest 33342
F
Co_EM/DM_EdU/H
% Area EdU/% Area Hochest 33342
5.75 Co_EM
12.5 Co_EM
5.75 Co_DM
12.5 Co_DM
D1 D2 D3 D4

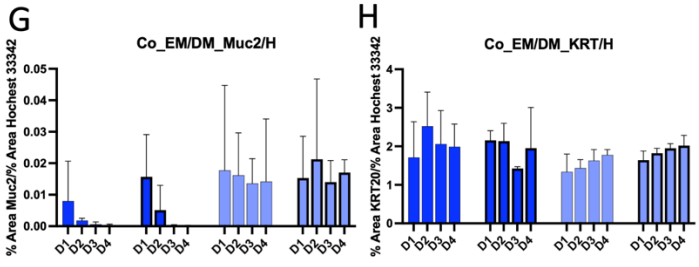
G
Co_EM/DM_Muc2/H
% Area Muc2/% Area Hochest 33342
H
Co_EM/DM_KRT/H
% Area KRT20/% Area Hochest 33342
D1 D2 D3 D4

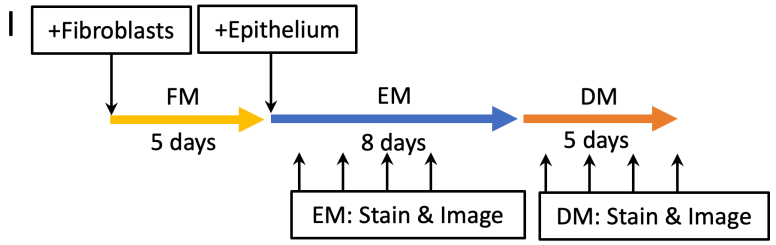
I
+Fibroblasts
+Epithelium
FM
5 days
EM
8 days
DM
5 days
EM: Stain & Image
DM: Stain & Image

Figure 3.4. Coculture expansion and differentiation on a soft or stiff substrate. First confocal fluorescence images shown of stained epithelium grown over fibroblasts in EM over four days on a (A) soft, and (B) stiff hydrogel. Next confocal images shown are stained epithelium grown over fibroblasts in DM over four days on a (C) soft, and (D) stiff hydrogel. (E) Hoechst 33342 fluorescent area above an empirical threshold on soft and stiff hydrogels in EM or DM. (F) EdU, (G) Muc2, and (H) KRT20 fluorescent area above an empirical threshold divided by Hoechst 33342 positive area on soft and stiff hydrogels in EM or DM. (I) Experimental timeline. ns = not significant, * = p-value < 0.05, ** = p-value < 0.01, *** = p-value < 0.001, **** = p-value < 0.0001. Panels E-H display the average data with a single standard deviation marked by the error bar with (n=3).

3.3.5. Culture of epithelial cells on soft and stiff molded 3D crypt scaffolds

The 3D crypt architecture present *in vivo* is a crucial feature of intestinal health. Spatially specific stimuli help define phenotypically distinct regions at the basal and luminal sides of the tissue and this enables the maintenance of proliferating stem cells which support continuous, healthy tissue regeneration. Molded, 3D collagen scaffolding (soft and stiff) was formed to mimic the shape of colonic crypts and enable formation of a chemical gradient of growth factors along the long axis of the crypts. Polarization, i.e., varied phenotypes along the vertical axis, in the epithelial layer is especially important to intestinal tissue function. Soft and stiff 3D crypt scaffolds were seeded with epithelial cells and cultured for 8 days in EM followed by 5 days in a chemical gradient with SM from the base and DM from the lumen. Samples were then fixed and stained for Hoechst 33342, EdU, Muc2, and KRT20. Image analysis software was used to extract the precise number and location (y-position) of Hoechst 33342+ objects and EdU+ objects so that crypt height, nuclear density, proliferative cell number and proliferative cell location could be compared.

Crypt height was significantly shorter in softer scaffolds compared to stiff, with an average height of 408 μm on soft substrates and 510 μm on stiff (n = 9, 17, Figure 3.5 A). The nuclear density (Hoechst 33342+ objects divided by crypt height) was significantly lower in stiff crypts compared to soft, indicative of a less tightly packed epithelial monolayer (Figure 3.5 B). Additionally, there were fewer EdU+ objects observed in the stiff crypts as compared to the soft (Figure 3.5 C). This aligns with trends noted on planar scaffolds and it is in line with prior observations that epithelium may proliferate more atop a scaffold that is softer. For further interrogation of the proliferative cell zone, crypts were split (mathematically) into four regions and the EdU+ object count for each crypt was averaged within the four quartiles. A significantly higher number of EdU+ cells were observed soft crypts versus stiff in the bottom two quartiles, suggesting that the proliferative cell zone was more densely packed and reached higher within softer, epithelium-only crypts (Figure 3.5 D, E). Muc2 was scarcely observed in soft crypts, though a few examples of Muc2 signal could be found in stiff, epithelium-only crypts (Figure 5F). KRT20 was observed on the luminal size of all crypts showing that both soft and stiff crypts exhibit a polarized behavior with a luminal differentiated cell zone (Figure 3.5 E). Using KRT20, which is expressed at the extents of differentiated epithelial cells, the height to width ratio was assessed to determine if cells were more columnar or squamous on each scaffold (Figure 3.6 A). It was found that epithelial cells are more squamous on the stiffer scaffold, consistent with a fibrotic environment (Figure 3.6 B). Finally, the EdU+ area for full tissue samples was used to evaluate, relatively, how many crypts could support cell proliferation in their base. On the stiffer substrate EdU+ area was found to be less, though no statistical significance was found (Figure 3.6 C). Taken together these data seem to show that the stiffer scaffold discourages proliferation

and encourages differentiation while the softer scaffold can support a denser monolayer of columnar cells.

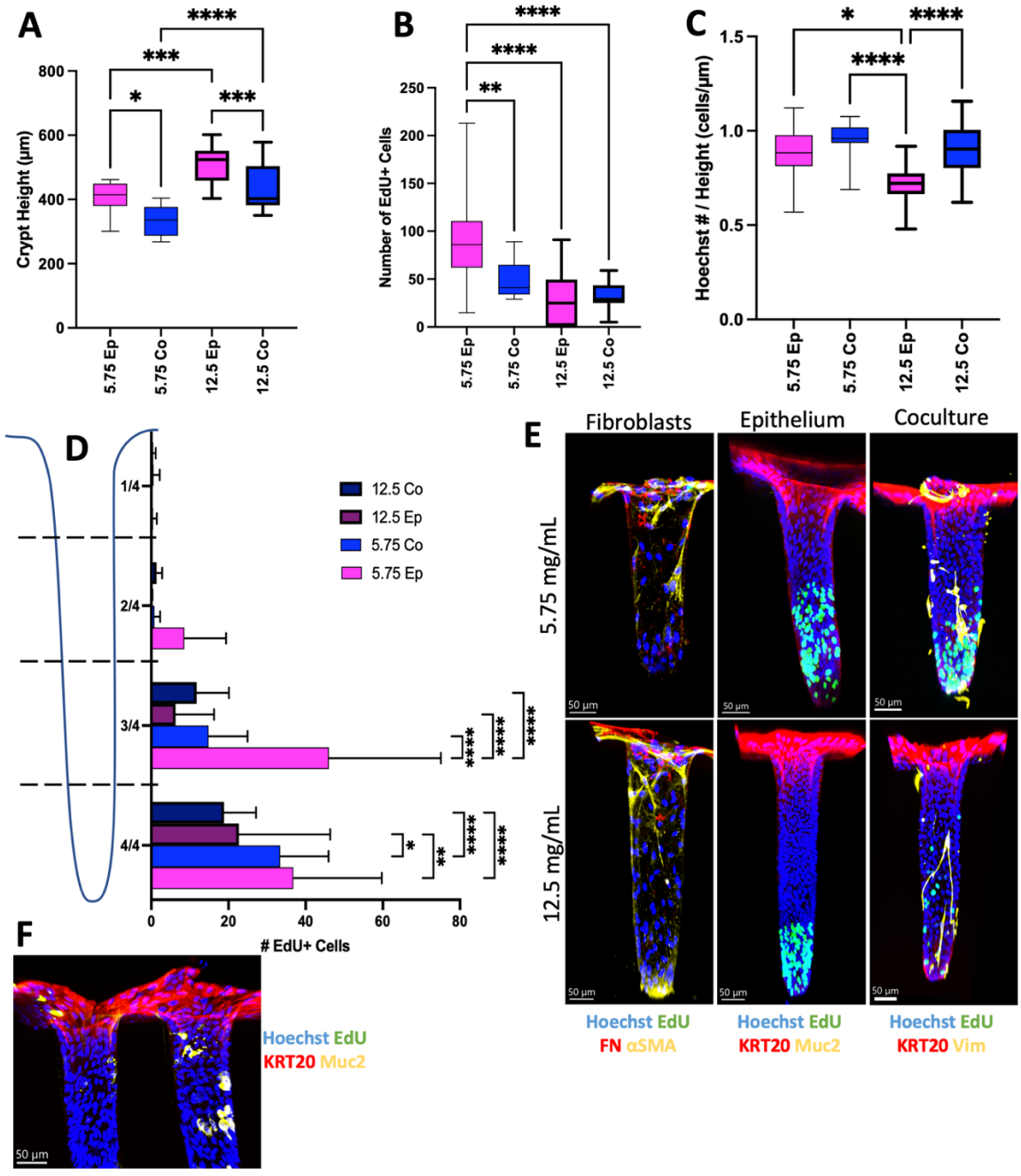

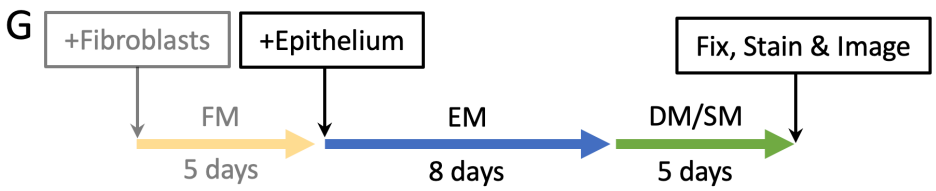

Figure 3.5. Characterizing molded 3D crypts with epithelium and fibroblasts on soft and stiff hydrogel substrates. (A) Crypt total height, (B) total number of EdU positive cells, and (C) total nuclei divided by crypt height for soft and stiff crypts with epithelium alone or epithelium in coculture with fibroblasts (n = 9, 15, 17, 29). (D) Distribution of EdU positive cells along the crypt vertical axis separated into quartiles. (E) Sample crypts for soft and stiff scaffold with monoculture or coculture fibroblasts and epithelium. (F) Crypts positively stained for differentiation markers KRT20 and Muc2. (G) Experimental timeline. ns = not significant, * = p-value < 0.05, ** = p-value < 0.01, *** = p-value < 0.001, **** = p-value < 0.0001. Panels A-C display the average data with a single standard deviation marked by the error bar with (n=3).

3.3.6. Coculture of mesenchymal and epithelial cells on soft and stiff molded 3D crypt scaffolds

As discussed, the interplay of pericryptal fibroblasts and epithelium is important for determining the fate of healthy and fibrotic intestinal tissue. The spatial organization within crypts can be influenced by these inter-cell type interactions and so it was important to study how coculture of these cells in soft and stiff crypt-shaped scaffolds might change *in vitro* behavior. Fibroblasts were first established for 5 days in FM, then epithelium was added on top and samples were grown in EM for 8 days followed by 5 days in a chemical gradient (SM/DM). Hoechst 33342, EdU, and KRT20 were used for comparison while Vimentin immunostaining was conducted to visualize pericryptal fibroblasts.

In coculture the crypt height was again significantly lower in softer scaffolds when compared to stiff (334 μm vs. 436 μm), and each coculture crypt was shorter than the epithelial monoculture crypt grown on the same stiffness substrate (Figure 3.5 A). Nuclei density was not significantly different between soft and stiff scaffolds in coculture and the number of EdU+ objects was also not significantly different, though the EdU+ cell count was significantly lower in both coculture conditions when compared to epithelial monoculture on a soft substrate (Figure 3.5 B, C). When considering EdU+ object distribution, there was no significant difference in coculture in any of the four quartiles (Figure 3.5 D). Vimentin coverage was low compared to

KRT20, indicating far fewer fibroblasts than epithelial cells (Figure 3.5 E). Epithelial aspect ratio was diminished on the stiff scaffold compared to soft, with cells exhibiting a more squamous morphology on the 12.5 mg/mL collagen hydrogel (Figure 3.6 A, B). Finally, there was slightly lower EdU+ area on the full scaffolds in soft and stiff coculture, though this measured difference was not statistically significant with just three replicate tissues (Figure 3.6 C). These data demonstrate that when fibroblasts are present, there is less proliferation within crypts on the softer scaffolds. On the other hand, the impact of a stiff scaffold versus soft is comparatively lower when measuring epithelial cell proliferation and nuclei density. Additionally, crypts were found to be shorter in coculture when compared to monoculture indicating that fibroblasts may be manipulating their physical environment on both soft and stiff substrates. That said, fibroblast presence alone is not enough to mitigate the change in morphology observed in epithelial cells when placed on a stiffer scaffold.

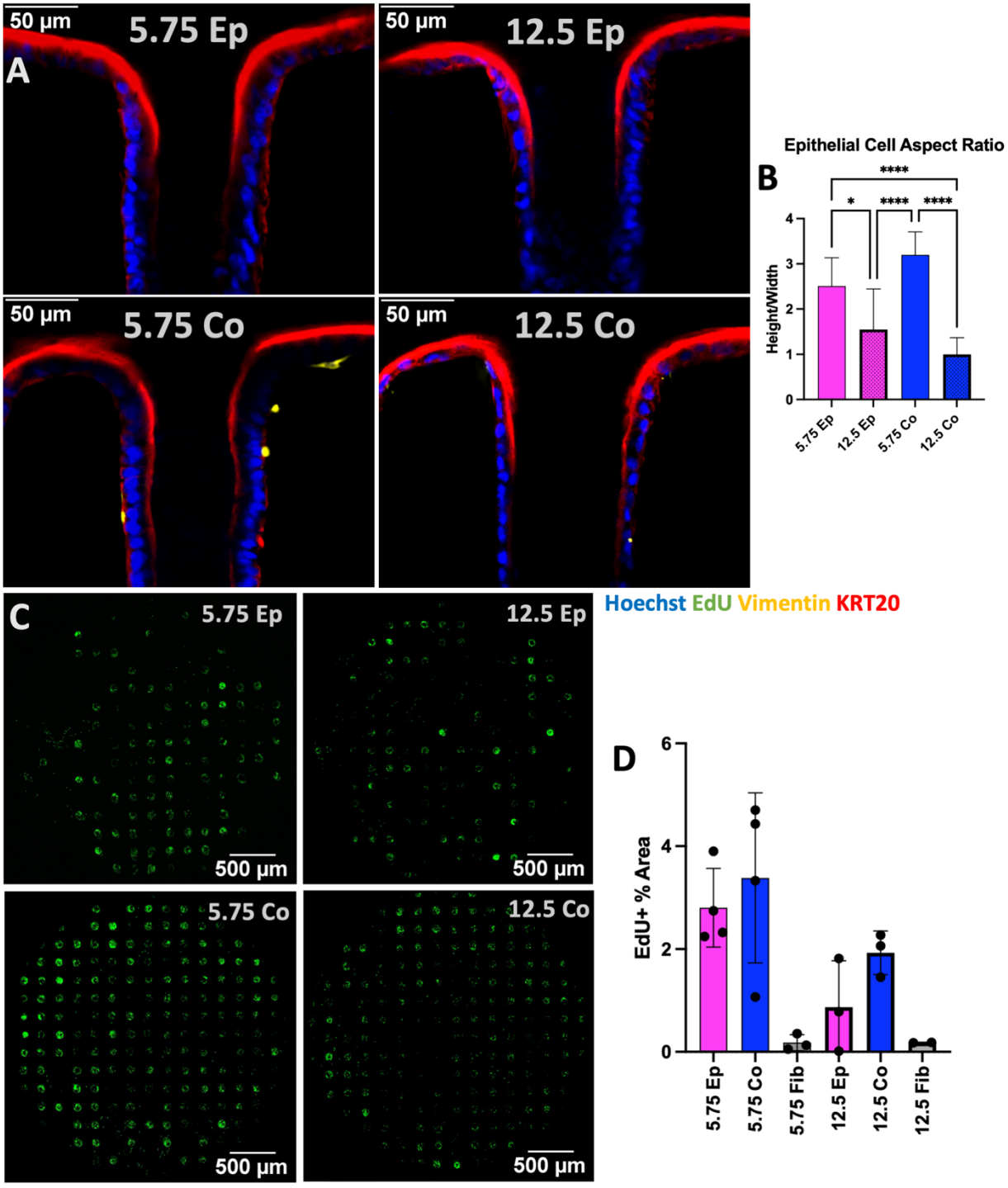

Figure 3.6. Epithelium morphology and proliferation behavior on soft and stiff scaffolds with and without fibroblasts. (A) Fluorescent single-slice images displaying epithelial cells within 3D crypts. (B) Epithelial cell morphology quantified via aspect ratio (height/width) as visualized with KRT20 staining (n=10). (C) Full 3D crypt array maximum z-projection images displaying EdU in green. (D) Quantified area occupied by EdU above an empirical threshold within the circular crypt array area (n=3). ns = not significant, * = p-value < 0.05, ** = p-value < 0.01, ***

= p-value < 0.001, **** = p-value < 0.0001. Panel B and D display the average data with a single standard deviation marked by the error bar.

3.4. Discussion

Two substrates were developed to represent healthy and fibrotic colon tissue which could be molded into an easily imaged planar scaffold or a physiological 3D crypt scaffold. The diffusivity characteristics and Young's modulus for each substrate was representative of a healthy and fibrotic colon and it was possible to grow primary intestinal fibroblasts and epithelium on the scaffolds *in vitro*. It was discovered that these primary fibroblasts behave largely the same on both scaffolds within this context, though epithelial cell proliferation, differentiation and morphology was altered atop stiff scaffolds when compared to the softer, healthy-stiffness substrate. Coculture of fibroblasts and epithelial cells revealed that fibroblasts aid in epithelial cell survival, but that coculture does not mitigate the morphological impact of a stiff substrate on epithelial cell aspect ratio. In 3D crypts, proliferative and differentiated cell zones were formed while crypt height and epithelial cell proliferation was altered by scaffold stiffness. In cocultured *in vitro* crypts fibroblast survival was minimal and their phenotype was not altered by scaffolds stiffness, though their effect was still noted in epithelial cells perhaps because of the ECM components laid down by fibroblasts before epithelial addition. In the future it will be useful to improve this system by mimicking chemical aspects of fibrosis through the addition of inflammatory factors like TGF-β while removing TGF-β inhibitors from the growth medium. This system properly recapitulates several aspects of the biophysical changes observed in intestinal fibrosis and it will be helpful in the future for investigations of the cellular mechanisms of intestinal fibrosis and for fibrosis-related drug testing.

3.5. Methods

3.5.1. Measuring hydrogel moduli

The hydrogels were cast by mixing N-(3-dimethylaminopropyl)-N ′-ethylcarbodiimide hydrochloride (EDC, 0.6 M (Oakwood Chemical, cat. no. 25952-53-8)) and N-hydroxysuccinimide (NHS, 0.15 M (Millipore-Sigma, cat. no. 130672)) with rat tail type I collagen (Corning, cat. no. 354236) which had been lyophilized and then dissolved in MES buffer (Millipore-Sigma, cat. no. M8250, 0.1 M, pH 5) at a ratio of 1:1:8, as described by Hinman et al. [100]. The collagen concentration prior to crosslinking with EDC and NHS was 5.75 mg/mL or 12.5 mg/mL to represent either healthy or fibrotic ECM, respectively. Prior to rheometric measurements, the hydrogel was cast between two glass slides covered by parafilm with 1 mm washer spacer. The resultant 1 mm tall collagen hydrogel slabs were cut into 8 mm diameter discs and taken to an Anton Paar MCR-301 Rheometer (Anton Paar USA, Ashland VA) equipped with an 8 mm diameter parallel plate platen. The gap was set at 0.8 mm and a frequency sweep was conducted between 0.1 and 100 rad s^{-1} with 1% strain amplitude. The shear storage and loss moduli were calculated from the linear region of the frequency sweep from 0.251 – 2.51 rad s^{-1}. From the shear storage modulus (G') the young's modulus was calculated using the Theory of Elasticity (E' = 2G'(1+v)) assuming a Poisson Ratio (v) in hydrogel of 0.49 [134].

3.5.2. Diffusion measurement with fluorescence recovery after photobleaching (FRAP)

For diffusion measurements, hydrogel samples for both 5.75 and 12.5 mg/mL conditions were cast between two glass slides covered with parafilm without a washer spacer to produce a thin hydrogel (< 0.5 mm). From the slab, 3 mm diameter discs were cut with a biopsy punch and

these samples were placed into a solution containing 100 ng/mL of various sized FITC-conjugated dextran (4, 10, 40, and 150 kDa) and allowed to soak for 2 h. Next the dextran soaked hydrogels were placed on a glass slide on the stage of a confocal microscope (Olympus Fluoview 3000 equipped with 405, 488, 561, and 640 nm laser diodes). With the 20x objective at 5x zoom a small circular area was photobleached with the 405 nm laser at the maximum allowable laser power (80-100%) for 1 minute. Immediately following photobleaching, the 20x objective at 1x zoom was used to obtain images every 1.1 seconds for 100 frames with the 405 nm laser providing 2-4% power. Following procedures outlined by Kang et al. for obtaining a diffusion coefficient from confocal FRAP data, a bleach profile at time 0 s was used to determine the effective radius (r_e) of the bleached area, a fluorescence recovery curve was used to determine the half-time of recovery (*Tau*) and the nominal radius (r_n) was set as 75 μm for each test[135,136]. From these the diffusion coefficient was determined by the following equation:

$$D_{confocal} = \frac{{r_e}^2 + {r_n}^2}{8\tau_{1/2}}$$

3.5.3. Cassette construction and scaffold casting

As described previously, collagen hydrogel scaffolds were placed within a modified well-insert that was used so that media conditions could be controlled on basal and luminal sides of the tissue. In brief, the factory-supplied membrane on the base of a 12-well culture insert (Corning, cat. no. 354236) was removed and replaced with a permeable membrane (Millipore-Sigma, cat. no. BGCM00010) and then below that an impermeable membrane (McMaster-Carr, cat. no. 8689K44) was placed with a 3 mm diffusion window to restrict diffusion between the basal or luminal compartments. Hydrogel scaffolds were cast following the same procedure described above (mixing EDC/NHS/rat tail type 1 collagen), but molding was done *in situ* such

that the result was either a uniform flat surface or an array of crypt-shaped microwells. To cast flat scaffolds, 50 µL or mixed EDC/NHS/collage was pipetted onto the diffusion window of a modified well-insert and then a 24-well insert, with parafilm on the bottom, was pushed down to flatten the droplet. For 3D-crypt microstructures a PDMS stamp with 80 µm wide, 500 µm tall posts was pushed down into collagen and in both flat and crypt-shaped scaffolds the mold was left in place for 1 h while the whole construct was under pressure (25 psi). The PDMS stamp was fabricated and surface-treated with PEG according to Hinman et al. so that it could be easily removed after the collagen hydrogel was set. Before adding cells to the scaffolds, the well-inserts with set collagen were soaked in deionized water over night (2L per 12 inserts) to leech out excess cross-linking reagents and then then the constructs were sterilized by soaking in 75% ethanol for 5 minutes. Once sterile scaffolds were rinsed with PBS three times and then a solution of PBS containing 10 ng/mL human type I collagen (VitroCol, Advanced BioMatrix, cat. no. 5007-20ML) was added to the luminal compartment and allowed to incubate overnight thus pre-treating the surface for cell attachment.

3.5.4. Cell culture

Human colon epithelial cells from a transverse colon tissue sample (male, 23 years old, RRID: CVCL_ZR41) were expanded and maintained atop a neutralized collagen slab according to previously described methods[74]. Primary fibroblasts isolated from descending colon (male, 12 years old, RRID: CVCL_D6WE) were expanded and maintained within a culture flask stored horizontally with Dulbecco's Modified Eagle Medium (DMEM, Thermo Fisher, cat. no. 11995065) supplemented with 10% heat-inactivated fetal bovine serum, 100 U/mL penicillin, and 100 µg/mL streptomycin (Table 2.1).

For seeding within molded scaffolds, fibroblasts were added to the luminal side of well-inserts in 1mL FM at a concentration of $3x10^5$ – $5x10^5$ cells/mL for both planar and 3D crypt scaffolds. Then FM was replenished daily. For subsequent epithelium addition, epithelial stem cells grown on 6-well plate above soft neutralized collagen were isolated and dissociated according to previous protocol using collagenase type 4 (Worthington Biochemical Corporation, cat. no. LS004189) and TrypLE express enzyme (Thermo Fisher, cat. no. 12605028)[113]. Epithelial cells were then added directly to the scaffolds for monoculture, or directly on top of fibroblasts for coculture, at a ratio of 1:3 (1 well from 6-well maintenance plate to 3 well-inserts). In 3D crypts, cells were grown in EM for 8 d (replenished daily) and then polarization was executed by replacing basal medium with stem medium (SM, Table 2.1) and luminal medium with differentiation medium (DM, Table 2.1). After 5 days of polarization (media replenished daily), the samples were fixed and stained for endpoint analysis.

3.5.5. Fluorescence staining and confocal imaging

5-ethynyl-2'-deoxyuridine (EdU, 1 μg/mL) was added to the culture medium 24 h before sample fixation. Cells were fixed with Prefer fixative (Anatech Ltd., cat. no.NC9053360) for 20 min, permeabilized with 0.5% Triton X-100 at 20°C, and then blocked with 1% bovine serum albumin (BSA) for 1 h. Subsequently, integrated EdU was stained with sulfo-Cy5-azide (1.25 μg/mL) and then primary antibodies were added[114]. In this study, a DNA stain (Hoechst 33342, Sigma-Aldrich, cat. no. B2261) and antibodies for mucin-2 (MUC2, Santa Cruz, cat. no. sc-15334), cytokeratin-20 (KRT20, Cell Signaling Technology, cat. no. 13063S), and vimentin (VIM, Santa Cruz, cat. no. sc-6260) were used (all 1:500 dilution). After overnight incubation at 4 °C with primary antibodies, the samples were rinsed and matched secondary antibodies with

Alexa Fluor 488 (goat anti-mouse, Life Technologies Corp., cat. no. A28175), and Alexa Fluor 555 (donkey anti-rabbit, Life Technologies Corp., cat. no. A31572) fluorophores were added and then rinsed away after overnight incubation at 4 °C. Confocal microscopy was performed with an inverted Olympus Fluoview 3000 equipped with 405, 488, 561, and 640 nm laser diodes and 4x, 10x, or 20x magnifying objectives were used to obtain images.

For image analysis in planar systems, Cell Profiler (cellprofiler.org[115]) was used to segment and measure area occupied by each fluorescent marker. Planar samples were each imaged with a 10x objective to capture the full tissue that was above the 3 mm diffusion window and a maximum intensity projection of the z-stack (step size 4 μm) was analyzed. For 3D crypts, 4x overview images were obtained from the top (z-stack, slice 25.4 μm) and a maximum intensity z-projection was used to analyze EdU positive area on full crypt arrays. Next, the membrane was detached from the insert base and cut in half using microdissection scissors, the crypt area was situated perpendicular to the objective and imaged from the side. The 20x objective (step size 4 μm) was used to obtain images and the z-stacks were reconstructed in 3D using IMARIS X64 v9.8.2 (imaris.oxinst.com, Oxford Instruments) for analysis. The number and position of nuclei (Hoechst 33342+), and proliferative nuclei (EdU+) were counted using the IMARIS spots module.

3.5.6. Statistics

Data are presented as mean ± standard deviation on all plots. Differences between means from separate groups (epithelium, fibroblasts and coculture) were determined using two-way ANOVA multiple comparisons by multiple comparisons with Bonferroni correction applied, unless otherwise specified. Statistical analysis and graphical illustration were performed using

GraphPad PRISM 9 software, version 9.5.0 (GraphPad Software, San Diego, CA) at a significance level (α) of 0.05 unless otherwise noted.

Chapter 4: A suspended collagen hydrogel for modeling epithelial and immune cell interactions

Chapter 4 is adapted from the following manuscript:

S. S. Hinman, A. Massaro, Y. Wang, C. E. Sims, R. Kim, N. L. Allbritton, Suspended Collagen Hydrogels to Replicate Human Colonic Epithelial Cell Interactions with Immune Cells. *Adv. Biology* 2022, 6, 2200129.

4.1. Abstract

The human colon plays a critical role in fluid and salt absorption and harbors the largest immune compartment. There is a widespread need for *in vitro* models of human colon physiology with its innate immune system. A method is described to produce a cassette with a network of struts supporting a suspended, non-chemically cross-linked collagen hydrogel scaffold compatible with the coculture of primary gastrointestinal epithelium and migratory inflammatory cells. The epithelial monolayer cultured on the suspended collagen possesses a population of polarized and differentiated cells like that present *in vivo*. This epithelial layer displays proper barrier function with a transepithelial electrical resistance (TEER) ≥ 1,500 Ω cm^2 and an apparent permeability ≤10−5 cm^2 s^{-1}. Immune cells plated on the basal face of the scaffold transmigrated over a period of 24 h to the epithelial layer in response to epithelial production of IL-8 induced by luminal stimulation of Clostridium difficile Toxin A. These studies demonstrate that this *in vitro* platform possesses a functional primary colonic epithelial layer with an immune cell compartment capable of recruitment in response to pro-inflammatory cues coming from the epithelium.

4.2. Introduction

CRC often coincides with a defective interaction between the intestinal epithelium, subepithelial immune cells, and bacteria (or their metabolites and toxins)[137]. The normal intestinal epithelium acts as a tight barrier preventing the movement of bacteria, noxious bacterial metabolites, and undigested foodstuffs in the intestinal lumen from crossing into the bloodstream[4,138–140]. An epithelium-microbiome-immune (EMI) axis continuously regulates homeostatic responses at the intestinal wall via intricate intercellular crosstalk of microbial metabolites, cytokines, antigens, and hormones[139,141,142]. To maintain homeostasis, the intestinal epithelium and tissue resident mononuclear (e.g., monocyte, macrophage) and polymorphonuclear (e.g., neutrophil) immune cells deep within the lamina propria continuously monitor and actively respond to chemical signals foretelling intestinal damage [4,139,140]. For example, epithelial cells secrete cytokines, including interleukin-8 (IL-8) and monocyte chemoattractant protein-1 (MCP-1), that act as chemoattractants for the rapid recruitment of immune cells to the epithelial surface [139,141,142]. [7,10,11] This sentinel signaling system is thought to be chronically activated in many intestinal diseases including IBD, celiac disease, and CRC [139,143–146].

Model systems to understand the interactions of the EMI axis are essential to fulfill the promise of the next generation of gut therapeutics targeting the immune system-epithelial cell interaction. Given the importance of the EMI axis, a multitude of model systems strive to mimic these complex intercellular interactions. Most of our knowledge regarding the intestinal immune system has been gleaned from germ-free animal models [147–149]. However, these models do not adequately mimic human physiology due to the differing genetics, diets, and microbiomes

between mice and humans [30,150–153]. The coculture of human intestinal tumor cells and human immune cells has been performed by several groups using hanging basket inserts and microfluidic formats[154–158]. Although tumor cell lines are not reflective of *in vivo* human physiology due to their dedifferentiated state, aberrant signaling, and a plethora of genetic mutations,[29–31] the majority of these *in vitro* models have utilized these tumor cell lines by virtue of their robustness and ease of culture[159–163]. While often employed for pre-clinical pharmaceutical trials, these cell lines lack the cellular subtypes of the intestinal epithelium and fail to duplicate the important interactions between these subtypes, thus they fall short in replicating human physiology and predicting *in vivo* response[161]. To address these shortcomings, primary human intestinal epithelial cells and immune cells are being incorporated into microscale systems with the goal of replicating key attributes of the EMI axis. Tissue explant models are available, but are short-lived, thus limiting their usefulness [164,165]. Intestinal organoids offer another approach for creating a more accurate model; however, their spheroid morphology poses challenges due to the inaccessibility of the luminal compartment as well as possessing a basal surface embedded deeply within a hydrogel making assays of permeability, transport and luminal versus basal cytokine production a challenge[138]. Tumor cells have been combined with other tissues to mimic the intestinal epithelium but these abnormal cells do not replicate primary human epithelial cells' biochemistry or physiology [82,166].

To overcome these challenges, human gastrointestinal stem cells have been successfully cultured and differentiated to form a monolayer when plated on a hydrogel scaffold and porous membrane under the combined influence of growth and morphogenic factors[167,168]. These primary intestinal epithelial monolayers have been cocultured with human macrophages seeded

on the opposing face of a track-etched membrane[169]. While communication between the epithelium and immune cells was demonstrated, the macrophages were incapable of migration to the epithelium due to the small pore size of the track-etched membrane. We and others have had similar experiences in the coculture of human peripheral blood mononuclear cells (PBMCs) separated from the intestinal monolayer by the porous membrane support that while allowing chemical crosstalk, limits physical contact [156,170]. Dual cylindrical layers of silk scaffold have been seeded with primary intestinal cells on the interior of the inner tube and macrophages on its outer surface[171]. The porous properties of the collagen-impregnated silk allowed macrophage migration toward the intestinal cells under a chemical gradient, but throughput was severely limited due to the required device assembly steps throughout the culture. There remains a need to develop an immune cell-intestinal coculture platform relying on a soft extracellular matrix (ECM) that enables both native primary human intercellular interactions including cell migration and cytokine exchange through the ECM. The ability to readily assay cells as well as the luminal and basal tissue compartments in an easy-to-use, scalable cassette would be of high value in investigations of intestinal physiology and compound screens [163].

In this work, an immunocompetent intestinal mucosal interface was developed. To accomplish this, an open polymer support structure was used to suspend a thick hydrogel layer compatible with both stem-cell-derived gastrointestinal epithelial tissue and migration competent inflammatory cells. The aim was to develop an easy-to-use cassette for coculture of primary human colonic epithelium with immune cells to enable the assay of intercompartmental communication, permit immune cell migration to the epithelium and assess bacterial toxin-induced disruption of the intestinal barrier. The device was designed with simplicity in mind so that no specialized valves, pumps, or flow controllers were incorporated with the goal that the

method could be employed within labs lacking biomaterials or microdevice expertise. A standard hanging basket design with widely spaced supporting struts was used to provide a culture platform with access to the luminal and basal fluid compartments. The intestinal monolayer was created on the luminal surface of the strut-supported hydrogel. Inflammatory cells were plated on the basal aspect of the suspended collagen. The large open area between the polyester struts allowed these cells to migrate through the unobstructed soft collagen regions between the struts and into the hydrogel to interact directly with the intestinal tissue. This format enabled several assays pertinent to such a coculture system to be conducted to demonstrate the design's functionality.

4.3. Results

4.3.1. Design Overview

The design goal was to develop a platform to support a functional relationship between intestinal epithelial cells and the underlying resident immune cells. In a normal human, the immune cells reside in the lamina propria or connective tissue just below the epithelial cells which line the intestinal lumen and maintain constant vigilance with a goal of detecting loss of barrier integrity (Figure 4.1a). In defending against potential microbial invaders, the immune cells secrete a host of cytokines and other molecules to attract additional immune cells and block microbial incursion. To recapitulate these epithelial cell-immune cell interactions, a cassette comprised of four components was constructed: i) a modified hanging basket for luminal media containment, ii) a neutralized suspended collagen hydrogel for primary intestinal epithelial cell culture, iii) polyester struts for basal support of the suspended collagen scaffold, and iv) an underlying multi-well plate for provision of a basal medium (Figure 4.1b). In order to support a

normal human intestinal epithelium in close proximity to immune cells, the supported scaffold required several attributes: i) display of native ECM contacts and an appropriate stiffness (Young's modulus: 0.1–1 kPa) to support the primary intestinal epithelial cells, ii) sufficient porosity so that microbial metabolites and toxins might diffuse across the scaffold, and iii) support migration of immune cells (10–20 μm diameter) into the scaffold matrix. For facile microscopy and immunoassay performance, the device needed to be optically transparent with accessible luminal and basal reservoirs. To encourage ready adoption of the method, the device should utilize a standard multi-well plate format without complex instrumentation such as valves and pumps. Additionally, the large intestine acts largely as a static waste storage organ and does not normally experience high luminal fluid flows (in contrast to the small intestine), so continuous fluid flow in the luminal compartment was not desirable.

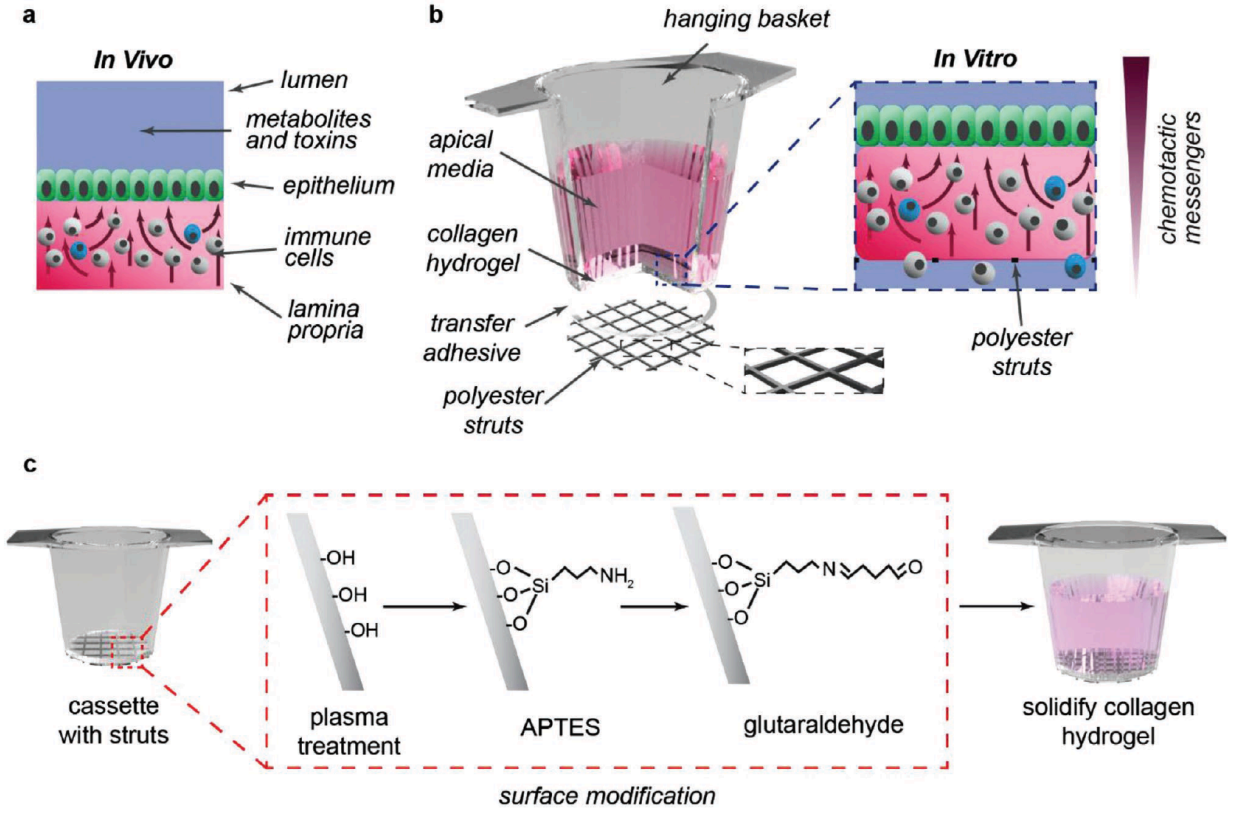

Figure 4.1. Design of cassettes for the suspended collagen scaffolds. a) Schematic of the *in vivo* relationship between the epithelium (green) and immune (white and blue) compartments of the large intestine. The arrows demonstrate the movement of the immune cells within the intestinal stroma (pink). b) Schematic of the components of the cassette with polyester struts supporting the collagen hydrogel (pink). The inset demonstrates the *in vitro* cell relationships. The basal fluid reservoir in which the cassette is placed is not shown. c) Schematic of device surface coating steps.

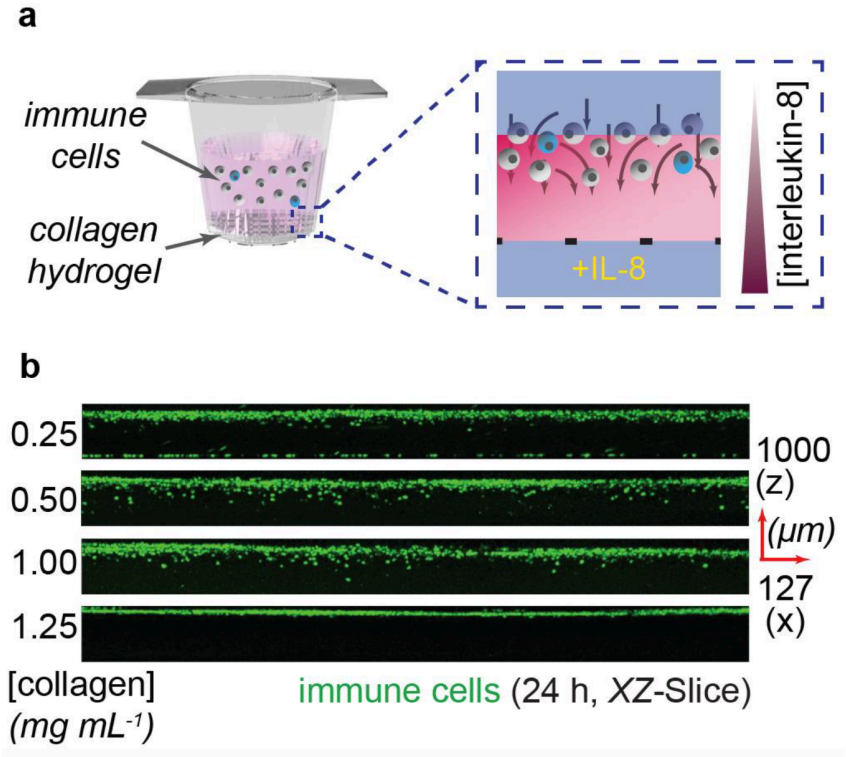

Figure. 4.2. Immune cell placement and behavior in the cassette with a supported scaffold. Scaffolds were formed from collagen at varying concentrations and then assayed for the ability of dHL60 immune cells (green) to migrate into the scaffold under an IL-8 gradient.

4.3.2. Cassette Construction and Fabrication

Most intestinal epithelial cell culture systems such as hanging baskets or microfluidic devices, use track-etched membranes or microfabricated films with small-sized openings to support the epithelial cells[157,172]. While these devices have enabled high-impact discoveries, the devices possess challenges in recreating epithelial-immune cell interactions. For example, the

membranes or films possess small pore openings, low porosity, and high stiffness (>1 MPa) and so they do not permit a physiologic contact between epithelial cells and white blood cells since the white blood cells are unable to move freely through these membranes or films (Table 4.1). In contrast, woven polyester stands possess large openings (up to 2.5 mm) and a very high percent open area (up to 60%). The polyester strands are also sufficiently rigid so that the strands could act as a network of supporting struts for soft hydrogels. Woven polyester strands with a range of openings (0.04–1.3 mm, 25%–59% open area) were affixed to the base of a polystyrene hanging basket (after removal of the hanging basket membrane) using a biomedical transfer adhesive (Figure 4.1b). Neutralized collagen was selected as the hydrogel since it is soft (100–200 Pa Young's modulus) and porous, supports colonic epithelial cell growth and can be invaded by immune cells (Figure 4.2) [167]. After placement of the basket on a sterile surface, collagen was loaded into and gelled within the lumen of the hanging basket to form a 3.33 mm thick slab at the base of the hanging basket and above the rigid polyester strands. For all openings between the struts except the 1.3 mm size, the collagen slab maintained its integrity when the basket was removed from the surface yielding a collagen hydrogel suspended above the polyester strands. Thus, the polyester strands acted as a system of supporting struts for the soft collagen hydrogel while leaving nearly all of the basal surface of the collagen hydrogel in direct contact with the basal medium (air in this instance or medium during cell culture). When visualized by transmitted light microscopy, the polyester strands were opaque but the collagen between the fibers was transparent, and most of the collagen basal surface was not obstructed by the polyester strands (Figure 4.3a). When the fluorescein-labeled collagen was placed into the basket and visualized by fluorescence microscopy, homogenous fluorescence across the hydrogel was present for all sizes of strand openings except the 1.3 mm size. For this biggest woven polyester

stand openings, the supporting polyester struts or strands were too far apart to support the soft collagen and the 1.3 mm size was not used further. Next, primary human colonic epithelial cells were loaded onto the suspended collagen and placed into an expansion medium (EM) rich in growth factors (Wnt-3A, R-spondin, and Noggin). The cells were cultured over 4 days until a confluent monolayer was formed. During this time all cultures demonstrated detachment of the hydrogel from basket inserts (Figure 4.3b). While the soft collagen supports colonic stem cell expansion and self-renewal, this hydrogel is susceptible to deformation from cellular contractile forces leading to collagen deformation[151,167,173]. To circumvent this issue, the polyester struts and polystyrene hanging basket were chemically modified to covalently bind to the suspended collagen with the goal of increasing collagen adhesion and decreasing the deformation of the hydrogel over time (Figure 4.1c). The hanging basket was incubated with 3-(aminopropyl)triethoxysilane (APTES) to add surface amino groups followed by incubation with glutaraldehyde to place reactive aldehydes on the surface of the basket and struts. These chemical moieties then reacted with amino acids (Cys, Lys, Arg) on the collagen covalently linking the collagen to the support structure. Since the reactive groups were localized to the strut/hanging basket surface, the collagen bulk was not cross-linked. When colonic epithelial cells were cultured on the suspended collagen scaffold, 100% of the suspended collagen hydrogels remained in place ($n > 50$). Since hanging baskets with a strut separation of 0.5 mm possessed the greatest percentage of open area and a stable suspended collagen scaffold, these baskets were used in all subsequent experiments.

Class	Available materials	Pore sizes (Openings)	Porosity (Open area)
Woven strands/inter-strut distances	Polyethylene, polypropylene, PTFE	0.01-67 mm^2	16%-61%
Track-etched membranes	Polycarbonate, PET	0.04-64.0 μm^2	$<1.5 \times 10^{-5}$%
Fibrous membranes	Biopore PTFE, mixed cellulose esters	0.04-0.16 μm^2	<80%

Table 4.1. Comparison of cell culture-compatible supports.

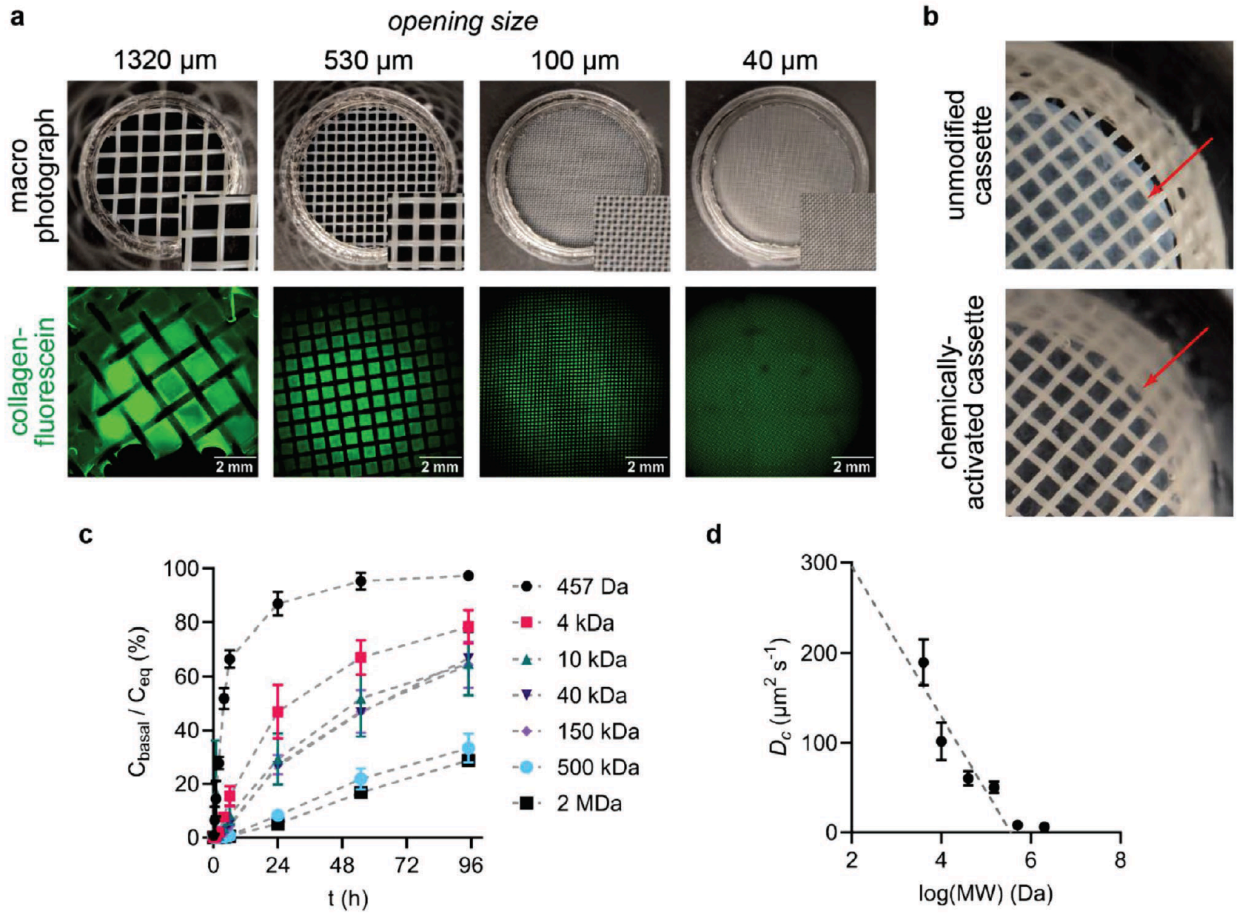

Figure 4.3. Characterization of the suspended collagen scaffold. a) Photographs (upper panels) and fluorescence images (lower panels) of polyester struts of varying spacing. The struts were attached to the base of the hanging basket and overlaid with fluorescein-labeled collagen. In the upper panels, the polyester struts are white and the suspended clear collagen between the struts is transparent and so appears black. Insets in the lower right hand of the image show a higher magnification view of the struts. The openings between the struts with a 40 µm spacing are difficult to visualize under these magnifications due to the small opening size. In the lower panels, the opaque struts are black and the fluorescein-labeled collagen is green. b) Photographs of suspended collagen on which epithelial cells were cultured. Upper panel - The collagen was overlaid onto non-activated polystyrene hanging basket/polyester struts. The red arrow marks where the collagen has pulled away from the hanging basket wall. Lower panel - The collagen was overlaid onto a chemically activated polystyrene hanging basket/polyester struts with cross-linking of the collagen to the hanging basket/struts at points of contact. c,d) Determination of diffusion coefficients for varying molecular weight compounds and estimation of molecular weight cutoff. c) Shown is the concentration of each dye in the basal compartment (C_{basal}) relative to its theoretical equilibrium concentration (C_{eq}) over the incubation period. Measurement of the movement of a low molecular weight dye (lucifer yellow) and varying molecular weight fluorescein-dextrans through the scaffold (n = 3). d) Plot of the measured diffusion coefficient (D_c) against the logarithmic transformation of the molecular weight to determine a theoretical molecular weight cutoff for the suspended collagen scaffolds (n = 3).

Molecular weight	Log (molecular weight) [Da]	Measured apparent D_c[$\mu m^2 s^{-1}$]	Theoretical D_c in H_2O [$\mu m^2 s^{-1}$]
457 Da	2.660	1014 ± 32	605
4 kDa	3.602	190 ± 15	223
10 kDa	4.000	102 ±12	146
40 kDa	4.602	60 ± 5	42
500 kDa	5.699	8 ± 1	24
2 MDa	6.301	6 ± 0.5	13

Table 4.2. Measured apparent and theoretical diffusion coefficients (D_c). Theoretical diffusion coefficients are derived from a Stokes–Einstein relation with hydrodynamic radii approximated according to Aimar et al. [174].

4.3.3. Characterization of the Suspended Scaffold

In vivo, the lamina propria is comprised of basement membrane and connective tissue that not only house stromal cells underlying the epithelium (e.g., immune and mesenchymal cells), but also facilitate their migration in response to bacterial invasion or biochemical messengers[175]. While it is established that the basement membrane, primarily composed of a fibrous network of collagen, enables free movement of these cell types in vivo, physicochemical properties such as density, porosity, and flexibility remain largely uncharacterized for isolated extracellular matrix devoid of cells[157,176]. The diffusion of solutes across in vitro scaffolds and culture systems has been subjected to rigorous study, however, with collagen-coated, track-etched membranes provide fractional diffusivities of solutes compared to their free diffusion in water,[51] and perforated PDMS culture systems impede transmigration of immune cells between segregated compartments [142,157,177]. We, therefore, benchmarked the permeability of our suspended hydrogel culture system by measuring the diffusivities of solutes possessing a range of molecular weights through the suspended collagen scaffold. Comparisons to their theoretical diffusivities in water were made to determine the degree of hindrance that the suspended scaffold provided and whether it might be suitable for immune cell migration assays. A concentrated fluorescent dye was added to the luminal compartment above a suspended collagen scaffold to generate a

gradient across the scaffold with dye passively diffusing from the luminal "source" compartment, through the suspended collagen, and into the basal "sink" compartment [178]. Dyes with a wide range of molecular weights (457 Da – 2 MDa) were used to determine the theoretical molecular weight cutoff (MWCO) for the scaffolds. The lowest molecular weight dye (457 Da) demonstrated rapid diffusion through the scaffold when incubated at 37 °C with near-identical luminal and basal dye concentration by 96 h (Figure 4.2c). Increasing the molecular weight of dissolved solutes predictably lowered the speed at which they diffused through the scaffold (Table 2), though remarkably, even the largest solute tested (2 MDa) demonstrated measurable diffusion (5 ± 4% of equilibrium concentration) over 24 h. Large biomolecules such as IgGs and IgMs possess molecular weights of ≈150 kDa and 1 MDa, respectively, so they and smaller molecules are able to migrate between the compartments of this system. To determine the degree to which diffusion of these compounds may be hindered by the scaffold, apparent diffusion coefficients were extracted by fitting the basal concentrations over time to a linearized model based on Fick's law [179]. This model assumes a two-compartment system separated by a membrane of a known thickness, which we define here as the suspended collagen scaffold. Binding sites for dextrans within collagen were assumed to be negligible. The measured apparent diffusion coefficients (D_c's) were similar to that derived from hydrogel photobleaching assays (Table 2) [179–181]. As expected the D_c for 40 kDa FITC-dextran in this system without bulk cross-linking of the collagen was higher than that reported for covalently cross-linked collagen (34 μm2 s−1), as the extensive covalent modifications within the collagen bulk decrease collagen permeability[182]. Diffusion was minimally hindered for the low molecular weight dyes as compared to dyes in an aqueous solution suggesting that the assumption of negligible binding sites for dextran within collagen was reasonable. But the diffusion of larger molecular weight

dyes was slowed by the scaffold. Thus, diffusional hindrance in these suspended collagen scaffolds was substantially less than that of conventionally used porous membrane supports. For example, track-etched membranes in common use demonstrate a solute diffusivity ratio for small molecules (<150 Da) of <0.25 [177]. Analysis of the linear range of a logarithmic transformation of solute molecular weight against measured D_c suggested a molecular weight exclusion limit of 357 kDa (Figure 4.2d). Since cytokines are soluble proteins with a lower molecular weight (≈6–70 kDa) than 357 kDa, the scaffold supports the movement of these molecules through the scaffold. Even very large molecules such as immunoglobulins (≈150 kDa) are predicted to cross the scaffold. Thus the epithelial cells and immune cells can communicate by secretion of cytokines and other molecules below the exclusion limit since these higher molecular weight molecules will permeate through the scaffold [178,183]. Lenzini and colleagues demonstrated that the mechanical properties of the extracellular matrix are responsible for regulating the transport of large biomolecules through nanoporous ECMs possessing a smaller pore size; here, a similar effect may be facilitated through flexible collagen fibers assembled into a soft hydrogel network, enabling molecules larger than the pore size to migrate or squeeze through [167,173]. The lack of cross-linking within the hydrogel bulk and the large open area between the struts was critical to supporting the movement of molecules of a wide range of molecular weights through the scaffold. In the context of cellular migration, it is also important to note that invasive cells are capable of deforming their three-dimensional shape and degrading their tissue microenvironment [184]. Taking these findings together with the high measured diffusivities, the suspended collagen system is likely suitable for cellular migration and crosstalk studies where other *in vitro* systems have fallen short due to diffusional or mechanical hindrance.

4.3.4. Growth of Primary Epithelial Cells on the Suspended Collagen

The epithelium of the colon is comprised of a monolayer of the following principal cell types: proliferative stem and transit amplifying cells, absorptive colonocytes, and mucous secreting goblet cells. Hormone-producing enteroendocrine cells are also present but are few in number. To determine the growth characteristics and establish the cell types within the intestinal epithelium on the suspended collagen, the monolayer was stained by immunocytochemistry and imaged at multiple time-points during expansion and differentiation. Human-derived colonic intestinal epithelial stem cells were seeded over the suspended collagen and cultured as a self-renewing monolayer [75,167]. The cells were cultured for 6 days in a growth factor-rich medium with Wnt, R-spondin, and Noggin (EM, Table 2.1) to support cell number expansion (Figure 4.4a). Once the cells formed a confluent monolayer (day 6), the medium was switched to a growth factor-depleted medium (DM) to support the differentiation of the cells. After varying days of culture, the cellular phenotype was measured by staining for EdU incorporation (S-phase proliferative cells), alkaline phosphatase (ALP, for colonocytes), mucin 2 (Muc2, for goblet cells), and Hoechst 33342 (DNA)[75,167]. The cells were then imaged by confocal fluorescence microscopy (Figure 4.4a). As expected, a majority of cells cultured in the presence of the growth-factor-rich medium remained proliferative (EdU+) with very few absorptive colonocytes (ALP+) [167]. Secretory goblet cells (MUC2+), one of the major cell types in the luminal differentiated epithelium in vivo were present on all days of culture as observed in prior culture systems (Figure 4.4a,c) [167]. After the removal of the growth factors, the number of EdU+ cells was significantly decreased suggesting the formation of a terminal, differentiated epithelium (Figure 4.4b) [167]. The intensity of ALP staining (on day 2 vs 8) increased significantly after conversion to a growth factor depleted medium as previously reported (Figure 4.4d) [167]. These

data suggested that the epithelial cell cultures on the suspended collagen were similar to that on a collagen slab with respect to cell proliferation and formation of the major differentiated cell types.

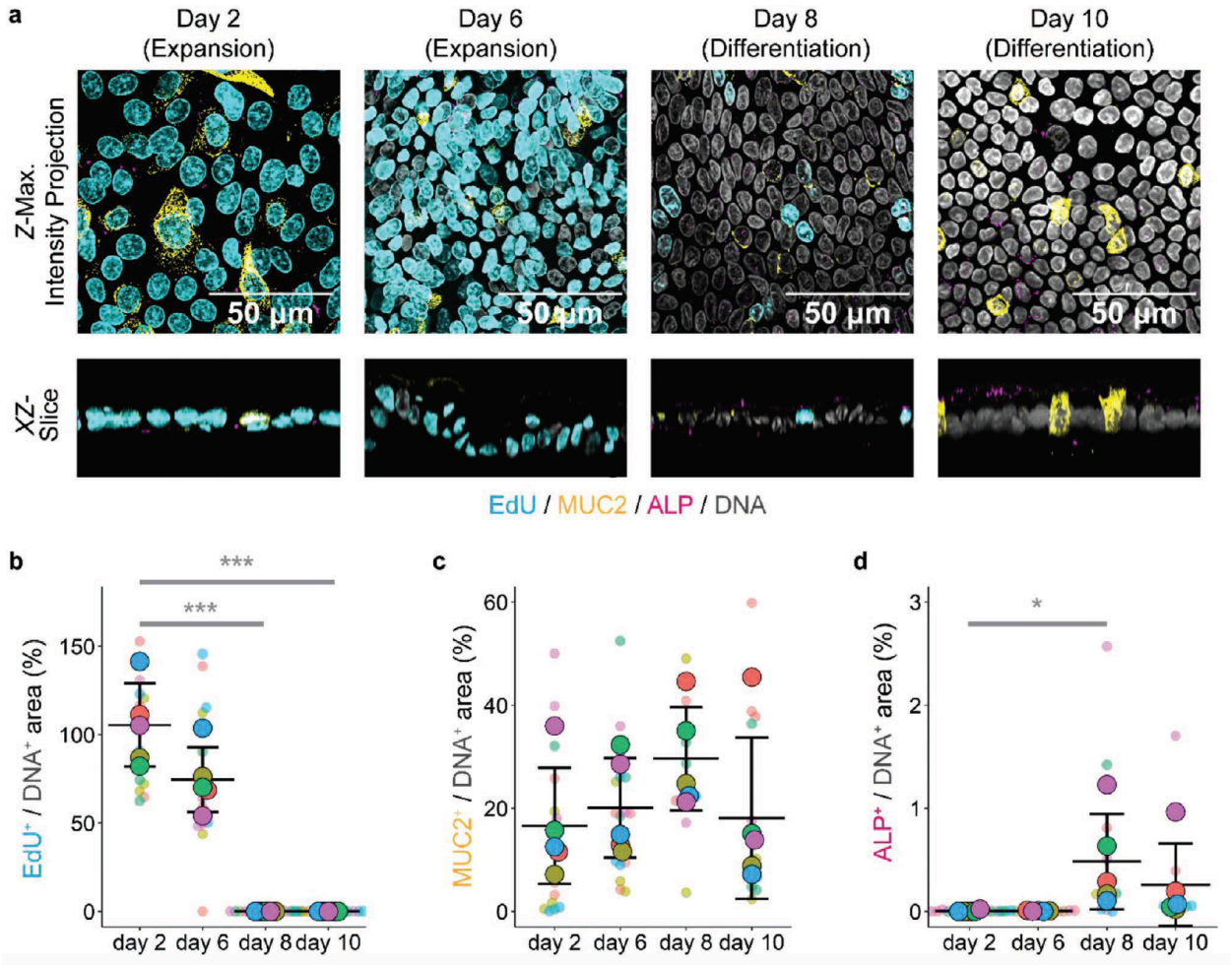

Figure 4.4. Cell growth and maturation on the suspended collagen. a) Images acquired by fluorescence confocal microscopy of cells labeled with Hoechst 33342 (white), stained for EdU incorporation (cyan), immunostained for anti-Muc2 (yellow), and assayed for ALP activity (magenta) on different days of culture. The top row of images is a z-focus stack projection (XY) view of the cultures while the lower row represents XZ cross-sections through the monolayer. b–d) Fluorescence staining was quantified by plotting the percentage of the culture area positive for b) EdU incorporation, c) MUC2 immunostaining or d) ALP activity relative to that stained by Hoechst 33342 (DNA). The transparent data points represent individual fields of view (FOVs) for each sample (5 FOVs imaged per cassette) and are color-coded by technical replicate, while the solid data points represent the mean value for each technical replicate (n = 5). The mean crossbar, error bars, and t-tests were calculated from the solid data points.

4.3.5. Characterization of Barrier Integrity of Primary Epithelial Cells on the Suspended Collagen

One of the chief functions of the colonic epithelium is to act as a barrier to prevent colonic microbiota, microbial products, and toxins from entering the body. This barrier function also serves to enable the colon to carry out its function of controlled absorption of ions and water from the feces. The ability of the confluent monolayer grown on the suspended collagen to act as a barrier to the movement of ions and larger molecules was assessed by measuring the transepithelial electrical resistance (TEER) and the permeability of lucifer yellow (LY). TEER values reflect ionic conductance via paracellular pathways across the epithelial layer [185]. TEER was measured as the monolayers grew to confluency in EM and then differentiated in DM (Figure 4.5a). On day 2 when the cells were present largely in isolated patches, the TEER was not significantly different from that of the scaffold in the absence of cells (31.2 ± 7.9 Ω cm2 vs 12.6 ± 2.4 Ω cm2, n = 9). By day 6, the cells formed a confluent monolayer in EM with TEER increasing to 176.5 ± 28.5 Ω cm2. Upon inducing differentiation of the monolayer under DM, TEER rapidly increased to a maximum on day 11 (Figure 4.5a). Over subsequent days, TEER began to decrease likely as a result of apoptosis of the terminally differentiated colonocytes as occurs in vivo [167].[38] These results suggest that once differentiated, the epithelial monolayer was resistant to the flow of ions through the paracellular spaces as is present in vivo [185]. Permeability reflects the ability of the colonic epithelium to act as a barrier to the passive transfer of small and large molecules. This property is dependent on the integrity of tight junctions between the cells and can be interrupted by inflammatory cells and factors [186]. Permeation of the small fluorescent, non-transported molecule LY was used to further evaluate the integrity of the monolayers. The apparent permeability (P_{app}) of LY through the cell monolayer was

measured over time and compared to that of the scaffold alone. The confluent monolayers on both days 8 and 10 displayed a P_{app} that was significantly lower than that of the suspended collagen without cells (Figure 4.5b). Since a P_{app} of <1 × 10−6 cm2 s−1 is considered impermeable and suitable for transport assays, these monolayers displayed barrier properties consistent with a mature colonic epithelium[187]. The colonic epithelium is made up of polarized cells having a luminal brush border and a basal surface adherent to the basement membrane of the lamina propria [188]. The intercellular borders are rich in tight and adherens junction proteins to enable the epithelium's barrier function [186]. To further analyze the characteristics of the differentiated epithelium on the supported hydrogel scaffold, the monolayers were immunostained for the presence and localization of proteins involved in intercellular adhesion, and establishment of luminal-to-basal polarity *in vivo* human gastrointestinal epithelium. Cross-section views (XZ confocal images) of the monolayers clearly demonstrated the appropriate columnar geometry of the cells (Figure 4.5c). Monolayers stained for actin and villin, proteins enriched in the brush border of the epithelium, demonstrated the proper luminal localization of these proteins in the monolayer [189,190]. Likewise, staining for integrins, proteins that recognize collagens and laminins in the lamina propria, demonstrated enriched staining at the basal surface of the monolayer adjacent to the hydrogel. These results suggest that the epithelial monolayer grown on the suspended collagen was properly polarized in a basal-to-luminal direction. The expression and localization of tight junction and adherens junction proteins were also assessed. Zonula occludens-1 (ZO-1), occludin, and claudin are luminally restricted tight junction proteins between cells (Figure 4.5c). These proteins showed rich staining at cell-cell junctions and were localized along the luminal aspect of the monolayer in the cross-section. Likewise, the cells expressed E-cadherin, a basolateral adherens junction

protein, in a proper orientation as seen in the cross-section. These data demonstrate that the monolayer cultures were grown on the supported hydrogel scaffold to express structural proteins in the appropriate cellular locations.

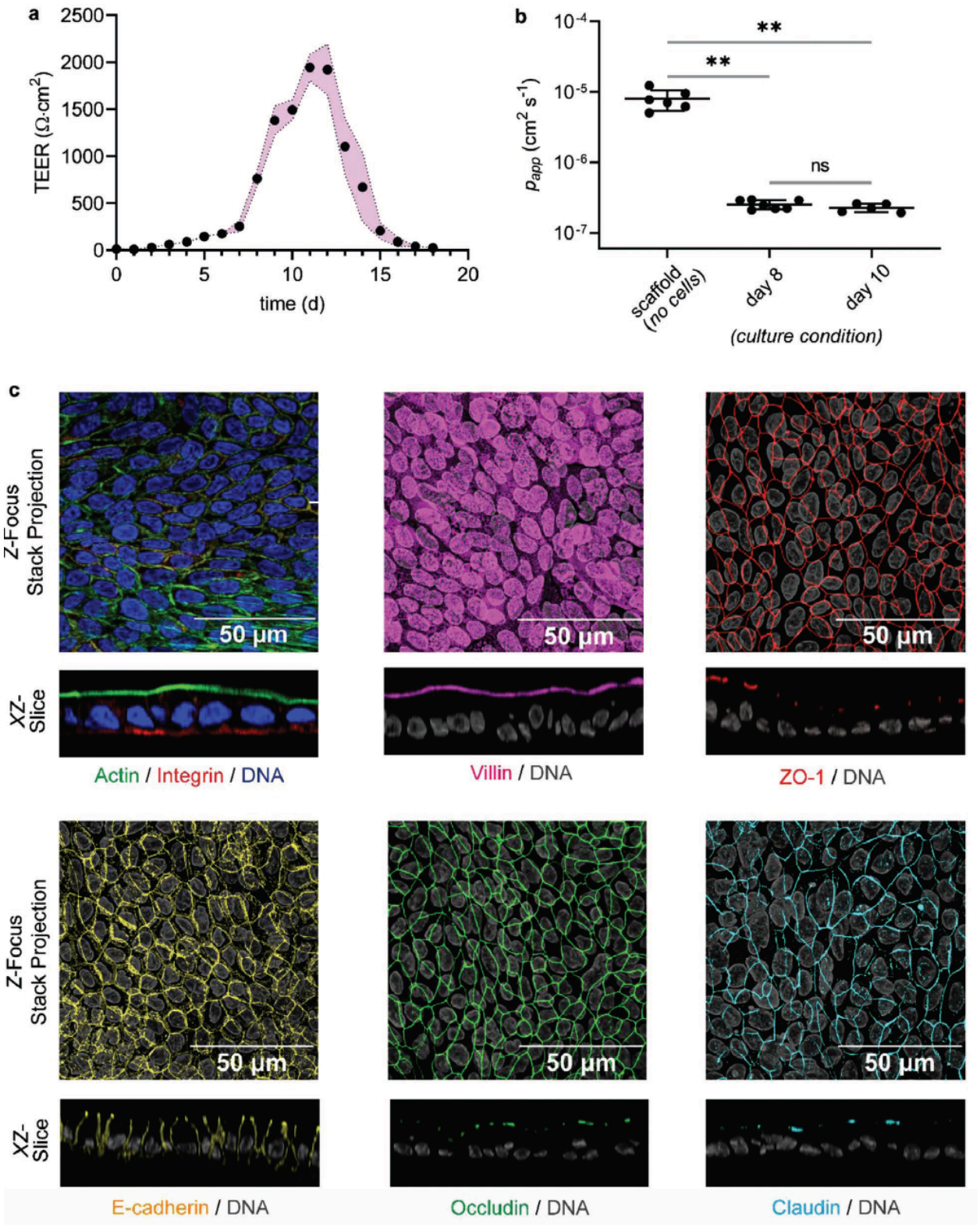

Figure 4.5. Barrier integrity of suspended epithelial monolayers. a) Measurements of TEER values for cultures during the culture protocol are shown in Figure 3a. The pink-shaded region

represents a single standard deviation (n = 5). b) Apparent permeability of epithelial monolayers to lucifer yellow at different times of culture (n = 8, with ROUT q = 1% removing outliers due to manually damaged scaffolds). c) Fluorescence confocal microscopy of day-10 cells stained for various proteins. The top row of images is the maximum intensity Z-projections (XY) of the cultures while the lower row represents XZ cross-sections through the monolayer. Hoechst 33342 labeling of DNA is depicted in blue in the top left panel but white in all other panels.

4.3.6. Epithelial-Immune Cell Response to Clostridium difficile Toxin A

The coculture system was exposed to a well-characterized bacterial toxin known to incite an innate immune response, previously demonstrated to disrupt colonic barrier integrity and cytoskeletal organization, and elicit rapid and directional IL-8 secretion [170,191]. The wide openings between the supporting struts of the cassette facilitate the interaction of the epithelial and immune cells (i.e., dHL-60s), as both the luminal and basal faces of the hydrogel scaffold remain exposed to their respective media compartments throughout the entire culture period. The epithelial cells were seeded, expanded, and differentiated over the suspended collagen for 8 d of culture (Figure 4.6a). On day 8, the epithelial cells on the scaffold were stained with CellMask DeepRed. The cassette with epithelial cells was inverted and a suspension of immune cells pre-labeled CellTracker Green CMFDA was applied to the basal surface of the scaffold. After a 30 min adhesion time, the hanging basket was inverted and returned to a multi-well plate with media. The immune cells remained attached to the basal surface of the scaffold for >24 h of suspended culture (Figure 4.6b). This suggests the establishment of focal adhesions that would be hindered if extracellular matrix proteins were not present or if cell-binding domains on the scaffold were quenched through covalent cross-linking within the collagen [92,96]. Toxin A derived from C. difficile (TcdA) was added to the luminal compartment of the basket insert to elicit IL-8 secretion for the *in situ* recruitment of immune cells toward the epithelial surface. In the presence of TcdA, the immune cells migrate upward toward the epithelial surface, eventually

transmigrating across the epithelium and into the luminal compartment, as in vivo [157]. This effect can be observed as early as after 4 h of TcdA exposure (Figure 4.6c). By 24 h of exposure, immune cell recruitment into the scaffold was further enhanced relative to that of cultures without TcdA. To assess whether secreted chemoattractants might be inducing migration of the immune cells, IL-8 was assayed in the basal medium compartment. The basal IL-8 concentration was significantly higher in the basal compartment in the presence of luminal TcdA compared to that without (Figure 4.6d). These results demonstrate the feasibility for in vitro immune cell recruitment by primary colonic epithelium followed by transmigration of the immune cells.

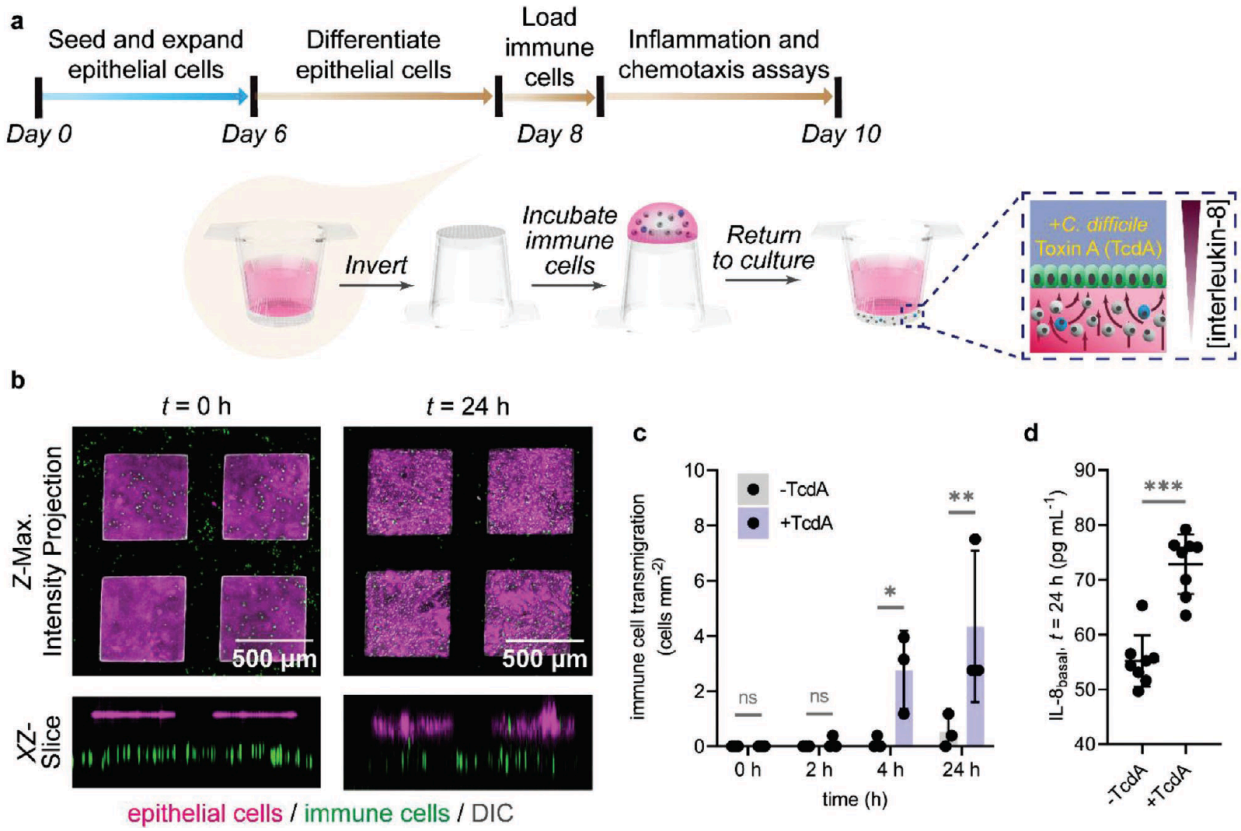

Figure 4.6. Immune cell chemotaxis in response to C. difficile toxin A. a) Timeline of the experiment. The right panel illustrates the cell relationships shortly after the addition of the toxin. b) Fluorescence images acquired by confocal microscopy at 0 and 24 h after toxin addition to the immune epithelial cell culture. The top row of images is a summed Z-stack (XY) view while the lower row represents an XZ cross-section through the monolayer. Shown are epithelial cells (magenta) and CellTracker Green stained dHL-60 cells (green). The opaque polyester struts are

black and the cells on the suspended collagen (2 × 2 regions) between the struts are shown. c) Density of cells measured as the number of cells crossing the scaffold per scaffold surface area over 24 h with and without TcdA exposure. The solid bars represent the average of the data points (black circles) while the error bars represent a single standard deviation (n = 3). d) IL-8 measurements after 24 h with and without TcdA exposure in the basal reservoir (n = 8). Data points are shown as black circles while the upper and lower bars represent a single standard deviation from the mean (middle bar).

4.4. Discussion

A suspended collagen hydrogel supported by and cross-linked to widely spaced, polyester struts provided a scaffold possessing biophysical properties compatible with the simultaneous culture of normal stem-cell-derived colonic epithelium and migratory inflammatory cells. The immune cells were capable of migrating through the hydrogel toward an innate cytokine source produced by the epithelium in response to a biological insult. This system was able to maintain a TEER > 500 Ω cm2 for 7 days and is, therefore, most suitable to mimic the acute inflammation. IL-8 secretion was readily measured in response to acute inflammation and in the future additional cytokines (IL-6, TNF-α, and IL-1β) should be measured due to the presence of the immune cells since the entire cytokine network plays a role in the acute inflammation process. To mimic chronic inflammation for IBD studies, a self-renewing intestine tissue (such as the in vitro 3D crypt possessing a stem cell niche and differentiated cell zone with a long lifespan) can be used [75]. This in vitro microphysiological system recapitulated several tissue-scale responses that result from gastrointestinal infection including immune cell infiltration of the scaffolding/ stroma. In the future, it will be important to further refine the system to incorporate primary immune cells including those isolated from infiltrates within the human large intestine. The platform can be expected to be of value in conducting high-content assays of cellular interactions between the human colonic epithelium and its immune compartment.

4.5. Methods

4.5.1. Formation of Suspended Collagen Hydrogels

Each cassette with a suspended collagen hydrogel was fabricated from three components held together with a biocompatible transfer adhesive (1504XL, 3M): i) a modified polystyrene hanging basket (353180, Corning), ii) a neutralized collagen hydrogel, and iii) woven polyester struts or strands (9218T68, McMaster–Carr). Hanging baskets (353180, Corning) were disassembled by removal of the pre-installed membrane using a razor blade. Woven polyester strands or struts (9218T68, McMaster–Carr) were manually fixed to the base of the hanging basket with a biocompatible transfer adhesive (1504XL, 3M). The hanging basket with attached struts was immersed in a solution of 1% (w/v) Alconox dissolved in deionized (DI) water (18.2 MΩ·cm, Milli-Q IQ 7000, Millipore-Sigma), bath sonicated for 1 h, and incubated at ambient temperature (20 °C) overnight. Thereafter, the cassettes were sequentially rinsed five times with DI water and once with 75% (v/v) ethanol prior to drying under compressed air and plasma treating at 30 W for 5 min (PDC-001, Harrick Plasma). The devices were then immediately immersed in a 5% (v/v) (3-aminopropyl) triethoxysilane (APTES) (440140, Millipore-Sigma) in DI water solution and incubated for 30 min. The silane-treated surfaces were then rinsed in 1 L of DI water five times, dried under compressed air, and immersed in the second solution of 1% (w/v) glutaraldehyde (G6257, Millipore-Sigma) in DI water for 30 min. These devices with aminereactive surfaces (struts and hanging basket walls) were sequentially rinsed in 1 L DI water five times and cleansed in 75% (v/v) ethanol for 5 min before transferring into an aseptic biosafety cabinet for collagen hydrogel formation.

To prevent aqueous collagen from flowing around the struts prior to gelation and out of the hanging basket, parafilm was applied to the base of each insert below the struts and the

assemblies were placed into 12-well companion plates (353503, Corning). Collagen Type 1, rat tail in 20 mM acetic acid (354236, Corning) was diluted to 1.25 mg mL^{-1} in an ice-cold neutralization buffer.[38] The neutralization buffer was formulated so that the final constituent concentrations equated to: 1 × PBS (46-013- CM, Corning), 20 mM HEPES (25-060-CI, Corning), 53 mM sodium bicarbonate (25-035-CI, Corning), and NaOH (S2270, Millipore-Sigma) equimolar to acetic acid, at pH 7.4. 300 μL of neutralized collagen (1.25 mg mL^{-1}) was added to the luminal side of the hanging well basket with attached struts and placed at 37 °C under 5% CO2 for 2 h to solidify the hydrogel. The hydrogels were then overlaid with 1 mL of 1× PBS and incubated for at least 24 h at 37 °C. Any residual amine-reactive sites on the surfaces of the hanging basket or struts were quenched by incubation of 1 mL of 10 μg mL^{-1} Type 1 human collagen (#5007, Advanced Biomatrix) in 1× PBS overnight at ambient temperature (20 °C). Prior to cell culture, the parafilm was removed and each scaffold was rinsed with 3 mL of 1× PBS (1 mL luminal, 2 mL basal), followed by the expansion medium (EM, Supporting Information, 0.5 mL luminal only). Schematics of the hanging baskets with the strut-supported hydrogel were created using Autodesk Fusion 360 (San Rafael, CA).

4.5.2. Culture of Primary Human Colon Epithelial Cells

The human colonic epithelial biopsy specimen (male, 52 y) was obtained during a routine screening colonoscopy performed at the University of North Carolina (UNC) Hospitals Meadowmount Endoscopy Center under UNC IRB #14-2013. The epithelial cells were expanded following a previously reported monolayer culture protocol (RRID:CVCL_ZL23, Supplementary Material) [100,167]. For seeding onto the suspended hydrogels, cells were passaged from a six-well maintenance/expansion plate (9.6 cm2 well−1, ≥ 80% confluency) with one well from a six-

well plate being subcultured into four suspended collagen scaffolds. These cultures were expanded to confluency for 6 days within an expansion medium (EM) containing Wnt3a, R-spondin 3, and noggin, before differentiation for 4 days within a differentiation medium (DM) that was absent in these growth factors. Medium (1 mL) was added to the luminal reservoir above the suspended collagen hydrogel, and 2 mL of medium was added to each basal reservoir below the suspended hydrogel, with media replenishments occurring every 48 h. The primary cells tested negative for mycoplasma contamination (LT07-118, Lonza) and were discarded after passage 15 to minimize genetic drift. To induce acute inflammation, toxin A derived from C. difficile (ab123999, Abcam) at 0 or 12 μg mL^{-1} was added to the luminal side of the human colonic epithelial monolayers. Barrier Integrity Measurements: Throughout culture, transepithelial electrical resistance (TEER) was measured using an EVOM2 Epithelial Voltohmmeter (World Precision Instruments, Sarasota, FL). Background measurements in ohms were obtained from suspended collagen scaffolds without cells, which were subtracted from each experimental measurement and normalized to the basal surface area of the suspended collagen scaffold (0.9 cm2). Paracellular transport of lucifer yellow (LY, 457 Da) was also utilized as an endpoint assessment of barrier integrity [192]. Stock solutions of LY (L453, ThermoFisher Scientific) were prepared in 1.5 mL aliquots at a concentration of 2 mM in HBSS (14025076, ThermoFisher Scientific) and stored at −20 °C until the time of assay. For LY permeability measurements, each suspended collagen scaffold was rinsed with 3 mL of 1× PBS (1 mL luminal, 2 mL basal) and 0.5 mL of LY solution (200 μM in phenol red-free differentiation medium, Supporting Information) was dispensed into each luminal reservoir. Basal reservoirs were each filled with 1.5 mL of phenol red free differentiation medium possessing no LY. The samples were incubated within a humidified CO_2 incubator set to 37 °C and 5% CO_2 for 6 h.

Thereafter, media from the basal reservoirs was sampled and LY fluorescence from each solution was measured on a Spectramax M5 plate reader (Ex: 430 nm, Em: 535 nm, Molecular Devices Corporation, San Jose, CA). The apparent permeability (P_{app}) of the epithelial monolayers was calculated using the following equation, where C_b is the measured LY concentration in the basal compartment at 6 h, V is the basal reservoir volume (1.5 cm^3), A is the monolayer surface area (0.9 cm^2), t is the incubation time (6 h), and C_a is the LY concentration in the luminal compartment at 0 h:

$$P_{app} = \frac{[C_b] \times V}{A \times t \times [C_a]}$$

4.5.3. Culture of HL-60 Model Immune Cell Line

HL-60 cells (human acute promyelocytic leukemia, ATCC No. CCL-240, RRID:CVCL_0002) were obtained from American Type Culture Collection (ATCC, Manassas, VA) and cultured in IMDM with GlutaMAX and 25 mM HEPES (31980030, ThermoFisher Scientific), supplemented with 20% heat-inactivated FBS (S11150, Atlanta Biologicals) and 50 μg mL^{-1} primocin (ant-pm-2, InvivoGen). Cells were maintained at a density between 2 × 105 cells mL^{-1} and 2 × 106 cells mL^{-1} in T-75 flasks (353136, Corning) within a humidified incubator at 37 °C and 5% CO_2, requiring passaging into fresh medium every 5–6 days. Cell lines were discarded after passage 10 from the original ATCC stocks to minimize genetic drift interferences.

Chemotactic, neutrophil-like cells were derived from HL-60 cultures through differentiation with dimethylsulfoxide (DMSO) [193,194]. Once HL-60 cultures reached a density of 1.5 – 2 × 106 cells mL^{-1}, the cells were passaged into a fresh medium containing 1.5% (v/v) DMSO

(D2650, Millipore-Sigma) at a density of 2 × 105 cells mL^{-1} in T-25 flasks (10062-868, VWR). The cells were cultured in this medium for 5 days, during which proliferation ceased and the cells became migratory. On day 8 of culture under DMSO, the differentiated HL-60 (dHL-60) cells were harvested, stained with 10 μM Cell Tracker Green CMFDA (C2925, ThermoFisher) for 30 min, and loaded onto the inverted suspended collagen scaffold at a concentration of 250000 cells mL^{-1} (100 μL) for an additional 30 min in a humidified CO2 incubator.

4.5.4. Endpoint Image Acquisition and Analysis

Fixed cells were assayed by fluorescence imaging of DNA (Hoechst 33342, B2261, Millipore-Sigma), 5-ethynyl-2'-deoxyuridine (EdU) incorporation (A10044, ThermoFisher Scientific), alkaline phosphatase (ALP) activity (SK-5100, Vector Laboratories), mucin-2 (MUC2) presence (sc-515032 AF488, Santa Cruz Biotechnology), actin localization (R37110, ThermoFisher Scientific), integrin-β4 localization (sc-9090, Santa Cruz Biotechnology), villin localization (sc-28283, Santa Cruz Biotechnology), claudin localization (71-7800, ThermoFisher Scientific), occludin localization (13401-1-AP, Proteintech), E-cadherin localization (sc-7870, Santa Cruz Biotechnology), and zonula occludens-1 (ZO-1) localization (21773-1-AP, Proteintech Group) using established labeling methods [75,167,195]. Confocal fluorescence microscopy was performed on an inverted Olympus Fluoview 3000 (Waltham, MA) equipped with 405, 488, 561, and 640 nm laser diodes operating in conjunction with a galvanometer scanner. Emission wavelengths (Hoechst: 430–470 nm, Cy5: 650–750 nm, AF 488: 505–545 nm, Texas Red: 600–640 nm) were selected from manufacturer-provided control software. All samples were mounted over a glass coverslip in a fructose/glycerol clearing solution and imaged as separate ROIs. Using the 4× objective (N.A. 0.16, UPlanSApo4X), regions of interest (ROIs)

were manually selected and imaged at 1× digital zoom (3.11 μm px−1, 1024 px2 area) with at least three z-series optical sections collected at a step size of 25 μm to account for sample thickness[196]. For select proteins (F-actin, E-cadherin, ZO-1) and other representative markers specified in the main text, a 30× silicone oil immersion objective (N.A. 1.05, correction collar: 17 mm/23 °C, UPlanSApo30XS) with 2× digital zoom (0.21 μm px−1, 1024 px2 area) was employed.

Image areas positive for EdU incorporation, mucin-2, immunostaining, and alkaline phosphatase activity were quantitatively evaluated and normalized to the Hoechst 33342-positive area (DNA). Initially, z-series optical stacks were subjected to three-dimensional constrained iterative deconvolution in cellSens Dimension v1.18 (Olympus Corp.) utilizing 20 iterations of an advanced maximum likelihood algorithm, with automatic denoising, background removal, and edge protection options enabled. The deconvolved images were flattened into 2D representations through maximum intensity z-projections and thereafter imported into CellProfiler v4.1.3 for further processing and segmentation[196]. Each 2D image was flat-field corrected using a gaussian-smoothed illumination correction function (100 px filter size). The corrected images were converted to binary using a global 3-class Otsu threshold selection with the middle pixel intensity class assigned to the foreground (DNA, EdU) or background (MUC2). A global 2-class Otsu threshold selection was utilized for ALP. The area occupied by each fluorescent marker was measured and exported to a spreadsheet.

4.5.5. Live-Cell Image Acquisition and Analysis

Live colonic epithelial cells and differentiated HL-60 cells were stained with CellMask DeepRed (1:1000 dilution, C10046, ThermoFisher Scientific) and CellTracker Green CMFDA

(10 μM, C2925, ThermoFisher Scientific), respectively, for 30 min within a humidified CO2 incubator at 37 °C. Immune cells were placed onto the basal surface of the suspended collagen scaffolds as described above. The epithelial cells were then cultured on the luminal surface of the suspended collagen scaffold as above and the scaffold with cells was transferred to a humified Tokai Hit stage top incubator (Cat. no., STXG-IX3WX-SET, Flow rate: 75–250 mL min^{-1}, TOKAI HIT USA INC. Bala Cynwyd, PA) set to 37 °C with a continuous flow of 5% medical grade CO_2. Imaging via confocal fluorescence microscopy at 0, 2, 4, and 24 h of culture was performed on an inverted Olympus Fluoview 3000 (Waltham, MA) equipped with 405, 488, 561, and 640 nm laser diodes operating in conjunction with a high-speed resonant scanner. Emission wavelengths (CellMask DeepRed: 650–750 nm, CellTracker Green: 505–545 nm) were selected from manufacturer-provided control software. Using the 4× objective (N.A. 0.16, UPlanSApo4X), regions of interest (ROIs) were manually selected and imaged at 1× digital zoom (3.11 μm px^{-1}, 512 px2 area) with at least 20 z-series optical sections collected at a step size of 25 μm to account for sample thickness. Z-series optical stacks were subjected to three-dimensional constrained iterative deconvolution utilizing 20 iterations of an advanced maximum likelihood algorithm, with automatic denoising, background removal, and edge protection options enabled, and immune cell positions relative to the epithelial monolayer were manually annotated in cellSens Dimension v1.18 (Olympus Corp.).

4.5.6. Estimation of Theoretical Diffusion Coefficients for Dextran

The theoretical diffusion coefficient was estimated from the Stokes–Einstein equation for the diffusion of spherical particles through a liquid with a low Reynolds number D = (kT)/(6 phr) where k = Boltzman's constant, T = absolute temperature, h = dynamic viscosity and r = radius

of a spherical particle[197]. The approximate radius of the different molecular weight dextran was estimated from the equation relating molar mass to radius $r = 0.33(MM)^{0.46}$ where MM = molar mass [174,198]. The calculation assumes that the concentration of binding sites for dextran within the collagen was minimal.

4.5.7. Statistical Comparisons

Statistical analyses were performed using GraphPad Prism 8.1.2 (GraphPad Software, San Diego, CA) at a significance level (α) of 0.05 unless otherwise noted. Group means for permeability measurements (n = 6 condition–1) were compared by one-way Welch ANOVA to account for unequal variances (F-test, $p < 0.001$) followed by a Dunnett T3 test to determine p-values. Group means from the immune cell transmigration counts (n = 3 condition−1) were compared using two-way repeated measures ANOVA followed by Šidák's multiple comparison test to determine p-values. Group means from IL-8 ELISA measurements (n = 8 condition−1) were compared using an unpaired, two-tailed t-test.

Cell growth comparisons were performed in RStudio v1.3.1056 (RStudio Team, Boston, MA) running R x64 v4.0.2 (R Core Team, Vienna, Austria) [199]. SuperPlots were generated by pooling the means of the stained surface area percentages (EdU, MUC2, or ALP positive area normalized to DNA positive area) from each suspended collagen scaffold, reducing the sample size from the total fields of view that were imaged (n = 5 FOVs cassette−1, 5 cassettes condition−1 or 25 FOVs condition−1) to the number of technical replicates (n = 5 cassettes condition−1), followed by a one-way ANOVA with Dunnett's multiple comparison test to determine p values [200].

Unless specified, data are presented as sample means with error bars depicting one standard deviation from the mean, and for statistical comparisons, p values are represented as follows: * for $p \leq 0.05$, ** for $p < 0.01$, and *** for $p < 0.001$.

Chapter 5: Summary and conclusions

5.1. Development of an in vitro model of intestinal tissue to study fibroblast and epithelial cell interplay

The work conducted in chapter 2 demonstrates the feasibility of modeling fibroblast-epithelial cell interactions *in vitro*. The model systems exhibited characteristics similar to those witnessed *in vivo* with proper barrier function, cell phenotype, crypt organization and gene expression. The two distinct architectures, planar and molded 3D crypts, represent new tools that will be useful for drug testing, disease modeling, and other cellular biology investigations in the future. In these primary experiments it was found that fibroblasts act in a supportive role, leading to enhanced epithelial survival and an increased number of viable crypts. Though crypts with fibroblasts and epithelium had, on average, fewer proliferative cells overall, the proliferative cell zone was smaller and perhaps more representative of the *in vivo* microenvironment. Lastly, bulk RNA-sequencing of molded 3D crypt tissue samples revealed that gene expression is also altered when fibroblasts and epithelial cells are cultured together *in vitro,* and the genes identified merit further investigation.

This model is useful and representative of a human tissue, though there is still room for improvement. The system could be further characterized by interrogating fibroblast phenotype. Understanding the fibroblasts, and whether they exhibit a more active myofibroblast phenotype, could also be useful for devising a strategy to increase fibroblast coverage in coculture. Additionally, *in vivo* fibroblasts fill the entire lamina propria rather than just lining the walls of colonic crypts, so fibroblasts should be integrated throughout the scaffold in the next iterations of this model. Finally, spatial transcriptomic analysis of the *in vitro* crypts would make this tool extremely powerful. Single cell RNA-sequencing would allow for the study of rare phenotypes

and more minute changes to the *in vitro* tissue due to imposed conditions. Insights from this controlled environment would likely be impossible to extract from live human tissue further emphasizing the importance of this *in vitro* model.

5.2. Modeling colonic fibrosis with fibroblasts and epithelium on a stiffened collagen hydrogel

Intestinal fibrosis is the result of excessive ECM deposition, and it results in an obstructed, stiff bowel. In chapter 3 a model is described which mimics the biophysical characteristics of this pathology with a collagen hydrogel that has been formed from a high-concentration collagen stock. The result is a scaffold with diffusion and stiffness properties that mimic those found *in vivo* for both healthy and fibrotic tissue. Fibroblasts play an important role in fibrinogenesis and progression of fibrosis and in this case the mesenchymal cells could be cultured on the *in vitro* scaffold with or without epithelium for observation. While there was little change observed in fibroblasts on the stiff scaffold when compared to the softer, healthy stiffness hydrogel, the epithelium morphology and phenotype was altered in a fibrotic context. A bidirectional relationship between fibroblasts and epithelium was also observed within this *in vitro* model similar to what was seen in chapter 2, and this coculture method will enable future testing regarding fibroblasts role in fibrosis development or recovery. This fibrotic mimic could be improved by introducing some of the biochemical aspects of fibrosis. For example, inflammatory signaling is often a trigger of fibrosis and TGF-β stimulation (while omitting TGF-β antagonists from the cell medium) could be a simple way to mimic this effect *in vitro*. Additionally, fibrosis often accompanies Ulcerative Colitis or Crohn's disease, so integrating primary epithelium or fibroblasts from patients with these diseases could aid in understanding how tissue stiffness

impacts these conditions. Cancer is also more likely in patients with IBD and fibrosis so it could be useful to include CRC cells or even cancer associated fibroblasts within the pre-stiffened scaffold.

5.3. A suspended collagen hydrogel for modeling epithelial and immune cell interactions

In chapter 4 an easy to produce, mesh-suspended hydrogel model was devised and validated enabling observable epithelial cell culture and immune cell migration. Proliferative and differentiated epithelial cell phenotypes were observed and the monolayer exhibited increasing TEER and expressed several key tight junction markers (ZO-1, Claudin, Occludin, E-cadherin). Lastly, macrophages were able to traverse the collagen hydrogel and increased migration was observed in the immune cells in response to luminal stimuli following epithelial barrier injury. In the future it will be useful to monitor the migration of other cells, including a peripheral blood mononuclear cell (PBMC) population. Integrating other stimuli, like bacterial from the microbiota or digested nutrient components could also increase the number of applications for which this system could be useful. Migration is also an important characteristic of metastatic colon tumor cells and resident mesenchymal cells in the lamina propria, and the techniques described in chapter 4 could be used to observe these phenomena *in vitro* as well.

References

[1] L.L. Azzouz, S. Sharma, Physiology, Large Intestine, StatPearls (2021). https://www.ncbi.nlm.nih.gov/books/NBK507857/ (accessed June 10, 2022).

[2] J. Reinus, D. Simon, Gastrointestinal anatomy and physiology : the essentials, (n.d.) 188. https://www.wiley.com/en-us/Gastrointestinal+Anatomy+and+Physiology%3A+The+Essentials-p-9780470674840 (accessed May 10, 2023).

[3] D.S. Levine, R.C. Haggitt, Normal histology of the colon, Am. J. Surg. Pathol. 13 (1989) 966–984. https://doi.org/10.1097/00000478-198911000-00008.

[4] L.W. Peterson, D. Artis, Intestinal epithelial cells: regulators of barrier function and immune homeostasis, Nat. Rev. Immunol. 2014 143 14 (2014) 141–153. https://doi.org/10.1038/nri3608.

[5] R. Okumura, K. Takeda, Maintenance of gut homeostasis by the mucosal immune system, Proc. Jpn. Acad. Ser. B. Phys. Biol. Sci. 92 (2016) 423. https://doi.org/10.2183/PJAB.92.423.

[6] H. Clevers, The intestinal crypt, a prototype stem cell compartment, Cell 154 (2013) 274. https://doi.org/10.1016/j.cell.2013.07.004.

[7] J.N. 1711-1756 Lieberkühn, Dissertatio anatomico-physiologica de fabrica et actione villorum intestinorum tenuium hominis, (1760). https://archive.hshsl.umaryland.edu/handle/10713/3443 (accessed May 10, 2023).

[8] C.W. Tan, Y. Hirokawa, B.S. Gardiner, D.W. Smith, A.W. Burgess, Colon Cryptogenesis: Asymmetric Budding, PLoS One 8 (2013) e78519. https://doi.org/10.1371/JOURNAL.PONE.0078519.

[9] N. Barker, M. van de Wetering, H. Clevers, The intestinal stem cell, Genes Dev. 22 (2008) 1856. https://doi.org/10.1101/GAD.1674008.

[10] J. Paneth, Ueber die secernirenden Zellen des Dünndarm-Epithels, Arch. Für Mikroskopische Anat. 31 (1887) 113–191. https://doi.org/10.1007/BF02955706/METRICS.

[11] G. Bizzozero, Ueber die schlauchförmigen Drüsen des Magendarmkanals und die Beziehungen ihres Epithels zu dem Oberflächenepithel der Schleimhaut Dritte Mittheilung: Hierzu Tafel VII-X, Arch. Für Mikroskopische Anat. 42 (1893) 82–152.

https://doi.org/10.1007/BF02975307.

[12] G.E. Kaiko, S.H. Ryu, O.I. Koues, P.L. Collins, L. Solnica-Krezel, E.J. Pearce, E.L. Pearce, E.M. Oltz, T.S. Stappenbeck, The Colonic Crypt Protects Stem Cells from Microbiota-Derived Metabolites, Cell 165 (2016) 1708–1720. https://doi.org/10.1016/j.cell.2016.05.018.

[13] Carlos Andrés Chacón-Martínez, Janis Koester, Sara A Wickström, Signaling in the stem cell niche: regulating cell fate, function and plasticity, Development 145 (2018). https://doi.org/10.1242/DEV.165399.

[14] N. Pentinmikko, R. Lozano, S. Scharaw, S. Andersson, J.I. Englund, D. Castillo-Azofeifa, A. Gallagher, M. Broberg, K.Y. Song, A.S. Carvajal, A.T. Speidel, M. Sundstrom, N. Allbritton, M.M. Stevens, O.D. Klein, A. Teixeira, P. Katajisto, Cellular shape reinforces niche to stem cell signaling in the small intestine, Sci. Adv. 8 (2022) eabm1847. https://doi.org/10.1126/sciadv.abm1847.

[15] P. De Santa Barbara, G.R. Van Den Brink, D.J. Roberts, Development and differentiation of the intestinal epithelium, Cell. Mol. Life Sci. 60 (2003) 1322–1332. https://doi.org/10.1007/S00018-003-2289-3/METRICS.

[16] A.J.M. Santos, Y.H. Lo, A.T. Mah, C.J. Kuo, The Intestinal Stem Cell Niche: Homeostasis and Adaptations, Trends Cell Biol. 28 (2018) 1062–1078. https://doi.org/10.1016/J.TCB.2018.08.001.

[17] J. Schuijers, J.P. Junker, M. Mokry, P. Hatzis, B.K. Koo, V. Sasselli, L.G. Van Der Flier, E. Cuppen, A. Van Oudenaarden, H. Clevers, Ascl2 Acts as an R-spondin/Wnt-Responsive Switch to Control Stemness in Intestinal Crypts, Cell Stem Cell 16 (2015) 158–170. https://doi.org/10.1016/J.STEM.2014.12.006.

[18] N. Barker, J.H. Van Es, J. Kuipers, P. Kujala, M. Van Den Born, M. Cozijnsen, A. Haegebarth, J. Korving, H. Begthel, P.J. Peters, H. Clevers, Identification of stem cells in small intestine and colon by marker gene Lgr5, Nat. 2007 4497165 449 (2007) 1003–1007. https://doi.org/10.1038/nature06196.

[19] L.G. Van Der Flier, H. Clevers, Stem cells, self-renewal, and differentiation in the intestinal epithelium, Annu. Rev. Physiol. 71 (2009) 241–260. https://doi.org/10.1146/ANNUREV.PHYSIOL.010908.163145.

[20] Y. Yatabe, S. Tavaré, D. Shibata, Investigating stem cells in human colon by using

methylation patterns, Proc. Natl. Acad. Sci. U. S. A. 98 (2001) 10839–10844. https://doi.org/10.1073/PNAS.191225998.

[21] J. Milano, J. McKay, C. Dagenais, L. Foster-Brown, F. Pognan, R. Gadient, R.T. Jacobs, A. Zacco, B. Greenberg, P.J. Ciaccio, Modulation of notch processing by gamma-secretase inhibitors causes intestinal goblet cell metaplasia and induction of genes known to specify gut secretory lineage differentiation, Toxicol. Sci. 82 (2004) 341–358. https://doi.org/10.1093/TOXSCI/KFH254.

[22] J.H. Van Es, M.E. Van Gijn, O. Riccio, M. Van Den Born, M. Vooijs, H. Begthel, M. Cozijnsen, S. Robine, D.J. Winton, F. Radtke, H. Clevers, Notch/gamma-secretase inhibition turns proliferative cells in intestinal crypts and adenomas into goblet cells, Nature 435 (2005) 959–963. https://doi.org/10.1038/NATURE03659.

[23] J.M. Allaire, S.M. Crowley, H.T. Law, S.Y. Chang, H.J. Ko, B.A. Vallance, The Intestinal Epithelium: Central Coordinator of Mucosal Immunity, Trends Immunol. 39 (2018) 677–696. https://doi.org/10.1016/J.IT.2018.04.002.

[24] A. Gregorieff, D. Pinto, H. Begthel, O. Destrée, M. Kielman, H. Clevers, Expression Pattern of Wnt Signaling Components in the Adult Intestine, Gastroenterology 129 (2005) 626–638. https://doi.org/10.1053/J.GASTRO.2005.06.007.

[25] X.C. He, J. Zhang, W.G. Tong, O. Tawfik, J. Ross, D.H. Scoville, Q. Tian, X. Zeng, X. He, L.M. Wiedemann, Y. Mishina, L. Li, BMP signaling inhibits intestinal stem cell self-renewal through suppression of Wnt-beta-catenin signaling, Nat. Genet. 36 (2004) 1117–1121. https://doi.org/10.1038/NG1430.

[26] A.P.G. Haramis, H. Begthel, M. Van Den Born, J. Van Es, S. Jonkheer, G.J.A. Offerhaus, H. Clevers, De novo crypt formation and juvenile polyposis on BMP inhibition in mouse intestine, Science 303 (2004) 1684–1686. https://doi.org/10.1126/SCIENCE.1093587.

[27] C. Kosinski, V.S.W. Li, A.S.Y. Chan, J. Zhang, C. Ho, Y.T. Wai, L.C. Tsun, R.C. Mifflin, D.W. Powell, T.Y. Siu, Y.L. Suet, X. Chen, Gene expression patterns of human colon tops and basal crypts and BMP antagonists as intestinal stem cell niche factors, Proc. Natl. Acad. Sci. U. S. A. 104 (2007) 15418–15423. https://doi.org/10.1073/PNAS.0707210104.

[28] K.A. Kim, M. Kakitani, J. Zhao, T. Oshima, T. Tang, M. Binnerts, Y. Liu, B. Boyle, E. Park, P. Emtage, W.D. Funk, K. Tomizuka, Mitogenic influence of human R-spondin1 on the intestinal epithelium, Science 309 (2005) 1256–1259.

https://doi.org/10.1126/SCIENCE.1112521.

[29] K.S. Yan, C.Y. Janda, J. Chang, G.X.Y. Zheng, K.A. Larkin, V.C. Luca, L.A. Chia, A.T. Mah, A. Han, J.M. Terry, A. Ootani, K. Roelf, M. Lee, J. Yuan, X. Li, C.R. Bolen, J. Wilhelmy, P.S. Davies, H. Ueno, R.J. Von Furstenberg, P. Belgrader, S.B. Ziraldo, H. Ordonez, S.J. Henning, M.H. Wong, M.P. Snyder, I.L. Weissman, A.J. Hsueh, T.S. Mikkelsen, K.C. Garcia, C.J. Kuo, Non-equivalence of Wnt and R-spondin ligands during Lgr5+ intestinal stem-cell self-renewal, Nat. 2017 5457653 545 (2017) 238–242. https://doi.org/10.1038/nature22313.

[30] T. Sato, R.G. Vries, H.J. Snippert, M. van de Wetering, N. Barker, D.E. Stange, J.H. van Es, A. Abo, P. Kujala, P.J. Peters, H. Clevers, Single Lgr5 stem cells build crypt-villus structures in vitro without a mesenchymal niche, Nat. 2009 4597244 459 (2009) 262–265. https://doi.org/10.1038/nature07935.

[31] Y. Wang, R. Kim, S.S. Hinman, B. Zwarycz, S.T. Magness, N.L. Allbritton, Bioengineered Systems and Designer Matrices That Recapitulate the Intestinal Stem Cell Niche, Cell. Mol. Gastroenterol. Hepatol. 5 (2018) 440-453.e1. https://doi.org/10.1016/J.JCMGH.2018.01.008.

[32] I. V. Pinchuk, R.C. Mifflin, J.I. Saada, D.W. Powell, Intestinal Mesenchymal Cells, Curr. Gastroenterol. Rep. 12 (2010) 310. https://doi.org/10.1007/S11894-010-0135-Y.

[33] M. Roulis, R.A. Flavell, Fibroblasts and myofibroblasts of the intestinal lamina propria in physiology and disease, Differentiation 92 (2016) 116–131. https://doi.org/10.1016/j.diff.2016.05.002.

[34] B. Hinz, Formation and Function of the Myofibroblast during Tissue Repair, J. Invest. Dermatol. 127 (2007) 526–537. https://doi.org/10.1038/SJ.JID.5700613.

[35] B. Eyden, A. Curry, G. Wang, Stromal cells in the human gut show ultrastructural features of fibroblasts and smooth muscle cells but not myofibroblasts, J. Cell. Mol. Med. 15 (2011) 1483–1491. https://doi.org/10.1111/J.1582-4934.2010.01132.X.

[36] M. Kurahashi, Y. Nakano, L.E. Peri, J.B. Townsend, S.M. Ward, K.M. Sanders, A novel population of subepithelial platelet-derived growth factor receptor α-positive cells in the mouse and human colon, Am. J. Physiol. Gastrointest. Liver Physiol. 304 (2013). https://doi.org/10.1152/AJPGI.00001.2013.

[37] M.D. Brugger, T. Valenta, H. Fazilaty, G. Hausmann, K. Basler, Distinct populations of

crypt-associated fibroblasts act as signaling hubs to control colon homeostasis, PLOS Biol. 18 (2020) e3001032. https://doi.org/10.1371/JOURNAL.PBIO.3001032.

[38] D.W. Powell, I. V. Pinchuk, J.I. Saada, X. Chen, R.C. Mifflin, Mesenchymal cells of the intestinal lamina propria, Annu. Rev. Physiol. 73 (2011) 213–237. https://doi.org/10.1146/ANNUREV.PHYSIOL.70.113006.100646.

[39] Z. Kabiri, G. Greicius, B. Madan, S. Biechele, Z. Zhong, H. Zaribafzadeh, Edison, J. Aliyev, Y. Wu, R. Bunte, B.O. Williams, J. Rossant, D.M. Virshup, Stroma provides an intestinal stem cell niche in the absence of epithelial Wnts, Development 141 (2014) 2206–2215. https://doi.org/10.1242/DEV.104976.

[40] T. Valenta, B. Degirmenci, A.E. Moor, P. Herr, D. Zimmerli, M.B. Moor, G. Hausmann, C. Cantù, M. Aguet, K. Basler, Wnt Ligands Secreted by Subepithelial Mesenchymal Cells Are Essential for the Survival of Intestinal Stem Cells and Gut Homeostasis, Cell Rep. 15 (2016) 911–918. https://doi.org/10.1016/J.CELREP.2016.03.088.

[41] R. Aoki, M. Shoshkes-Carmel, N. Gao, S. Shin, C.L. May, M.L. Golson, A.M. Zahm, M. Ray, C.L. Wiser, C.V.E. Wright, K.H. Kaestner, Foxl1-expressing mesenchymal cells constitute the intestinal stem cell niche, Cell. Mol. Gastroenterol. Hepatol. 2 (2016) 175–188. https://doi.org/10.1016/J.JCMGH.2015.12.004.

[42] I. Stzepourginski, G. Nigro, J.M. Jacob, S. Dulauroy, P.J. Sansonetti, G. Eberl, L. Peduto, CD34+ mesenchymal cells are a major component of the intestinal stem cells niche at homeostasis and after injury, Proc. Natl. Acad. Sci. U. S. A. 114 (2017) E506–E513. https://doi.org/10.1073/PNAS.1620059114.

[43] N. Chalkidi, C. Paraskeva, V. Koliaraki, Fibroblasts in intestinal homeostasis, damage, and repair, Front. Immunol. 13 (2022). https://doi.org/10.3389/FIMMU.2022.924866.

[44] H. Dang, T.J. Harryvan, L.J.A.C. Hawinkels, Fibroblast Subsets in Intestinal Homeostasis, Carcinogenesis, Tumor Progression, and Metastasis, Cancers 2021, Vol. 13, Page 183 13 (2021) 183. https://doi.org/10.3390/CANCERS13020183.

[45] B. Yang, G. Zhang, M. Elias, Y. Zhu, J. Wang, The role of cytokine and immune responses in intestinal fibrosis, J. Dig. Dis. 21 (2020) 308–314. https://doi.org/10.1111/1751-2980.12879.

[46] R. Curciarello, G.H. Docena, T.T. MacDonald, The Role of Cytokines in the Fibrotic Responses in Crohn's Disease, Front. Med. 4 (2017) 126.

https://doi.org/10.3389/FMED.2017.00126.

[47] T. Matsuoka, M. Yashiro, The Role of the Transforming Growth Factor-β Signaling Pathway in Gastrointestinal Cancers, Biomol. 2023, Vol. 13, Page 1551 13 (2023) 1551. https://doi.org/10.3390/BIOM13101551.

[48] V. Valatas, E. Filidou, I. Drygiannakis, G. Kolios, Stromal and immune cells in gut fibrosis: the myofibroblast and the scarface, Ann. Gastroenterol. 30 (2017) 393. https://doi.org/10.20524/AOG.2017.0146.

[49] F. Rieder, S.P. Kessler, G.A. West, S. Bhilocha, C. De La Motte, T.M. Sadler, B. Gopalan, E. Stylianou, C. Fiocchi, Inflammation-Induced Endothelial-to-Mesenchymal Transition: A Novel Mechanism of Intestinal Fibrosis, Am. J. Pathol. 179 (2011) 2660. https://doi.org/10.1016/J.AJPATH.2011.07.042.

[50] S. D'Alessio, F. Ungaro, D. Noviello, S. Lovisa, L. Peyrin-Biroulet, S. Danese, Revisiting fibrosis in inflammatory bowel disease: the gut thickens, Nat. Rev. Gastroenterol. Hepatol. 2021 193 19 (2021) 169–184. https://doi.org/10.1038/s41575-021-00543-0.

[51] I.C. Lawrance, G. Rogler, G. Bamias, C. Breynaert, J. Florholmen, G. Pellino, S. Reif, S. Speca, G. Latella, Cellular and Molecular Mediators of Intestinal Fibrosis, J. Crohn's Colitis 11 (2017) 1491–1503. https://doi.org/10.1016/J.CROHNS.2014.09.008.

[52] J.P. Burke, M.F. Cunningham, R.W.G. Watson, N.G. Docherty, J.C. Coffey, P.R. O'Connell, Bacterial lipopolysaccharide promotes profibrotic activation of intestinal fibroblasts, Br. J. Surg. 97 (2010) 1126–1134. https://doi.org/10.1002/BJS.7045.

[53] L. Luo, W. Zhang, S. You, X. Cui, H. Tu, Q. Yi, J. Wu, O. Liu, The role of epithelial cells in fibrosis: Mechanisms and treatment, Pharmacol. Res. 202 (2024) 107144. https://doi.org/10.1016/J.PHRS.2024.107144.

[54] R. Kiesslich, M. Goetz, E.M. Angus, Q. Hu, Y. Guan, C. Potten, T. Allen, M.F. Neurath, N.F. Shroyer, M.H. Montrose, A.J.M. Watson, Identification of Epithelial Gaps in Human Small and Large Intestine by Confocal Endomicroscopy, Gastroenterology 133 (2007) 1769–1778. https://doi.org/10.1053/J.GASTRO.2007.09.011.

[55] H. Sung, J. Ferlay, R.L. Siegel, M. Laversanne, I. Soerjomataram, A. Jemal, F. Bray, Global Cancer Statistics 2020: GLOBOCAN Estimates of Incidence and Mortality Worldwide for 36 Cancers in 185 Countries, CA. Cancer J. Clin. 71 (2021) 209–249. https://doi.org/10.3322/CAAC.21660.

[56] I. Mármol, C. Sánchez-de-Diego, A.P. Dieste, E. Cerrada, M.J.R. Yoldi, Colorectal Carcinoma: A General Overview and Future Perspectives in Colorectal Cancer, Int. J. Mol. Sci. 18 (2017). https://doi.org/10.3390/IJMS18010197.

[57] D. Cunningham, W. Atkin, H.J. Lenz, H.T. Lynch, B. Minsky, B. Nordlinger, N. Starling, Colorectal cancer, Lancet (London, England) 375 (2010) 1030–1047. https://doi.org/10.1016/S0140-6736(10)60353-4.

[58] K.A. Cronin, A.J. Lake, S. Scott, R.L. Sherman, A.-M. Noone, N. Howlader, S.J. Henley, R.N. Anderson, A.U. Firth, J. Ma, B.A. Kohler, A. Jemal, Annual Report to the Nation on the Status of Cancer, part I: National cancer statistics, Cancer 124 (2018) 2785–2800. https://doi.org/10.1002/CNCR.31551.

[59] E. Dekker, P.J. Tanis, J.L.A. Vleugels, P.M. Kasi, M.B. Wallace, Colorectal cancer, Lancet 394 (2019) 1467–1480. https://doi.org/10.1016/S0140-6736(19)32319-0.

[60] J. Schneikert, J. Behrens, The canonical Wnt signalling pathway and its APC partner in colon cancer development, Gut 56 (2007) 417–425. https://doi.org/10.1136/GUT.2006.093310.

[61] E.R. Fearon, B. Vogelstein, A genetic model for colorectal tumorigenesis, Cell 61 (1990) 759–767. https://doi.org/10.1016/0092-8674(90)90186-I.

[62] T.L. Whiteside, The tumor microenvironment and its role in promoting tumor growth, Oncogene 2008 2745 27 (2008) 5904–5912. https://doi.org/10.1038/onc.2008.271.

[63] P.P. Provenzano, D.R. Inman, K.W. Eliceiri, J.G. Knittel, L. Yan, C.T. Rueden, J.G. White, P.J. Keely, Collagen density promotes mammary tumor initiation and progression, BMC Med. 6 (2008). https://doi.org/10.1186/1741-7015-6-11.

[64] N.I. Nissen, M.A. Karsdal, T.R. Cox, N. Willumsen, The roles of collagens and fibroblasts in cancer, Biochem. Collagens, Laminins Elastin Struct. Funct. Biomarkers, Third Ed. (2024) 419–434. https://doi.org/10.1016/B978-0-443-15617-5.00029-9.

[65] N.I. Nissen, M. Karsdal, N. Willumsen, Collagens and Cancer associated fibroblasts in the reactive stroma and its relation to Cancer biology, J. Exp. Clin. Cancer Res. 38 (2019) 1–12. https://doi.org/10.1186/S13046-019-1110-6/TABLES/1.

[66] M. Fang, J. Yuan, C. Peng, Y. Li, Collagen as a double-edged sword in tumor progression, Tumor Biol. 35 (2014) 2871–2882. https://doi.org/10.1007/S13277-013-1511-7/FIGURES/6.

[67] L.A. Johnson, E.S. Rodansky, K.L. Sauder, J.C. Horowitz, J.D. Mih, D.J. Tschumperlin, P.D. Higgins, Matrix stiffness corresponding to strictured bowel induces a fibrogenic response in human colonic fibroblasts, Inflamm. Bowel Dis. 19 (2013) 891–903. https://doi.org/10.1097/MIB.0B013E3182813297.

[68] J. Zhu, F. Zhang, F. Liu, W. He, J. Tian, H. Han, P. Cao, Identifying the inflammatory and fibrotic bowel stricture: MRI diffusion-weighted imaging in Crohn's disease, Radiol. Infect. Dis. 2 (2015) 128–133. https://doi.org/10.1016/J.JRID.2015.11.005.

[69] M. Thormann, B. Melekh, C. Bär, M. Pech, J. Omari, A. Wienke, H.J. Meyer, A. Surov, Apparent diffusion coefficient for assessing Crohn's disease activity: a meta-analysis, Eur. Radiol. 33 (2023) 1677–1686. https://doi.org/10.1007/S00330-022-09149-9/FIGURES/6.

[70] T. Sato, D.E. Stange, M. Ferrante, R.G.J. Vries, J.H. Van Es, S. Van Den Brink, W.J. Van Houdt, A. Pronk, J. Van Gorp, P.D. Siersema, H. Clevers, Long-term Expansion of Epithelial Organoids From Human Colon, Adenoma, Adenocarcinoma, and Barrett's Epithelium, Gastroenterology 141 (2011) 1762–1772. https://doi.org/10.1053/J.GASTRO.2011.07.050.

[71] H. Miyoshi, R. Ajima, C.T.-Y. Luo, T.P. Yamaguchi, T.S. Stappenbeck, Wnt5a Potentiates TGF-β Signaling to Promote Colonic Crypt Regeneration after Tissue Injury, Science 338 (2012) 108. https://doi.org/10.1126/SCIENCE.1223821.

[72] H. Miyoshi, T.S. Stappenbeck, In vitro expansion and genetic modification of gastrointestinal stem cells in spheroid culture, Nat. Protoc. 2013 812 8 (2013) 2471–2482. https://doi.org/10.1038/nprot.2013.153.

[73] K.L. VanDussen, N.M. Sonnek, T.S. Stappenbeck, L-WRN conditioned medium for gastrointestinal epithelial stem cell culture shows replicable batch-to-batch activity levels across multiple research teams, Stem Cell Res. 37 (2019) 101430. https://doi.org/10.1016/J.SCR.2019.101430.

[74] Y. Wang, M. DiSalvo, D.B. Gunasekara, J. Dutton, A. Proctor, M.S. Lebhar, I.A. Williamson, J. Speer, R.L. Howard, N.M. Smiddy, S.J. Bultman, C.E. Sims, S.T. Magness, N.L. Allbritton, Self-renewing Monolayer of Primary Colonic or Rectal Epithelial Cells, CMGH 4 (2017) 165-182.e7. https://doi.org/10.1016/j.jcmgh.2017.02.011.

[75] Y. Wang, R. Kim, D.B. Gunasekara, M.I. Reed, M. Disalvo, D.L. Nguyen, S.J. Bultman,

C.E. Sims, S.T. Magness, N.L. Allbritton, Formation of Human Colonic Crypt Array by Application of Chemical Gradients Across a Shaped Epithelial Monolayer, Cell. Mol. Gastroenterol. Hepatol. 5 (2018) 113–130. https://doi.org/10.1016/j.jcmgh.2017.10.007.

[76] A.A. Ahmad, Y. Wang, C.E. Sims, S.T. Magness, N.L. Allbritton, Optimizing Wnt-3a and R-spondin1 concentrations for stem cell renewal and differentiation in intestinal organoids using a gradient-forming microdevice, RSC Adv. 5 (2015) 74881–74891. https://doi.org/10.1039/C5RA14923A.

[77] V. De Gregorio, G. Imparato, F. Urciuolo, P.A. Netti, 3D stromal tissue equivalent affects intestinal epithelium morphogenesis in vitro, Biotechnol. Bioeng. 115 (2018) 1062–1075. https://doi.org/10.1002/BIT.26522.

[78] M. Verhulsel, A. Simon, M. Bernheim-Dennery, V.R. Gannavarapu, L. Gérémie, D. Ferraro, D. Krndija, L. Talini, J.L. Viovy, D.M. Vignjevic, S. Descroix, Developing an advanced gut on chip model enabling the study of epithelial cell/fibroblast interactions, Lab Chip 21 (2021) 365–377. https://doi.org/10.1039/D0LC00672F.

[79] N.J. Darling, C.L. Mobbs, A.L. González-Hau, M. Freer, S. Przyborski, Bioengineering Novel in vitro Co-culture Models That Represent the Human Intestinal Mucosa With Improved Caco-2 Structure and Barrier Function, Front. Bioeng. Biotechnol. 8 (2020) 992. https://doi.org/10.3389/FBIOE.2020.00992/BIBTEX.

[80] S.E. Rudolph, B.N. Longo, M.W. Tse, M.R. Houchin, M.M. Shokoufandeh, Y. Chen, D.L. Kaplan, Crypt-Villus Scaffold Architecture for Bioengineering Functional Human Intestinal Epithelium, ACS Biomater. Sci. Eng. 8 (2022) 4942–4955. https://doi.org/10.1021/ACSBIOMATERIALS.2C00851/ASSET/IMAGES/LARGE/AB2C00851_0007.JPEG.

[81] Y. Guo, J.L. Ayers, K.T. Carter, T. Wang, S.K. Maden, D. Edmond, P. Newcomb P, C. Li, C. Ulrich, M. Yu, W.M. Grady, Senescence-associated tissue microenvironment promotes colon cancer formation through the secretory factor GDF15, Aging Cell 18 (2019). https://doi.org/10.1111/acel.13013.

[82] M.H. Macedo, A.S. Barros, E. Martínez, C.C. Barrias, B. Sarmento, All layers matter: Innovative three-dimensional epithelium-stroma-endothelium intestinal model for reliable permeability outcomes, J. Control. Release 341 (2021) 414–430. https://doi.org/10.1016/J.JCONREL.2021.11.048.

[83] G.J. Jasso, A.I. Jaiswal, M.I. Varma, T. Laszewski, A. Grauel, A. OmarID, N. Silva, G. Dranoff, J.A. Porter, K. Mansfield, V. Cremasco, A. Regev, R.J. XavierID, D.B. Graham, Colon stroma mediates an inflammation-driven fibroblastic response controlling matrix remodeling and healing, (2022). https://doi.org/10.1371/journal.pbio.3001532.

[84] J. Kinchen, H.H. Chen, K. Parikh, A. Antanaviciute, M. Jagielowicz, D. Fawkner-Corbett, N. Ashley, L. Cubitt, E. Mellado-Gomez, M. Attar, E. Sharma, Q. Wills, R. Bowden, F.C. Richter, D. Ahern, K.D. Puri, J. Henault, F. Gervais, H. Koohy, A. Simmons, Structural Remodeling of the Human Colonic Mesenchyme in Inflammatory Bowel Disease, Cell 175 (2018) 372. https://doi.org/10.1016/J.CELL.2018.08.067.

[85] N.Y. Lei, Z. Jabaji, J. Wang, V.S. Joshi, G.J. Brinkley, H. Khalil, F. Wang, A. Jaroszewicz, M. Pellegrini, L. Li, M. Lewis, M. Stelzner, J.C.Y. Dunn, M.G. Martín, Intestinal Subepithelial Myofibroblasts Support the Growth of Intestinal Epithelial Stem Cells, PLoS One 9 (2014) e84651. https://doi.org/10.1371/journal.pone.0084651.

[86] M. Nikolaev, O. Mitrofanova, N. Broguiere, S. Geraldo, D. Dutta, Y. Tabata, B. Elci, N. Brandenberg, I. Kolotuev, N. Gjorevski, H. Clevers, M.P. Lutolf, Homeostatic mini-intestines through scaffold-guided organoid morphogenesis, Nat. 2020 5857826 585 (2020) 574–578. https://doi.org/10.1038/s41586-020-2724-8.

[87] M.E. Viney, A.J. Bullock, M.J. Day, S. MacNeil, The co-culture of intestinal epithelial and stromal cells in 3D collagen-based environments, Regen. Med. 4 (2009) 397. https://doi.org/10.2217/RME.09.4.

[88] N. Lahar, N.Y. Lei, J. Wang, Z. Jabaji, S.C. Tung, V. Joshi, M. Lewis, M. Stelzner, M.G. Martín, J.C.Y. Dunn, Intestinal Subepithelial Myofibroblasts Support in vitro and in vivo Growth of Human Small Intestinal Epithelium, PLoS One 6 (2011) e26898. https://doi.org/10.1371/JOURNAL.PONE.0026898.

[89] A. Salari, K. Zhou, K. Nikolovska, U. Seidler, M. Amiri, Human Colonoid–Myofibroblast Coculture for Study of Apical Na+/H+ Exchangers of the Lower Cryptal Neck Region, Int. J. Mol. Sci. 24 (2023) 4266. https://doi.org/10.3390/IJMS24054266/S1.

[90] E. Strating, M.P. Verhagen, E. Wensink, E. Dünnebach, L. Wijler, I. Aranguren, A.S. De la Cruz, N.A. Peters, J.H. Hageman, M.M.C. van der Net, S. van Schelven, J. Laoukili, R. Fodde, J. Roodhart, S. Nierkens, H. Snippert, M. Gloerich, I.B. Rinkes, S.G. Elias, O. Kranenburg, Co-cultures of colon cancer cells and cancer-associated fibroblasts

recapitulate the aggressive features of mesenchymal-like colon cancer, Front. Immunol. 14 (2023) 1053920. https://doi.org/10.3389/FIMMU.2023.1053920/BIBTEX.

[91] V.S. Atanasova, C. de Jesus Cardona, V. Hejret, A. Tiefenbacher, T. Mair, L. Tran, J. Pfneissl, K. Draganić, C. Binder, J. Kabiljo, J. Clement, K. Woeran, B. Neudert, S. Wohlhaupter, A. Haase, S. Domazet, M. Hengstschläger, M. Mitterhauser, L. Müllauer, B. Tichý, M. Bergmann, G. Schweikert, M. Hartl, H. Dolznig, G. Egger, Mimicking Tumor Cell Heterogeneity of Colorectal Cancer in a Patient-derived Organoid-Fibroblast Model, Cell. Mol. Gastroenterol. Hepatol. 15 (2023) 1391–1419. https://doi.org/10.1016/J.JCMGH.2023.02.014.

[92] Y. Wang, D.B. Gunasekara, M.I. Reed, M. DiSalvo, S.J. Bultman, C.E. Sims, S.T. Magness, N.L. Allbritton, A microengineered collagen scaffold for generating a polarized crypt-villus architecture of human small intestinal epithelium, Biomaterials 128 (2017) 44–55. https://doi.org/10.1016/j.biomaterials.2017.03.005.

[93] L. Meran, L. Tullie, S. Eaton, P. De Coppi, V.S.W. Li, Bioengineering human intestinal mucosal grafts using patient-derived organoids, fibroblasts and scaffolds, Nat. Protoc. 2022 181 18 (2022) 108–135. https://doi.org/10.1038/s41596-022-00751-1.

[94] N. Torras, J. Zabalo, E. Abril, A. Carré, M. García-Díaz, E. Martínez, A bioprinted 3D gut model with crypt-villus structures to mimic the intestinal epithelial-stromal microenvironment, Biomater. Adv. 153 (2023) 213534. https://doi.org/10.1016/J.BIOADV.2023.213534.

[95] R.L. Howard, Y. Wang, N.L. Allbritton, Use of liquid lithography to form in vitro intestinal crypts with varying microcurvature surrounding the stem cell niche, J. Micromech. Microeng. 31 (2021). https://doi.org/10.1088/1361-6439/AC2D9C.

[96] Y. Wang, R. Kim, D.B. Gunasekara, M.I. Reed, M. DiSalvo, D.L. Nguyen, S.J. Bultman, C.E. Sims, S.T. Magness, N.L. Allbritton, Formation of Human Colonic Crypt Array by Application of Chemical Gradients Across a Shaped Epithelial Monolayer, CMGH 5 (2018) 113–130. https://doi.org/10.1016/j.jcmgh.2017.10.007.

[97] G. (1941-. . . .). Wypych, Handbook of Polymers, (n.d.).

[98] Y. Wang, R. Kim, D.B. Gunasekara, M.I. Reed, M. DiSalvo, D.L. Nguyen, S.J. Bultman, C.E. Sims, S.T. Magness, N.L. Allbritton, Formation of Human Colonic Crypt Array by Application of Chemical Gradients Across a Shaped Epithelial Monolayer, CMGH 5

(2018) 113–130. https://doi.org/10.1016/j.jcmgh.2017.10.007.

[99] S.H. Han, S. Shim, M.J. Kim, H.Y. Shin, W.S. Jang, S.J. Lee, Y.W. Jin, S.S. Lee, S.B. Lee, S. Park, Long-term culture-induced phenotypic difference and efficient cryopreservation of small intestinal organoids by treatment timing of Rho kinase inhibitor, World J. Gastroenterol. 23 (2017) 964. https://doi.org/10.3748/WJG.V23.I6.964.

[100] S.S. Hinman, Y. Wang, R. Kim, N.L. Allbritton, In vitro generation of self-renewing human intestinal epithelia over planar and shaped collagen hydrogels, Nat. Protoc. 16 (2021) 352–382. https://doi.org/10.1038/s41596-020-00419-8.

[101] P. Dalerba, T. Kalisky, D. Sahoo, P.S. Rajendran, M.E. Rothenberg, A.A. Leyrat, S. Sim, J. Okamoto, D.M. Johnston, D. Qian, M. Zabala, J. Bueno, N.F. Neff, J. Wang, A.A. Shelton, B. Visser, S. Hisamori, Y. Shimono, M. Van De Wetering, H. Clevers, M.F. Clarke, S.R. Quake, Single-cell dissection of transcriptional heterogeneity in human colon tumors, Nat. Biotechnol. 2011 2912 29 (2011) 1120–1127. https://doi.org/10.1038/NBT.2038.

[102] K.A. Breau, M.T. Ok, I. Gomez-Martinez, J. Burclaff, N.P. Kohn, S.T. Magness, Efficient transgenesis and homology-directed gene targeting in monolayers of primary human small intestinal and colonic epithelial stem cells, Stem Cell Reports 17 (2022) 1493. https://doi.org/10.1016/J.STEMCR.2022.04.005.

[103] G. Larrinaga, I. Perez, L. Blanco, B. Sanz, P. Errarte, M. Beitia, M.C. Etxezarraga, A. Loizate, J. Gil, J. Irazusta, J.I. López, Prolyl endopeptidase activity is correlated with colorectal cancer prognosis, Int. J. Med. Sci. 11 (2014) 199–208. https://doi.org/10.7150/IJMS.7178.

[104] M.D. Brügger, K. Basler, The diverse nature of intestinal fibroblasts in development, homeostasis, and disease, Trends Cell Biol. 33 (2023) 834–849. https://doi.org/10.1016/J.TCB.2023.03.007.

[105] L. Onfroy-Roy, D. Hamel, J. Foncy, L. Malaquin, A. Ferrand, Extracellular Matrix Mechanical Properties and Regulation of the Intestinal Stem Cells: When Mechanics Control Fate, Cells 9 (2020) 1–23. https://doi.org/10.3390/CELLS9122629.

[106] H. Miyoshi, Wnt-expressing cells in the intestines: guides for tissue remodeling, J. Biochem. 161 (2017) 19–25. https://doi.org/10.1093/JB/MVW070.

[107] A.J. Mikels, R. Nusse, Purified Wnt5a protein activates or inhibits beta-catenin-TCF

signaling depending on receptor context, PLoS Biol. 4 (2006) 570–582. https://doi.org/10.1371/JOURNAL.PBIO.0040115.

[108] A.M. Nik, A. Reyahi, F. Pontén, P. Carlsson, Foxf2 in intestinal fibroblasts reduces numbers of Lgr5(+) stem cells and adenoma formation by inhibiting Wnt signaling, Gastroenterology 144 (2013) 1001–1011. https://doi.org/10.1053/J.GASTRO.2013.01.045.

[109] J. Xie, X.Y. Zhu, L.M. Liu, Z.Q. Meng, Solute carrier transporters: potential targets for digestive system neoplasms, Cancer Manag. Res. 10 (2018) 153. https://doi.org/10.2147/CMAR.S152951.

[110] H.M. Chen, J.A. MacDonald, Death-associated protein kinases and intestinal epithelial homeostasis, Anat. Rec. 306 (2023) 1062–1087. https://doi.org/10.1002/AR.25022.

[111] A.A. Wolfarth, X. Liu, T.M. Darby, D.J. Boyer, J.B. Spizman, J.A. Owens, B. Chandrasekharan, C.R. Naudin, K.Z. Hanley, B.S. Robinson, E.A. Ortlund, R.M. Jones, A.S. Neish, Proline-Rich Acidic Protein 1 (PRAP1) Protects the Gastrointestinal Epithelium From Irradiation-Induced Apoptosis, Cell. Mol. Gastroenterol. Hepatol. 10 (2020) 713. https://doi.org/10.1016/J.JCMGH.2020.06.011.

[112] N. Chalkidi, C. Paraskeva, V. Koliaraki, Fibroblasts in intestinal homeostasis, damage, and repair, Front. Immunol. 13 (2022). https://doi.org/10.3389/FIMMU.2022.924866.

[113] S.S. Hinman, Y. Wang, R. Kim, N.L. Allbritton, In vitro generation of self-renewing human intestinal epithelia over planar and shaped collagen hydrogels, Nat. Protoc. 16 (2021) 352–382. https://doi.org/10.1038/s41596-020-00419-8.

[114] F.A. Flomerfelt, R.E. Gress, Analysis of Cell Proliferation and Homeostasis Using EdU Labeling, Methods Mol. Biol. 1323 (2016) 211. https://doi.org/10.1007/978-1-4939-2809-5_18.

[115] D.R. Stirling, M.J. Swain-Bowden, A.M. Lucas, A.E. Carpenter, B.A. Cimini, A. Goodman, CellProfiler 4: improvements in speed, utility and usability, BMC Bioinformatics 22 (2021) 1–11. https://doi.org/10.1186/S12859-021-04344-9/FIGURES/6.

[116] A. Dobin, C.A. Davis, F. Schlesinger, J. Drenkow, C. Zaleski, S. Jha, P. Batut, M. Chaisson, T.R. Gingeras, STAR: ultrafast universal RNA-seq aligner, Bioinformatics 29 (2013) 15–21. https://doi.org/10.1093/BIOINFORMATICS/BTS635.

[117] S. Andrews, FastQC: a quality control tool for high throughput sequence data., (2010). http://www.bioinformatics.babraham.ac.uk/projects/fastqc.

[118] D.S. Deluca, J.Z. Levin, A. Sivachenko, T. Fennell, M.D. Nazaire, C. Williams, M. Reich, W. Winckler, G. Getz, RNA-SeQC: RNA-seq metrics for quality control and process optimization, Bioinformatics 28 (2012) 1530. https://doi.org/10.1093/BIOINFORMATICS/BTS196.

[119] L. Wang, S. Wang, W. Li, RSeQC: quality control of RNA-seq experiments, Bioinformatics 28 (2012) 2184–2185. https://doi.org/10.1093/BIOINFORMATICS/BTS356.

[120] M.D. Robinson, D.J. McCarthy, G.K. Smyth, edgeR: a Bioconductor package for differential expression analysis of digital gene expression data, Bioinformatics 26 (2010) 139–140. https://doi.org/10.1093/BIOINFORMATICS/BTP616.

[121] F. Rieder, C. Fiocchi, G. Rogler, Mechanisms, Management, and Treatment of Fibrosis in Patients with Inflammatory Bowel Diseases, Gastroenterology 152 (2017) 340. https://doi.org/10.1053/J.GASTRO.2016.09.047.

[122] T.A. Wynn, Cellular and molecular mechanisms of fibrosis, J. Pathol. 214 (2008) 199. https://doi.org/10.1002/PATH.2277.

[123] Y. Sato, S. Tsujinaka, T. Miura, Y. Kitamura, H. Suzuki, C. Shibata, Inflammatory Bowel Disease and Colorectal Cancer: Epidemiology, Etiology, Surveillance, and Management, Cancers 2023, Vol. 15, Page 4154 15 (2023) 4154. https://doi.org/10.3390/CANCERS15164154.

[124] M. Yashiro, Molecular Alterations of Colorectal Cancer with Inflammatory Bowel Disease, Dig. Dis. Sci. 60 (2015) 2251–2263. https://doi.org/10.1007/S10620-015-3646-4/FIGURES/1.

[125] B. Piersma, M.K. Hayward, V.M. Weaver, Fibrosis and cancer: A strained relationship, Biochim. Biophys. Acta. Rev. Cancer 1873 (2020) 188356. https://doi.org/10.1016/J.BBCAN.2020.188356.

[126] F. Rieder, J. Brenmoehl, S. Leeb, J. Schölmerich, G. Rogler, Wound healing and fibrosis in intestinal disease, Gut 56 (2007) 130. https://doi.org/10.1136/GUT.2006.090456.

[127] V. Solitano, A. Dal Buono, R. Gabbiadini, M. Wozny, A. Repici, A. Spinelli, S. Vetrano, A. Armuzzi, Fibro-Stenosing Crohn's Disease: What Is New and What Is Next?, J. Clin.

Med. 2023, Vol. 12, Page 3052 12 (2023) 3052. https://doi.org/10.3390/JCM12093052.

[128] F. Rieder, S. Kessler, M. Sans, C. Fiocchi, Animal models of intestinal fibrosis: new tools for the understanding of pathogenesis and therapy of human disease, Am. J. Physiol. Gastrointest. Liver Physiol. 303 (2012). https://doi.org/10.1152/AJPGI.00059.2012.

[129] L.A. Johnson, E.S. Rodansky, A.J. Haak, S.D. Larsen, R.R. Neubig, P.D.R. Higgins, Novel Rho/MRTF/SRF Inhibitors Block Matrix-stiffness and TGF-β–Induced Fibrogenesis in Human Colonic Myofibroblasts, Inflamm. Bowel Dis. 20 (2014) 154–165. https://doi.org/10.1097/01.MIB.0000437615.98881.31.

[130] E.S. Rodansky, L.A. Johnson, S. Huang, J.R. Spence, P.D.R. Higgins, Intestinal organoids: A model of intestinal fibrosis for evaluating anti-fibrotic drugs, Exp. Mol. Pathol. 98 (2015) 346–351. https://doi.org/10.1016/J.YEXMP.2015.03.033.

[131] L. Kandilogiannakis, E. Filidou, I. Drygiannakis, G. Tarapatzi, S. Didaskalou, M. Koffa, K. Arvanitidis, G. Bamias, V. Valatas, V. Paspaliaris, G. Kolios, Development of a Human Intestinal Organoid Model for In Vitro Studies on Gut Inflammation and Fibrosis, Stem Cells Int. 2021 (2021). https://doi.org/10.1155/2021/9929461.

[132] S. Hahn, M.O. Nam, J.H. Noh, D.H. Lee, H.W. Han, D.H. Kim, K.B. Hahm, S.P. Hong, J.H. Yoo, J. Yoo, Organoid-based epithelial to mesenchymal transition (OEMT) model: from an intestinal fibrosis perspective, Sci. Reports 2017 71 7 (2017) 1–11. https://doi.org/10.1038/s41598-017-02190-5.

[133] J.R. Miller, The Wnts, Genome Biol. 3 (2002) reviews3001.1. https://doi.org/10.1186/GB-2001-3-1-REVIEWS3001.

[134] U. Chippada, B. Yurke, N.A. Langrana, Simultaneous determination of Young's modulus, shear modulus, and Poisson's ratio of soft hydrogels, J. Mater. Res. 25 (2010) 545–555. https://doi.org/10.1557/JMR.2010.0067/METRICS.

[135] M. Kang, C.A. Day, A.K. Kenworthy, E. DiBenedetto, Simplified equation to extract diffusion coefficients from confocal FRAP data, Traffic 13 (2012) 1589–1600. https://doi.org/10.1111/TRA.12008.

[136] M. Jay Unruh (Stowers Institute for Medical Research in Kansas City, Stowers ImageJ Plugins, (n.d.). https://research.stowers.org/imagejplugins/ (accessed August 5, 2024).

[137] M. Schmitt, F.R. Greten, The inflammatory pathogenesis of colorectal cancer, Nat. Rev. Immunol. 2021 2110 21 (2021) 653–667. https://doi.org/10.1038/s41577-021-00534-x.

[138] J.S. Dutton, S.S. Hinman, R. Kim, Y. Wang, N.L. Allbritton, Primary Cell-Derived Intestinal Models: Recapitulating Physiology, Trends Biotechnol. 37 (2019) 744–760. https://doi.org/10.1016/j.tibtech.2018.12.001.

[139] A.M. Mowat, W.W. Agace, Regional specialization within the intestinal immune system, Nat. Rev. Immunol. 14 (2014) 667–685. https://doi.org/10.1038/NRI3738.

[140] A.J. Macpherson, M.B. Geuking, K.D. McCoy, Immune responses that adapt the intestinal mucosa to commensal intestinal bacteria, Immunology 115 (2005) 153–162. https://doi.org/10.1111/J.1365-2567.2005.02159.X.

[141] C.P. Miller, W. Shin, E.H. Ahn, H.J. Kim, D.-H. Kim, Engineering Microphysiological Immune System Responses on Chips Trends in Biotechnology, Trends Biotechnol. 38 (2020) 857–872. https://doi.org/10.1016/j.tibtech.2020.01.003.

[142] Y.M. Ambrosini, W. Shin, S. Min, H.J. Kim, Microphysiological Engineering of Immune Responses in Intestinal Inflammation, Immune Netw. 20 (2020). https://doi.org/10.4110/IN.2020.20.E13.

[143] Y.R. Na, M. Stakenborg, S.H. Seok, G. Matteoli, Macrophages in intestinal inflammation and resolution: a potential therapeutic target in IBD, Nat. Rev. Gastroenterol. Hepatol. 16 (2019) 531–543. https://doi.org/10.1038/S41575-019-0172-4.

[144] S. De Schepper, S. Verheijden, J. Aguilera-Lizarraga, M.F. Viola, W. Boesmans, N. Stakenborg, I. Voytyuk, I. Schmidt, B. Boeckx, I. Dierckx de Casterlé, V. Baekelandt, E. Gonzalez Dominguez, M. Mack, I. Depoortere, B. De Strooper, B. Sprangers, U. Himmelreich, S. Soenen, M. Guilliams, P. Vanden Berghe, E. Jones, D. Lambrechts, G. Boeckxstaens, Self-Maintaining Gut Macrophages Are Essential for Intestinal Homeostasis, Cell 176 (2019) 676. https://doi.org/10.1016/J.CELL.2019.01.010.

[145] A.M. Hine, P. Loke, Intestinal Macrophages in Resolving Inflammation, J. Immunol. 203 (2019) 593–599. https://doi.org/10.4049/JIMMUNOL.1900345.

[146] M.G. Gareau, P.M. Sherman, W.A. Walker, Probiotics and the gut microbiota in intestinal health and disease, Nat. Rev. Gastroenterol. Hepatol. 7 (2010) 503–514. https://doi.org/10.1038/NRGASTRO.2010.117.

[147] B. Mørland, T. Midtvedt, Phagocytosis, peritoneal influx, and enzyme activities in peritoneal macrophages from germfree, conventional, and ex-germfree mice, Infect. Immun. 44 (1984) 750–752. https://doi.org/10.1128/IAI.44.3.750-752.1984.

[148] K. Haverson, Z. Rehakova, J. Sinkora, L. Sver, M. Bailey, Immune development in jejunal mucosa after colonization with selected commensal gut bacteria: a study in germ-free pigs, Vet. Immunol. Immunopathol. 119 (2007) 243–253. https://doi.org/10.1016/J.VETIMM.2007.05.022.

[149] T.B. Clarke, K.M. Davis, E.S. Lysenko, A.Y. Zhou, Y. Yu, J.N. Weiser, Recognition of peptidoglycan from the microbiota by Nod1 enhances systemic innate immunity, Nat. Med. 16 (2010) 228–231. https://doi.org/10.1038/NM.2087.

[150] T.L.A. Nguyen, S. Vieira-Silva, A. Liston, J. Raes, How informative is the mouse for human gut microbiota research?, Dis. Model. Mech. 8 (2015) 1–16. https://doi.org/10.1242/DMM.017400.

[151] N. Gjorevski, N. Sachs, A. Manfrin, S. Giger, M.E. Bragina, P. Ordóñez-Morán, H. Clevers, M.P. Lutolf, Designer matrices for intestinal stem cell and organoid culture, Nature 539 (2016) 560–564. https://doi.org/10.1038/NATURE20168.

[152] M. Van De Wetering, H.E. Francies, J.M. Francis, G. Bounova, F. Iorio, A. Pronk, W. Van Houdt, J. Van Gorp, A. Taylor-Weiner, L. Kester, A. McLaren-Douglas, J. Blokker, S. Jaksani, S. Bartfeld, R. Volckman, P. Van Sluis, V.S.W. Li, S. Seepo, C. Sekhar Pedamallu, K. Cibulskis, S.L. Carter, A. McKenna, M.S. Lawrence, L. Lichtenstein, C. Stewart, J. Koster, R. Versteeg, A. Van Oudenaarden, J. Saez-Rodriguez, R.G.J. Vries, G. Getz, L. Wessels, M.R. Stratton, U. McDermott, M. Meyerson, M.J. Garnett, H. Clevers, Prospective derivation of a living organoid biobank of colorectal cancer patients, Cell 161 (2015) 933–945. https://doi.org/10.1016/J.CELL.2015.03.053.

[153] T. Sato, H. Clevers, Growing self-organizing mini-guts from a single intestinal stem cell: mechanism and applications, Science 340 (2013) 1190–1194. https://doi.org/10.1126/SCIENCE.1234852.

[154] J.C. Brazil, W.Y. Lee, K.N. Kolegraff, A. Nusrat, C.A. Parkos, N.A. Louis, Neutrophil migration across intestinal epithelium: evidence for a role of CD44 in regulating detachment of migrating cells from the luminal surface, J. Immunol. 185 (2010) 7026–7036. https://doi.org/10.4049/JIMMUNOL.1001293.

[155] K.M. Blake, S.O. Carrigan, A.C. Issekutz, A.W. Stadnyk, Neutrophils migrate across intestinal epithelium using beta2 integrin (CD11b/CD18)-independent mechanisms, Clin. Exp. Immunol. 136 (2004) 262–268. https://doi.org/10.1111/J.1365-2249.2004.02429.X.

[156] H.J. Kim, H. Li, J.J. Collins, D.E. Ingber, Contributions of microbiome and mechanical deformation to intestinal bacterial overgrowth and inflammation in a human gut-on-a-chip, Proc. Natl. Acad. Sci. U. S. A. 113 (2016) E7–E15. https://doi.org/10.1073/PNAS.1522193112.

[157] W. Shin, H.J. Kim, Intestinal barrier dysfunction orchestrates the onset of inflammatory host-microbiome cross-talk in a human gut inflammation-on-a-chip, Proc. Natl. Acad. Sci. U. S. A. 115 (2018) E10539–E10547. https://doi.org/10.1073/PNAS.1810819115.

[158] M. Maurer, M.S. Gresnigt, A. Last, T. Wollny, F. Berlinghof, R. Pospich, Z. Cseresnyes, A. Medyukhina, K. Graf, M. Gröger, M. Raasch, F. Siwczak, S. Nietzsche, I.D. Jacobsen, M.T. Figge, B. Hube, O. Huber, A.S. Mosig, A three-dimensional immunocompetent intestine-on-chip model as in vitro platform for functional and microbial interaction studies, Biomaterials 220 (2019). https://doi.org/10.1016/J.BIOMATERIALS.2019.119396.

[159] H. Sun, E.C.Y. Chow, S. Liu, Y. Du, K.S. Pang, The Caco-2 cell monolayer: usefulness and limitations, Expert Opin. Drug Metab. Toxicol. 4 (2008) 395–411. https://doi.org/10.1517/17425255.4.4.395.

[160] P. Artursson, K. Palm, K. Luthman, Caco-2 monolayers in experimental and theoretical predictions of drug transport, Adv. Drug Deliv. Rev. 46 (2001) 27–43. https://doi.org/10.1016/S0169-409X(00)00128-9.

[161] C.A. Larregieu, L.Z. Benet, Drug discovery and regulatory considerations for improving in silico and in vitro predictions that use Caco-2 as a surrogate for human intestinal permeability measurements, AAPS J. 15 (2013) 483–497. https://doi.org/10.1208/S12248-013-9456-8.

[162] A. Bein, W. Shin, S. Jalili-Firoozinezhad, M.H. Park, A. Sontheimer-Phelps, A. Tovaglieri, A. Chalkiadaki, H.J. Kim, D.E. Ingber, Microfluidic Organ-on-a-Chip Models of Human Intestine, Cell. Mol. Gastroenterol. Hepatol. 5 (2018) 659–668. https://doi.org/10.1016/J.JCMGH.2017.12.010.

[163] S.S. Hinman, R. Kim, Y. Wang, K.S. Phillips, P.J. Attayek, N.L. Allbritton, Microphysiological System Design: Simplicity Is Elegance, Curr. Opin. Biomed. Eng. 13 (2020) 94–102. https://doi.org/10.1016/J.COBME.2019.12.010.

[164] C.L. Zindl, J.F. Lai, Y.K. Lee, C.L. Maynard, S.N. Harbour, W. Ouyang, D.D. Chaplin,

C.T. Weaver, IL-22-producing neutrophils contribute to antimicrobial defense and restitution of colonic epithelial integrity during colitis, Proc. Natl. Acad. Sci. U. S. A. 110 (2013) 12768–12773. https://doi.org/10.1073/PNAS.1300318110.

[165] M. Miyake, T. Koga, S. Kondo, N. Yoda, C. Emoto, T. Mukai, H. Toguchi, Prediction of drug intestinal absorption in human using the Ussing chamber system: A comparison of intestinal tissues from animals and humans, Eur. J. Pharm. Sci. 96 (2017) 373–380. https://doi.org/10.1016/J.EJPS.2016.10.006.

[166] A. Vila, N. Torras, A.G. Castaño, M. García-Díaz, J. Comelles, T. Pérez-Berezo, C. Corregidor, Ó. Castaño, E. Engel, V. Fernández-Majada, E. Martínez, Hydrogel co-networks of gelatine methacrylate and poly(ethylene glycol) diacrylate sustain 3D functional in vitro models of intestinal mucosa, Biofabrication 12 (2020). https://doi.org/10.1088/1758-5090/AB5F50.

[167] Y. Wang, M. DiSalvo, D.B. Gunasekara, J. Dutton, A. Proctor, M.S. Lebhar, I.A. Williamson, J. Speer, R.L. Howard, N.M. Smiddy, S.J. Bultman, C.E. Sims, S.T. Magness, N.L. Allbritton, Self-renewing Monolayer of Primary Colonic or Rectal Epithelial Cells, CMGH 4 (2017) 165-182.e7. https://doi.org/10.1016/j.jcmgh.2017.02.011.

[168] J.G. In, J. Foulke-Abel, E. Clarke, O. Kovbasnjuk, Human Colonoid Monolayers to Study Interactions Between Pathogens, Commensals, and Host Intestinal Epithelium, J. Vis. Exp. 2019 (2019). https://doi.org/10.3791/59357.

[169] G. Noel, N.W. Baetz, J.F. Staab, M. Donowitz, O. Kovbasnjuk, M.F. Pasetti, N.C. Zachos, A primary human macrophage-enteroid co-culture model to investigate mucosal gut physiology and host-pathogen interactions, Sci. Rep. 7 (2017). https://doi.org/10.1038/SREP45270.

[170] Y. Wang, R. Kim, S.H.J. Hwang, J. Dutton, C.E. Sims, N.L. Allbritton, Analysis of Interleukin 8 Secretion by a Stem-Cell-Derived Human-Intestinal-Epithelial-Monolayer Platform, Anal. Chem. 90 (2018) 11523–11530. https://doi.org/10.1021/ACS.ANALCHEM.8B02835.

[171] T.T. Roh, Y. Chen, H.T. Paul, C. Guo, D.L. Kaplan, 3D bioengineered tissue model of the large intestine to study inflammatory bowel disease, Biomaterials 225 (2019). https://doi.org/10.1016/J.BIOMATERIALS.2019.119517.

[172] C.P. Miller, W. Shin, E.H. Ahn, H.J. Kim, D.H. Kim, Engineering Microphysiological Immune System Responses on Chips, Trends Biotechnol. 38 (2020) 857–872. https://doi.org/10.1016/J.TIBTECH.2020.01.003.

[173] D.B. Gunasekara, J. Speer, Y. Wang, D.L. Nguyen, M.I. Reed, N.M. Smiddy, J.S. Parker, J.K. Fallon, P.C. Smith, C.E. Sims, S.T. Magness, N.L. Allbritton, A Monolayer of Primary Colonic Epithelium Generated on a Scaffold with a Gradient of Stiffness for Drug Transport Studies, Anal. Chem. 90 (2018) 13331–13340. https://doi.org/10.1021/ACS.ANALCHEM.8B02845.

[174] P. Aimar, M. Meireles, V.S.-J. of membrane science, undefined 1990, A contribution to the translation of retention curves into pore size distributions for sieving membranes, ElsevierP Aimar, M Meireles, V SanchezJournal Membr. Sci. 1990•Elsevier 54 (1990) 321–338. https://www.sciencedirect.com/science/article/pii/S0376738800806183 (accessed August 5, 2024).

[175] D.W. Powell, I. V. Pinchuk, J.I. Saada, X. Chen, R.C. Mifflin, Mesenchymal cells of the intestinal lamina propria, Annu. Rev. Physiol. 73 (2011) 213–237. https://doi.org/10.1146/ANNUREV.PHYSIOL.70.113006.100646.

[176] B. Roy, L. Yuan, Y. Lee, A. Bharti, A. Mitra, G. V. Shivashankar, Fibroblast rejuvenation by mechanical reprogramming and redifferentiation, Proc. Natl. Acad. Sci. U. S. A. 117 (2020) 10131–10141. https://doi.org/10.1073/PNAS.1911497117.

[177] K. Adatia, M. Raja, P. Vadgama, An electrochemical study of microporous track-etched membrane permeability and the effect of surface protein layers, Colloids Surf. B. Biointerfaces 158 (2017) 84–92. https://doi.org/10.1016/J.COLSURFB.2017.06.032.

[178] C.J. Lee, J.A. Vroom, H.A. Fishman, S.F. Bent, Determination of human lens capsule permeability and its feasibility as a replacement for Bruch's membrane, Biomaterials 27 (2006) 1670–1678. https://doi.org/10.1016/J.BIOMATERIALS.2005.09.008.

[179] S. Ramanujan, A. Pluen, T.D. McKee, E.B. Brown, Y. Boucher, R.K. Jain, Diffusion and convection in collagen gels: implications for transport in the tumor interstitium, Biophys. J. 83 (2002) 1650–1660. https://doi.org/10.1016/S0006-3495(02)73933-7.

[180] T. Kihara, J. Ito, J. Miyake, Measurement of biomolecular diffusion in extracellular matrix condensed by fibroblasts using fluorescence correlation spectroscopy, PLoS One 8 (2013). https://doi.org/10.1371/JOURNAL.PONE.0082382.

[181] M.H. Hettiaratchi, A. Schudel, T. Rouse, A.J. García, S.N. Thomas, R.E. Guldberg, T.C. McDevitt, A rapid method for determining protein diffusion through hydrogels for regenerative medicine applications, APL Bioeng. 2 (2018). https://doi.org/10.1063/1.4999925.

[182] S.S. Hinman, Y. Wang, N.L. Allbritton, Photopatterned Membranes and Chemical Gradients Enable Scalable Phenotypic Organization of Primary Human Colon Epithelial Models, Anal. Chem. 91 (2019) 15240–15247. https://doi.org/10.1021/ACS.ANALCHEM.9B04217.

[183] D.M. Ornoff, Y. Wang, A. Proctor, A.S. Shah, N.L. Allbritton, Co-fabrication of chitosan and epoxy photoresist to form microwell arrays with permeable hydrogel bottoms, Biomaterials 74 (2016) 77–88. https://doi.org/10.1016/J.BIOMATERIALS.2015.09.032.

[184] H.L. Nowotarski, P.J. Attayek, N.L. Allbritton, Automated platform for cell selection and separation based on four-dimensional motility and matrix degradation, Analyst 145 (2020) 2731–2742. https://doi.org/10.1039/C9AN02224D.

[185] B. Srinivasan, A.R. Kolli, M.B. Esch, H.E. Abaci, M.L. Shuler, J.J. Hickman, TEER measurement techniques for in vitro barrier model systems, J. Lab. Autom. 20 (2015) 107–126. https://doi.org/10.1177/2211068214561025.

[186] S.C. Bischoff, G. Barbara, W. Buurman, T. Ockhuizen, J.D. Schulzke, M. Serino, H. Tilg, A. Watson, J.M. Wells, Intestinal permeability--a new target for disease prevention and therapy, BMC Gastroenterol. 14 (2014). https://doi.org/10.1186/S12876-014-0189-7.

[187] I. Hubatsch, E.G.E. Ragnarsson, P. Artursson, Determination of drug permeability and prediction of drug absorption in Caco-2 monolayers, Nat. Protoc. 2 (2007) 2111–2119. https://doi.org/10.1038/NPROT.2007.303.

[188] L.W. Peterson, D. Artis, Intestinal epithelial cells: regulators of barrier function and immune homeostasis, Nat. Rev. Immunol. 14 (2014) 141–153. https://doi.org/10.1038/NRI3608.

[189] A.B. West, C.A. Isaac, J.M. Carboni, J.S. Morrow, M.S. Mooseker, K.W. Barwick, Localization of villin, a cytoskeletal protein specific to microvilli, in human ileum and colon and in colonic neoplasms, Gastroenterology 94 (1988) 343–352. https://doi.org/10.1016/0016-5085(88)90421-0.

[190] N. Hirokawa, L.G. Tilnfy, K. Fujiwara, J.E. Heuser, Organization of actin, myosin, and

intermediate filaments in the brush border of intestinal epithelial cells, J. Cell Biol. 94 (1982) 425–443. https://doi.org/10.1083/JCB.94.2.425.

[191] Y. Wang, R. Kim, C.E. Sims, N.L. Allbritton, Building a Thick Mucus Hydrogel Layer to Improve the Physiological Relevance of In Vitro Primary Colonic Epithelial Models, Cell. Mol. Gastroenterol. Hepatol. 8 (2019) 653-655.e5. https://doi.org/10.1016/J.JCMGH.2019.07.009.

[192] J.E. Speer, D.B. Gunasekara, Y. Wang, J.K. Fallon, P.J. Attayek, P.C. Smith, C.E. Sims, N.L. Allbritton, Molecular transport through primary human small intestinal monolayers by culture on a collagen scaffold with a gradient of chemical cross-linking, J. Biol. Eng. 13 (2019). https://doi.org/10.1186/S13036-019-0165-4.

[193] S.J. Collins, F.W. Ruscetti, R.E. Gallagher, R.C. Gallo, Terminal differentiation of human promyelocytic leukemia cells induced by dimethyl sulfoxide and other polar compounds, Proc. Natl. Acad. Sci. U. S. A. 75 (1978) 2458–2462. https://doi.org/10.1073/PNAS.75.5.2458.

[194] A. Millius, O.D. Weiner, Chemotaxis in neutrophil-like HL-60 cells, Methods Mol. Biol. 571 (2009) 167–177. https://doi.org/10.1007/978-1-60761-198-1_11.

[195] S.S. Hinman, Y. Wang, N.L. Allbritton, Photopatterned Membranes and Chemical Gradients Enable Scalable Phenotypic Organization of Primary Human Colon Epithelial Models, Anal. Chem. 91 (2019) 15240–15247. https://doi.org/10.1021/acs.analchem.9b04217.

[196] J.F. Dekkers, M. Alieva, L.M. Wellens, H.C.R. Ariese, P.R. Jamieson, A.M. Vonk, G.D. Amatngalim, H. Hu, K.C. Oost, H.J.G. Snippert, J.M. Beekman, E.J. Wehrens, J.E. Visvader, H. Clevers, A.C. Rios, High-resolution 3D imaging of fixed and cleared organoids, Nat. Protoc. 14 (2019) 1756–1771. https://doi.org/10.1038/S41596-019-0160-8.

[197] J. Crank, The mathematics of diffusion, 1979. https://books.google.com/books?hl=en&lr=&id=eHANhZwVouYC&oi=fnd&pg=IA4&ots=fBZ2C1flOV&sig=9SSfH8eFd8xePbyPQZfMOKFkC0E (accessed August 5, 2024).

[198] K.A. Granath, B.E. Kvist, Molecular weight distribution analysis by gel chromatography on Sephadex, J. Chromatogr. 28 (1967) 69–81. https://doi.org/10.1016/S0021-9673(01)85930-6.

[199] R.T.- Computing, 2020, RA language and environment for statistical computing, R Foundation for Statistical, Cir.Nii.Ac.Jp (n.d.). https://cir.nii.ac.jp/crid/1370298755636824325 (accessed August 5, 2024).

[200] S.J. Lord, K.B. Velle, R. Dyche Mullins, L.K. Fritz-Laylin, SuperPlots: Communicating reproducibility and variability in cell biology, J. Cell Biol. 219 (2020). https://doi.org/10.1083/JCB.202001064.